

CURRENT, CTD, AND PRESSURE MEASUREMENTS IN POSSIBLE DISPERSAL  
REGIONS OF THE CHUKCHI SEA

by

Knut Aagaard

School of Oceanography  
University of Washington  
Seattle, WA 98195

Final Report  
Outer Continental Shelf Environmental Assessment Program  
Research Unit 91

May 1984

## *Introduction*

The northwest coast of Alaska bordering the **Chukchi** Sea extends over 1200 km from **Bering** Strait to Point Barrow. The **Chukchi** is the north-eastern end of the great **arctic** continental shelf system, the world's largest, which surrounds the northern **Eurasian** land mass. These vast shelf seas are remarkably wide and shallow, **typically** 600-800 km and **50m** respectively, characteristics which greatly affect **marine** conditions.

**Oceanographically**, the **Chukchi** Sea is an area of great contrasts. While in many respects it is an **adjoining** shelf **sea** of the Arctic Ocean, much as the East Siberian or the Laptev Sea is, it is **also** anomalous in that it is the recipient of the large northward discharge of the North Pacific through Bering Strait. The importance of this influx can scarcely be exaggerated. The nutrient-rich waters, carrying Pacific **planktonic** life forms, define a migratory pathway between the Arctic and the Pacific for a great variety of animals, including marine mammals. The flow, in summer anomalously warm and of low salinity, causes the **Chukchi** to become ice-free much earlier in the year than it otherwise would, and it likewise extends the ice-free season far later into the **fall**. The influx has an important **effect** on the layering of the Arctic Ocean itself, and the influence of the Pacific water can be detected to the North **Pole** and beyond.

There is one major embayment along the Alaskan **Chukchi** coast, Kotzebue Sound, into which sufficient freshwater is discharged in **summer** to noticeably affect water characteristics in the eastern **Chukchi** Sea. Otherwise, the flow through Bering Strait contributes the only significant freshwater fraction from the North American side. **However**, this Bering Strait contribution is a very large one; its characteristics have been discussed by Coachman, Aagaard and Tripp (1975), hereafter referred to as CAT.

sea ice is an important feature of the **Chukchi** Sea, covering most of the area from about November-July, although the southern **Chukchi** may be ice-free somewhat longer. The ice has a number of *oceanographic* consequences. (1) During Ice formation, salt is rejected from the growing ice. The brine rejection drives gravitational convection, mixing the water **column**. Furthermore, the density increase associated with the **salinization** **alters** the oceanic pressure field and establishes horizontal circulation. (2) During melting, the ice serves as a freshwater source, and hence a buoyancy source, stabilizing the surface Layer. This in turn **leads to** solar heating of the upper layer, and also to a more favorable environment for primary production, **until** nutrients in the upper Layer are exhausted. **Inhomogeneties** in the buoyancy distribution will drive horizontal circulation. (3) The ice provides thermostatic control, buffering the temperature **field** so as to keep the water at the freezing point. (4) The wind stress acting through the medium of the ice is in general altered. In the extreme **case of landfast** ice, no direct momentum transfer occurs.

Tides in the **Chukchi** Sea are **small**, with the largest constituent, the  $M_2$ , having a maximum amplitude in the eastern **Chukchi** of about 5 cm (Kowalik, 1981). However, large sea **level** changes (of order 2-3 m) can be generated by meteorological surges (Matthews, 1970).

### *Study objectives*

There have been two primary objectives for **RU91**. The first has been to determine the **longshore** transport, and in particular that between Cape **Lisburne** and Point Barrow. The presence of a strong flow along this coast has been known for **many** years, with the mean set being northeastward and representing an extension of the Bering Strait **inflow** (cf. CAT for a

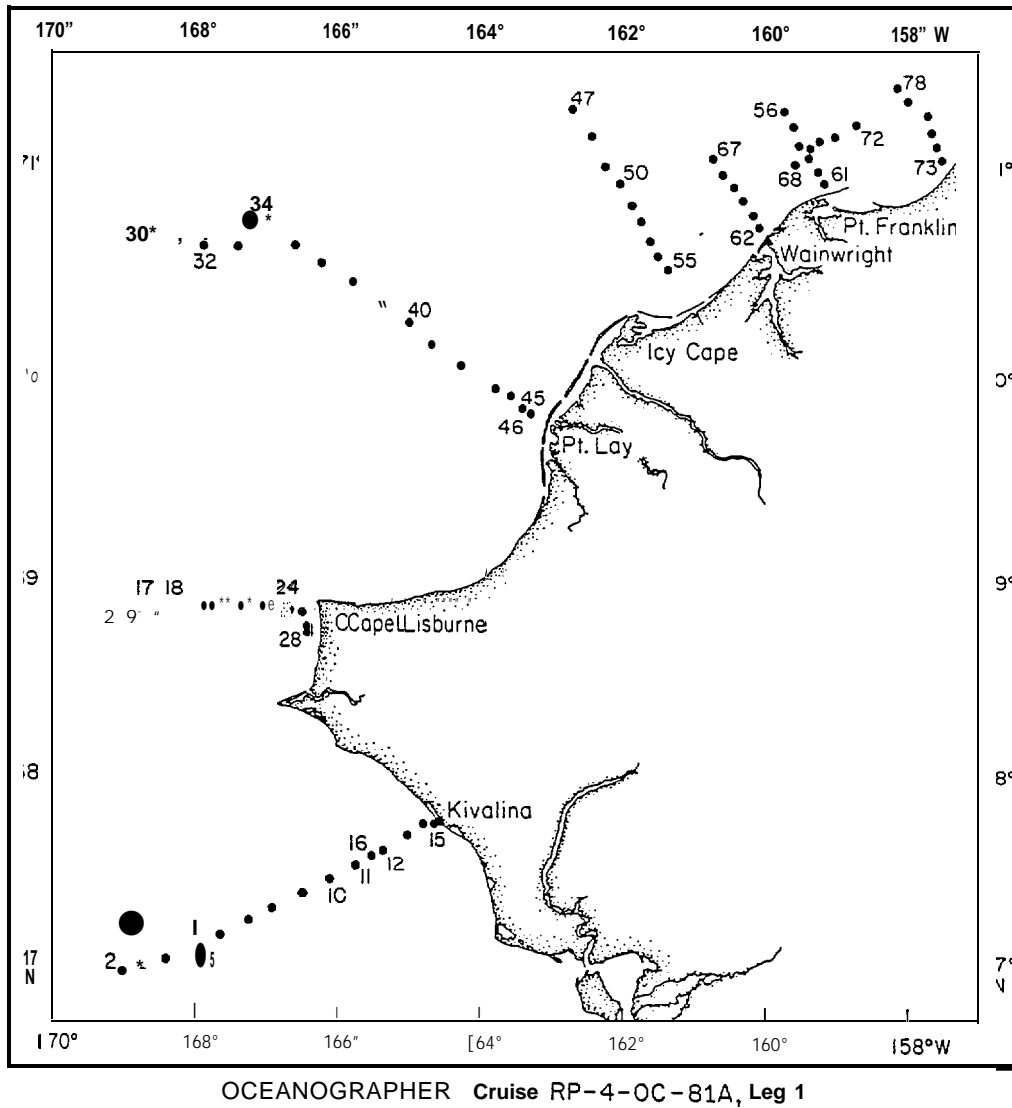
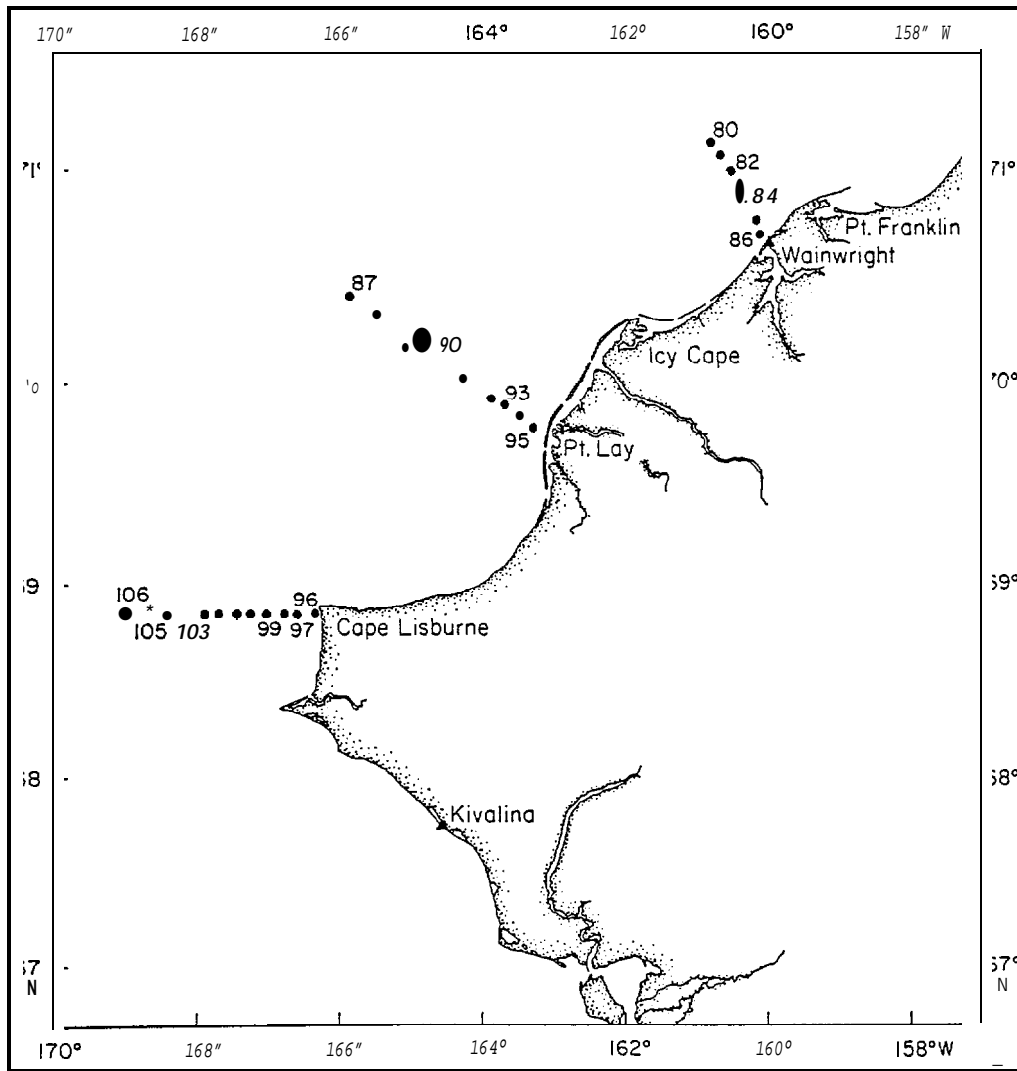
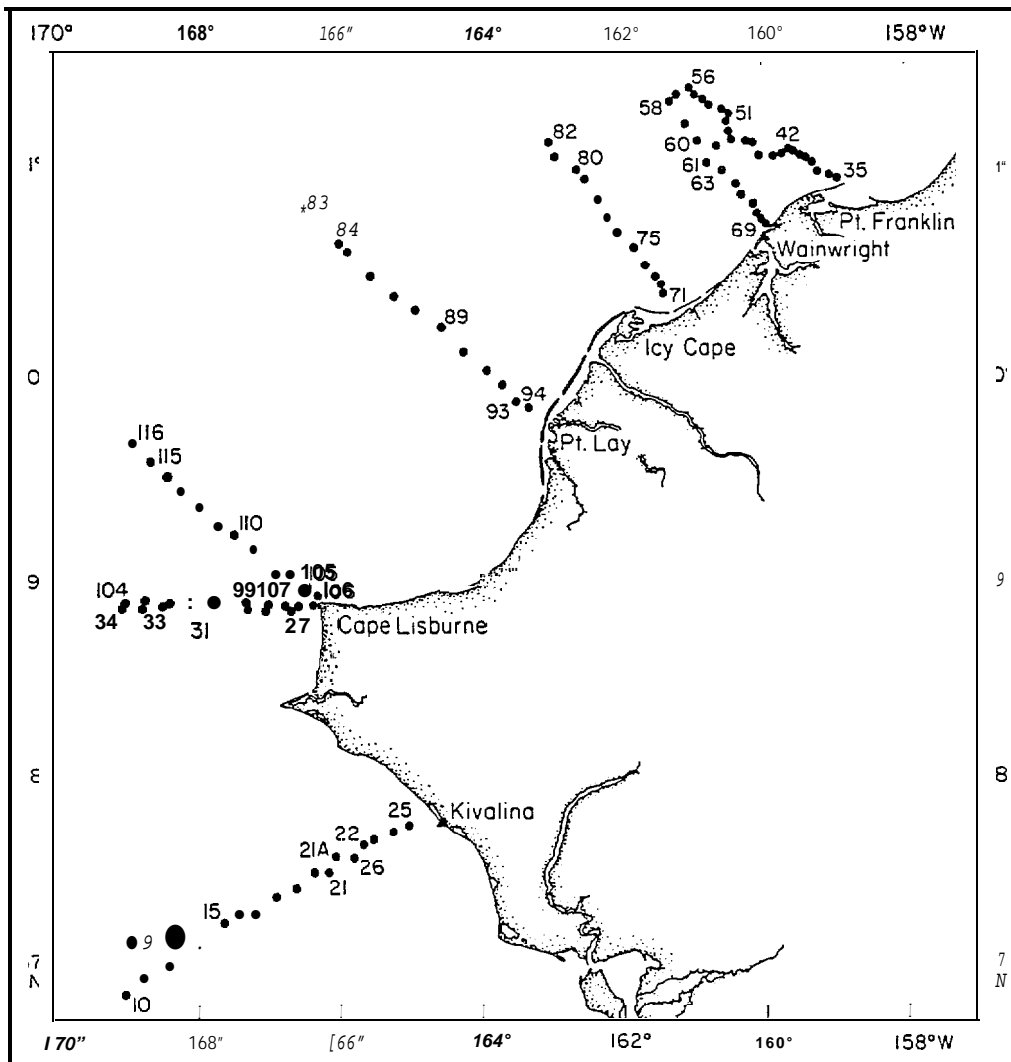


Figure 1. Station positions, 4-12 September 1981



OCEANOGRAPHER Cruise RP-4-OC-81A, Leg II

Figure 2. Station positions, 14-19 September 1981



DI SCOVERER Cruise RP-4-DI-82A, Leg II

Figure 3. Station positions, 16-27 August 1982

262

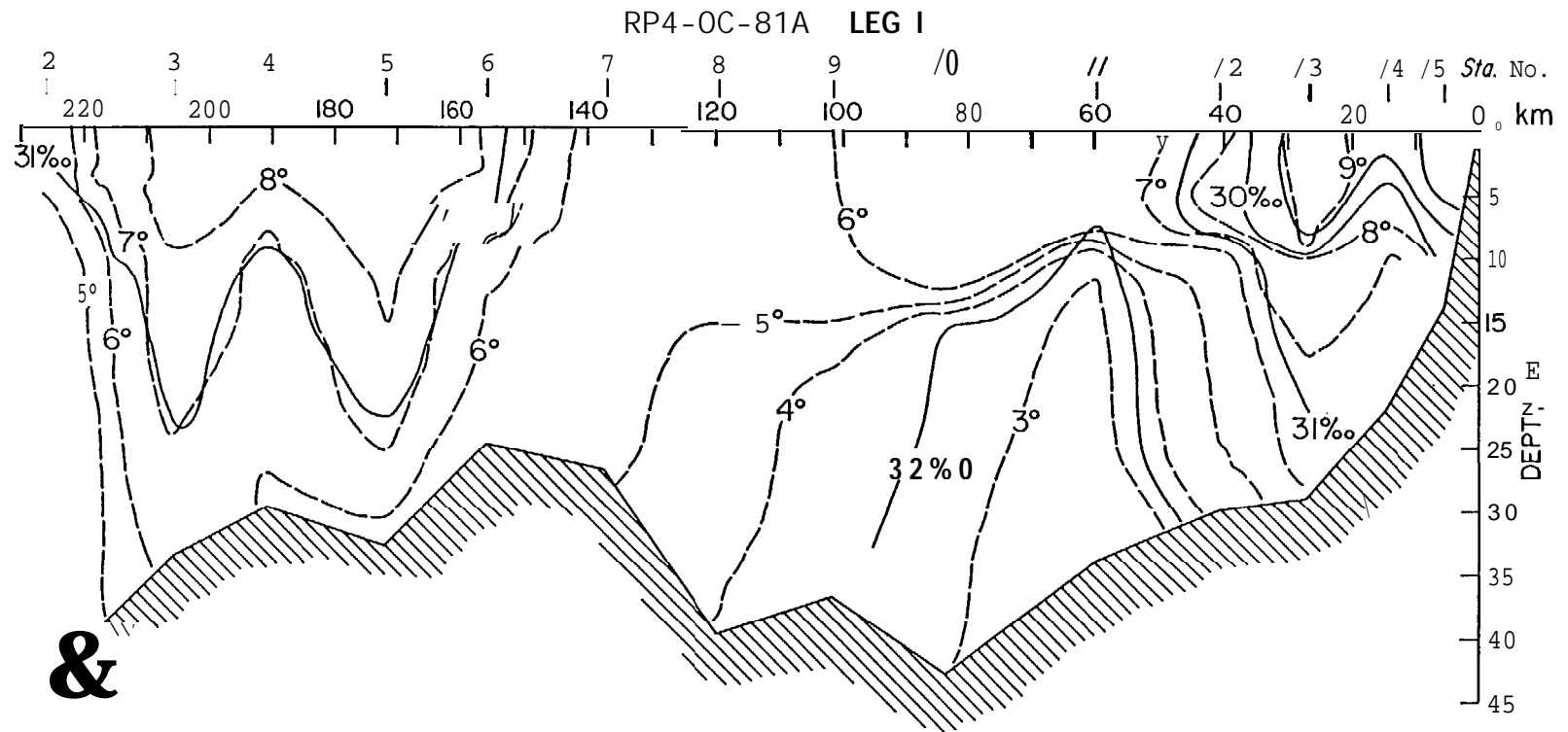


Figure 4. Kivalina section

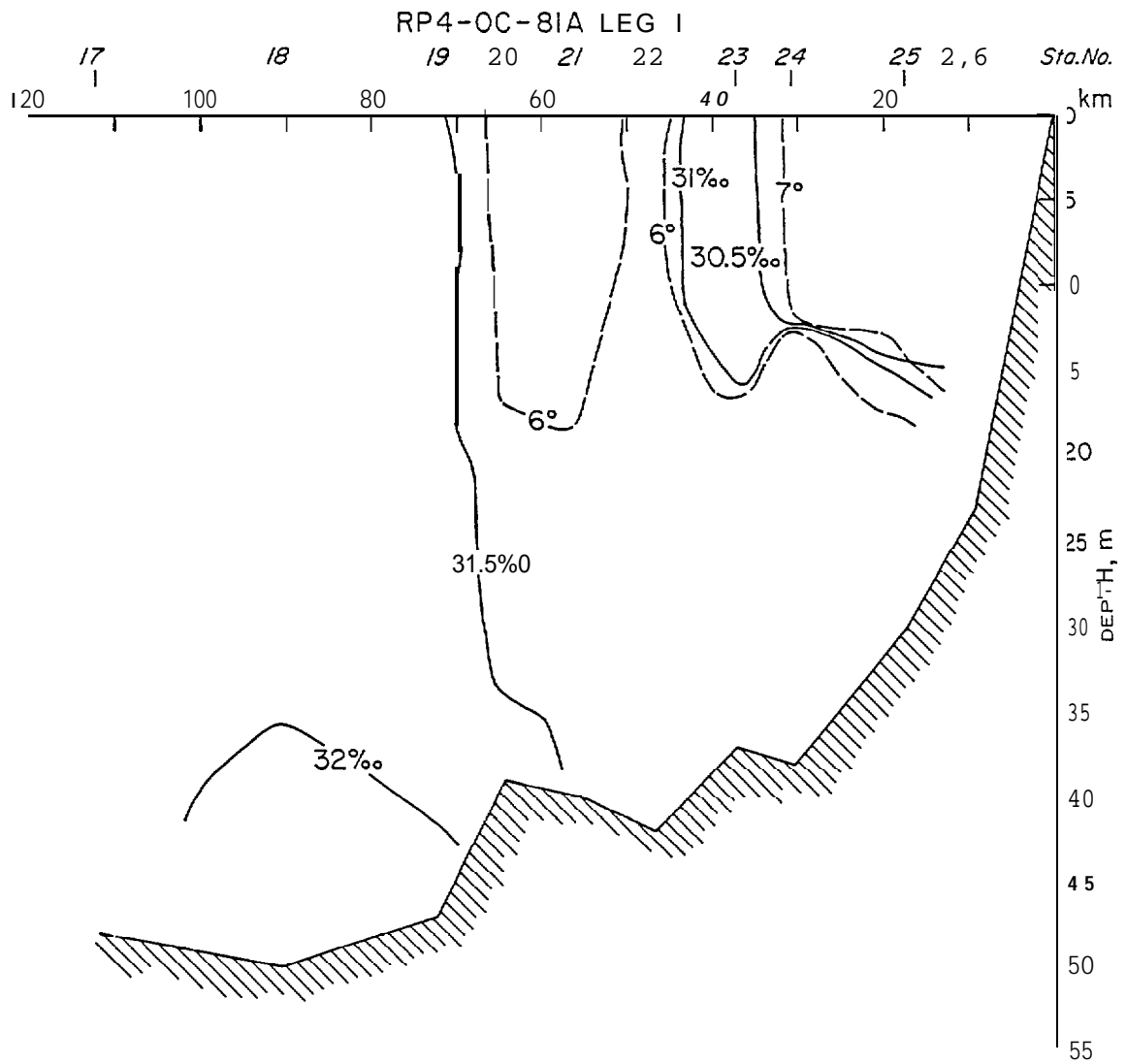


Figure 5. Cape Lisburne section

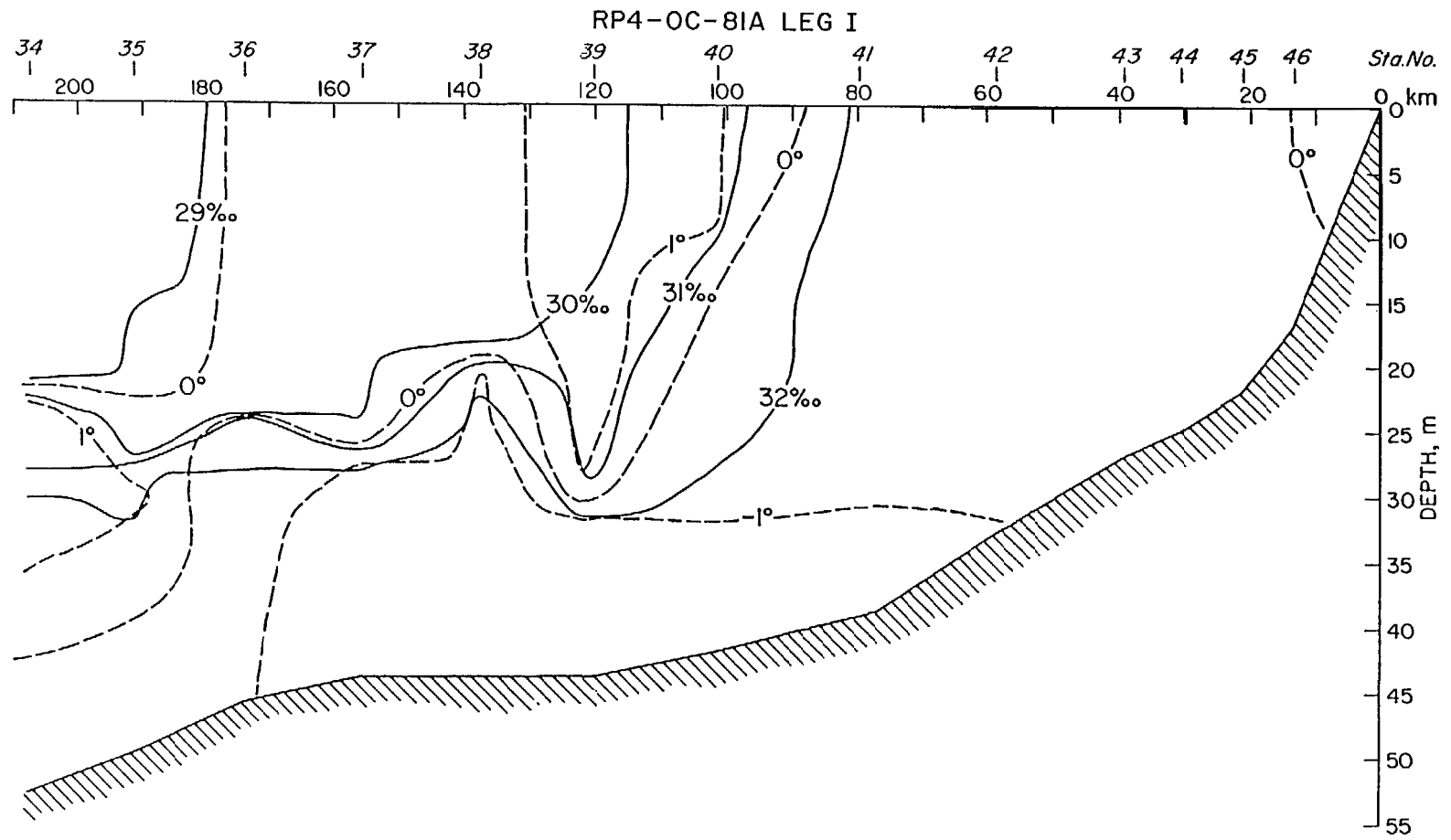


Figure 6. Pt. Lay section

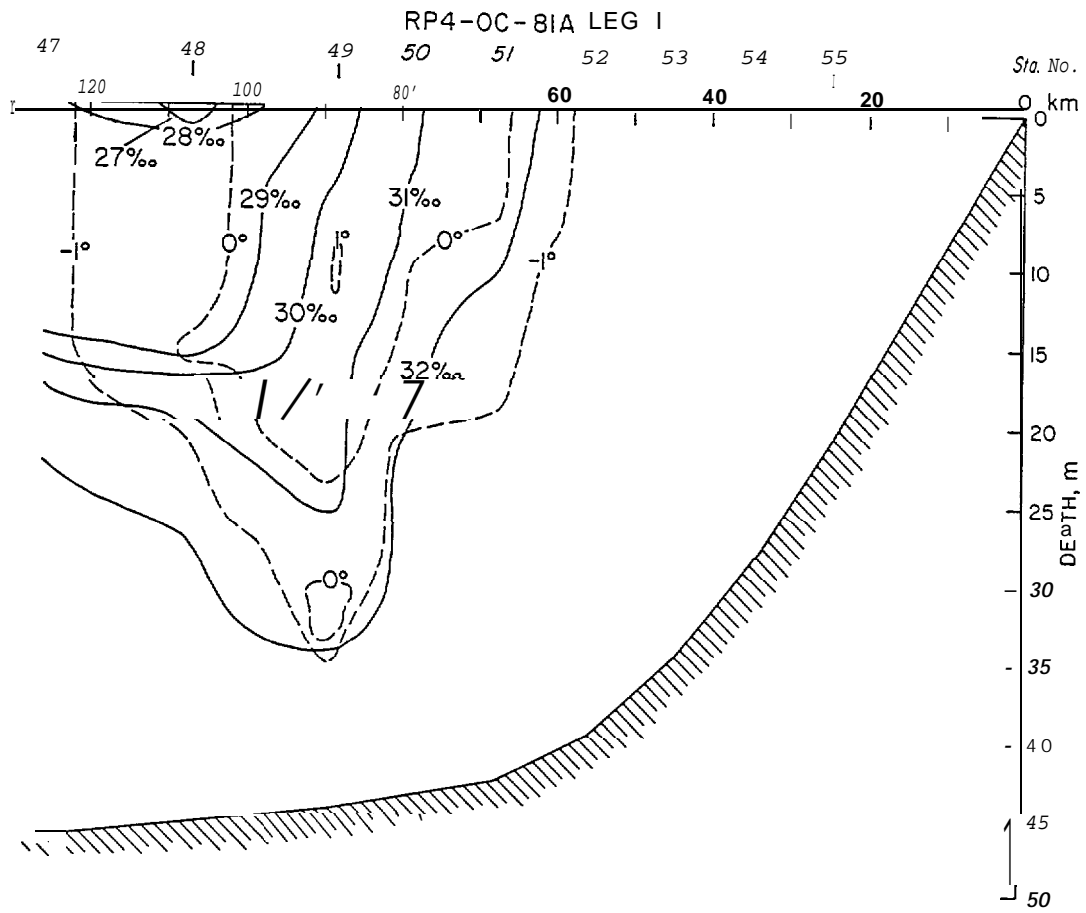


Figure 7. Icy Cape section

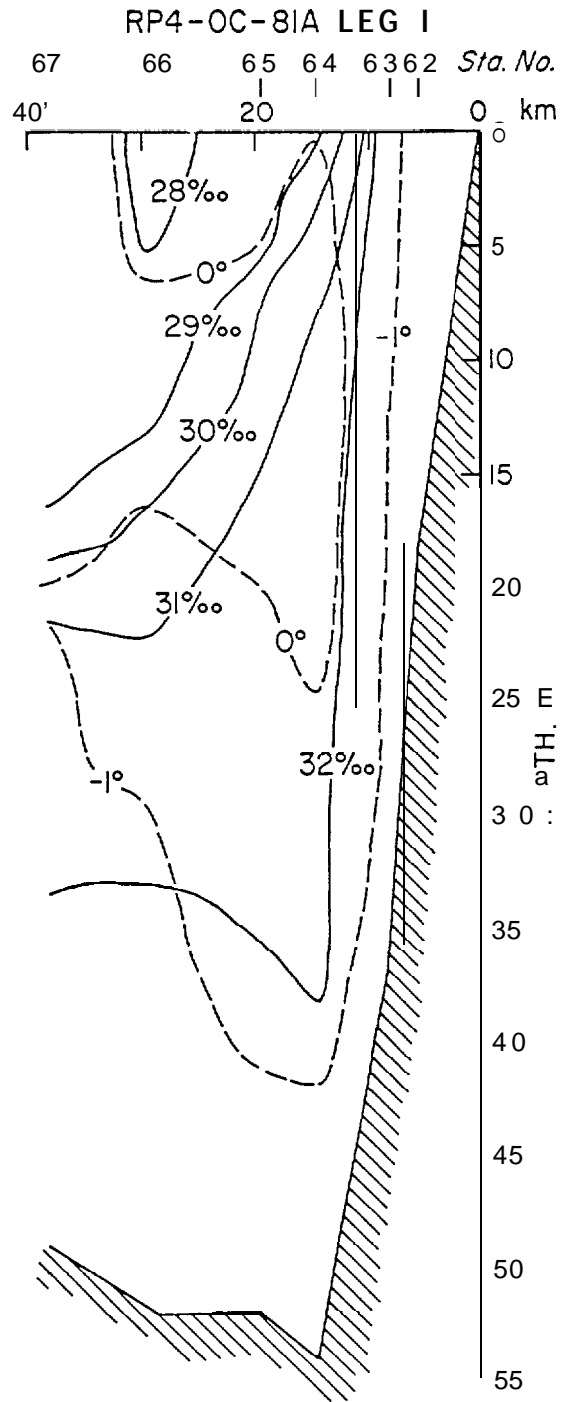


Figure 8. Wainwright section

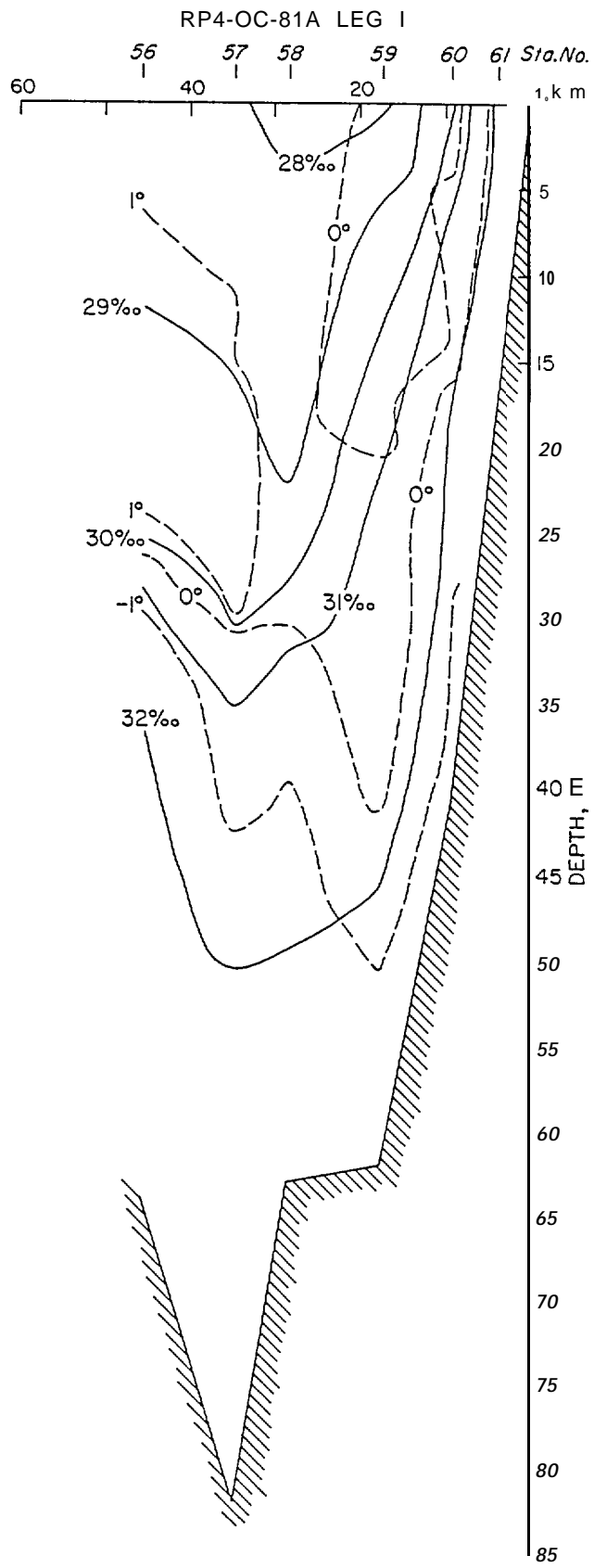


Figure 9. Pt. Franklin section

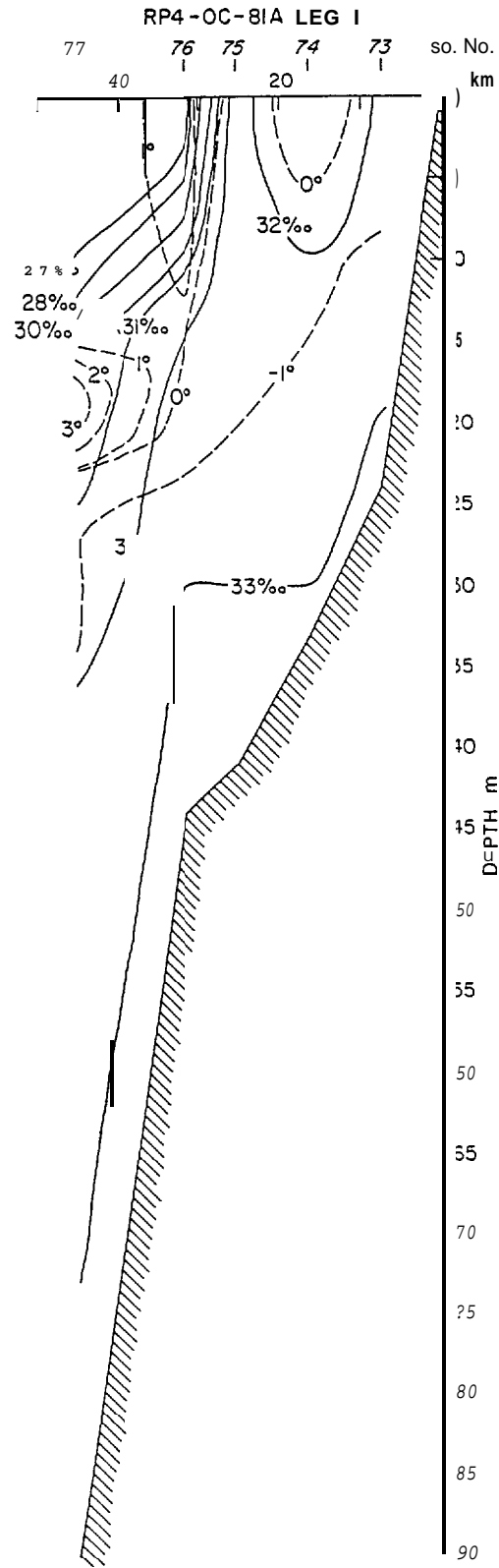


Figure 10. Pt. Barrow/Pt. Franklin section

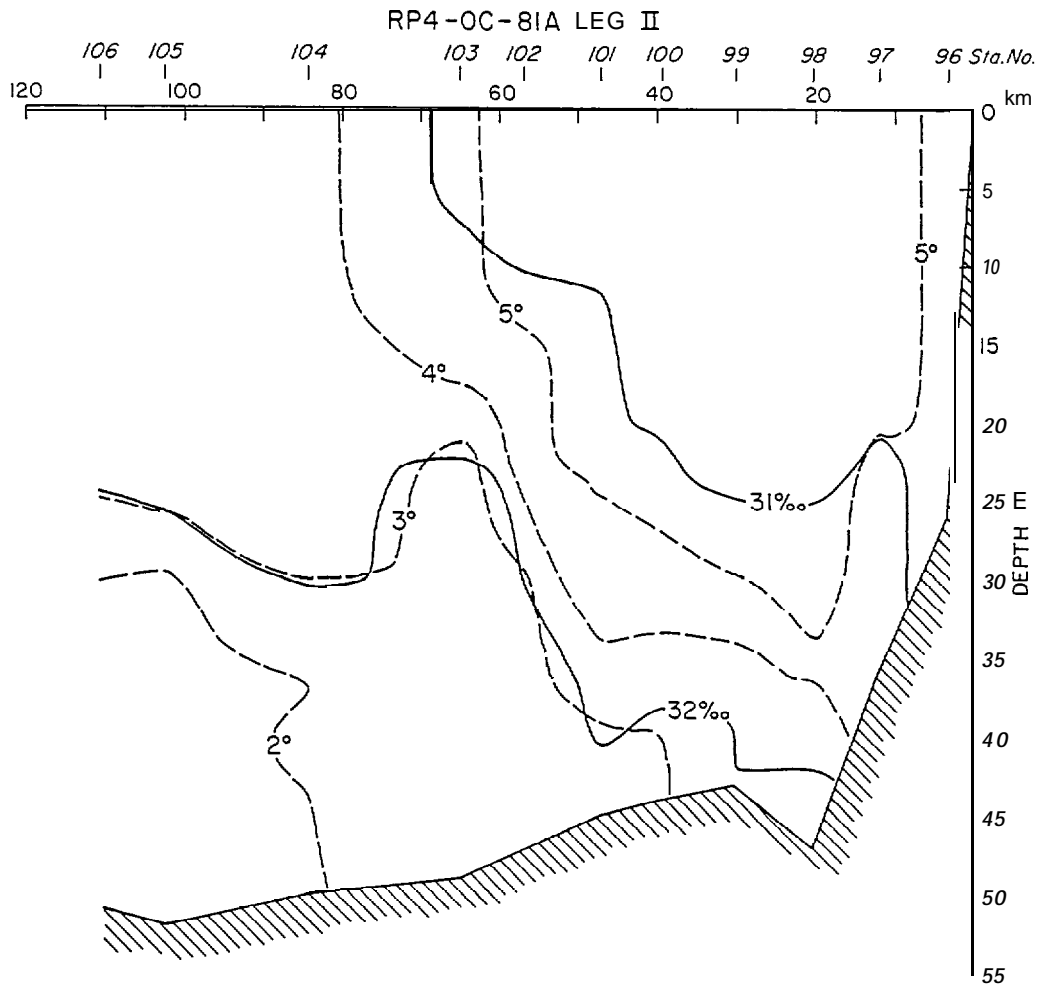


Figure 11. Cape Lisburne section

270

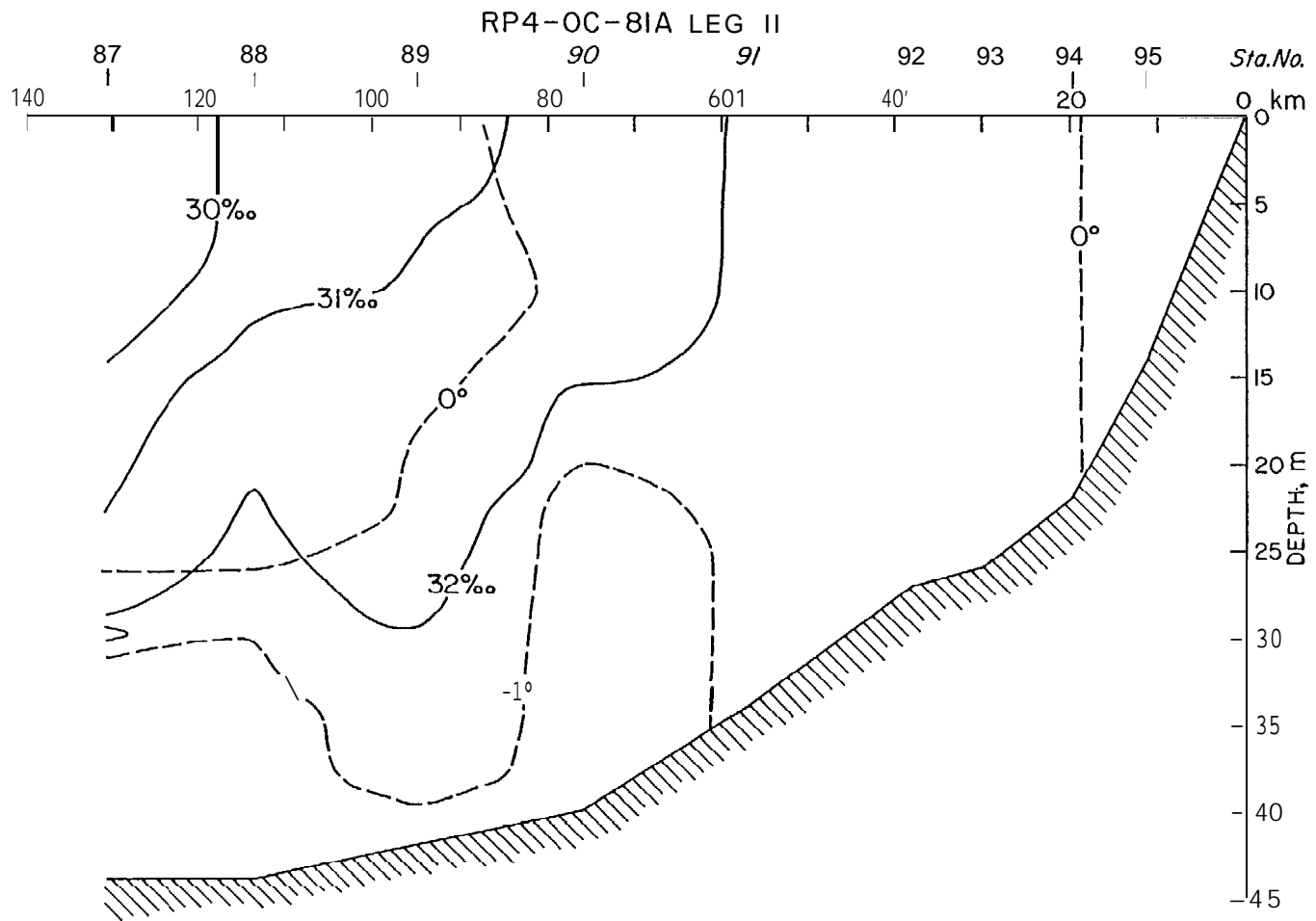


Figure 12. Pt. Lay section

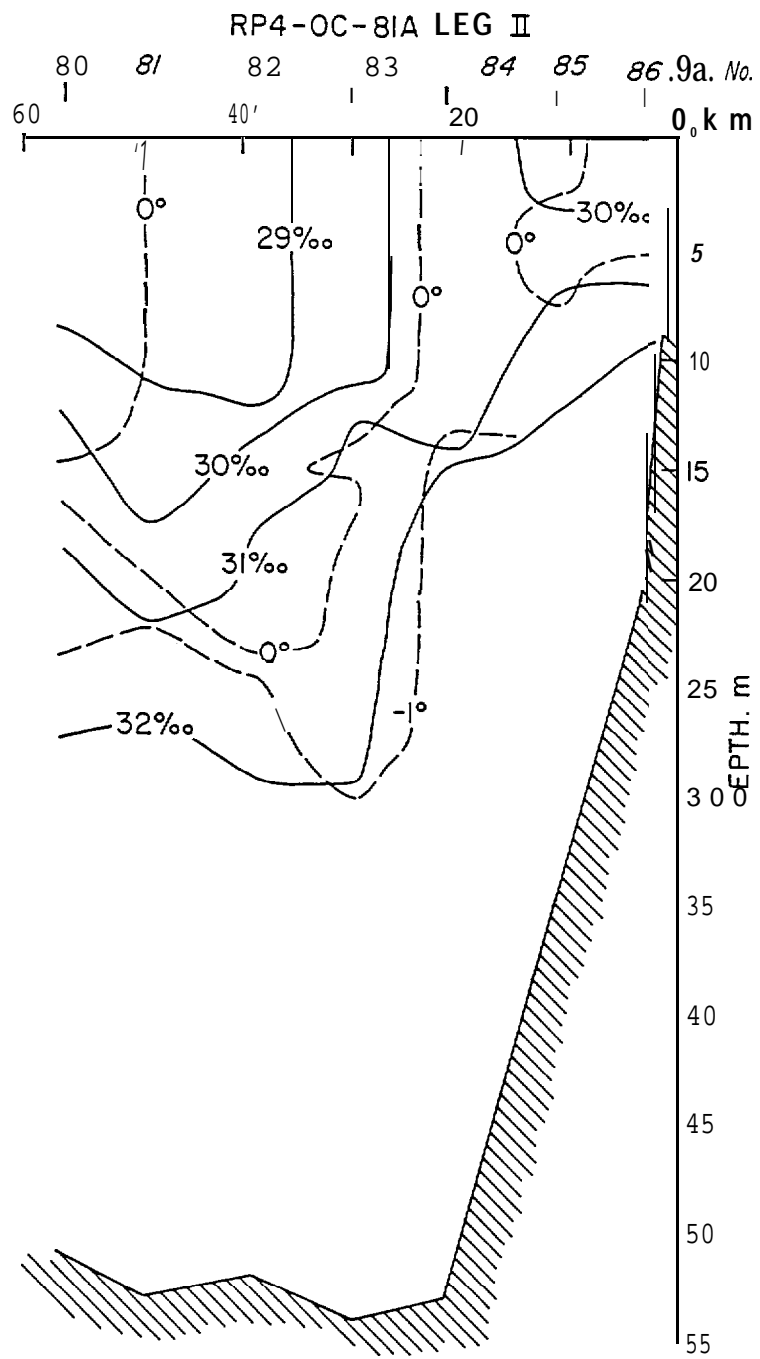


Figure 13. Wainwright section

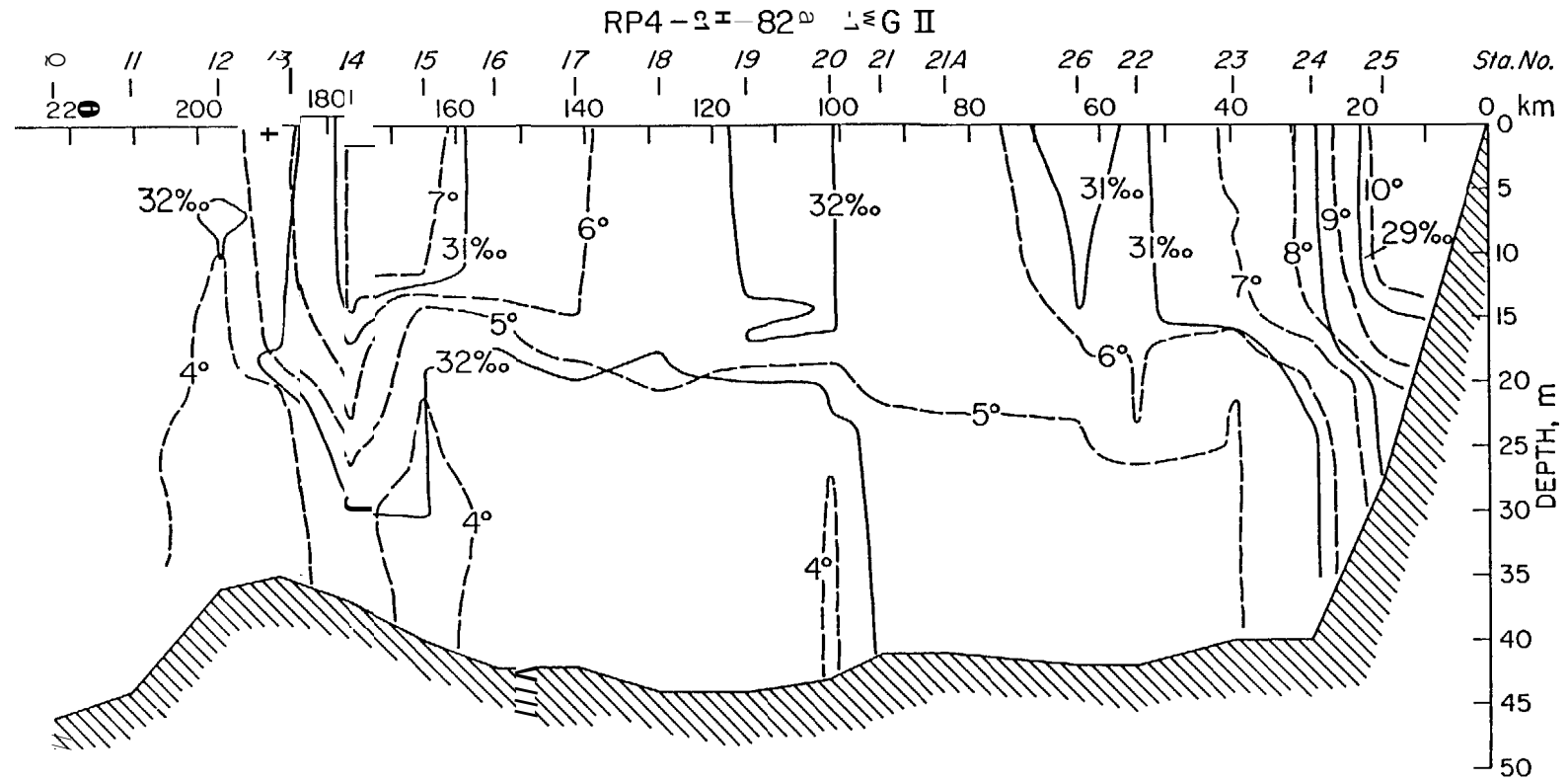


Figure 14. Kivalina section

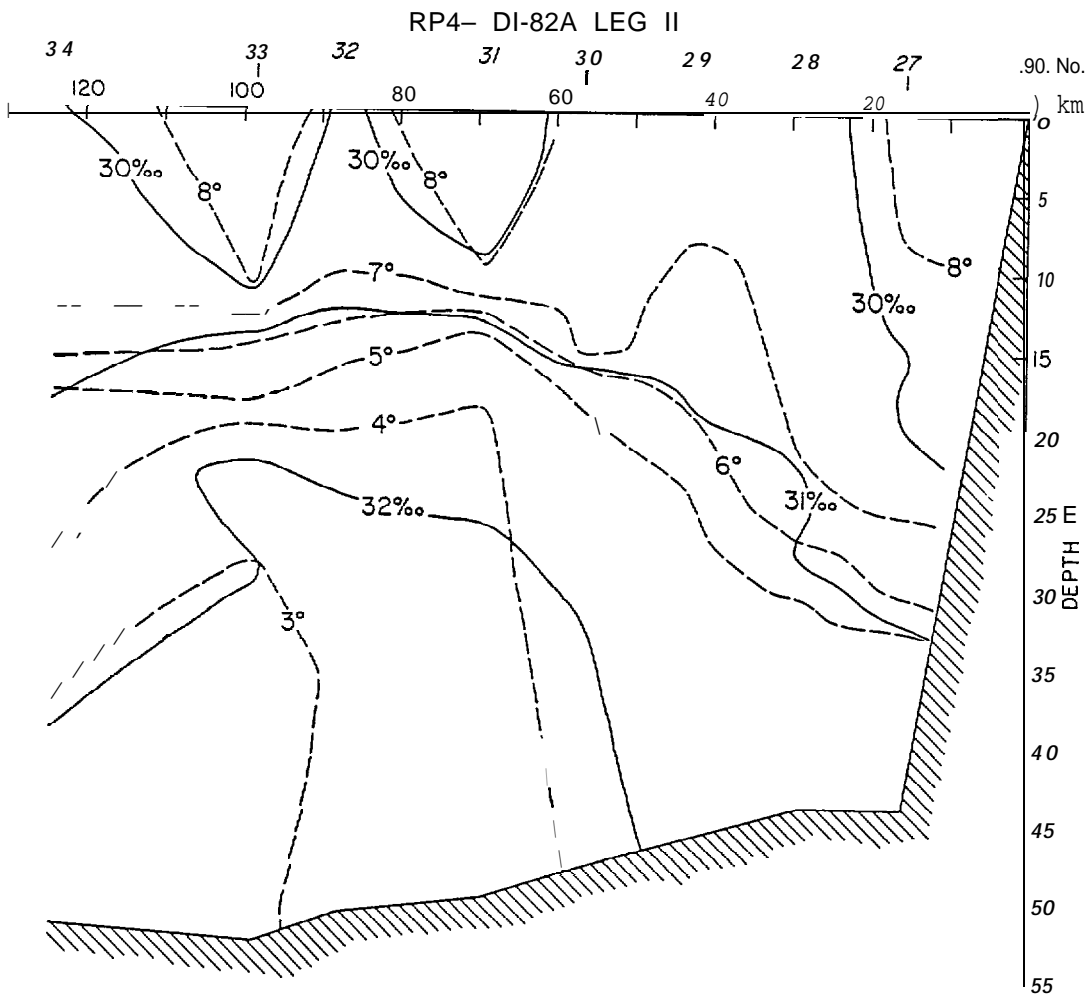


Figure 15. Cape Lisburne section

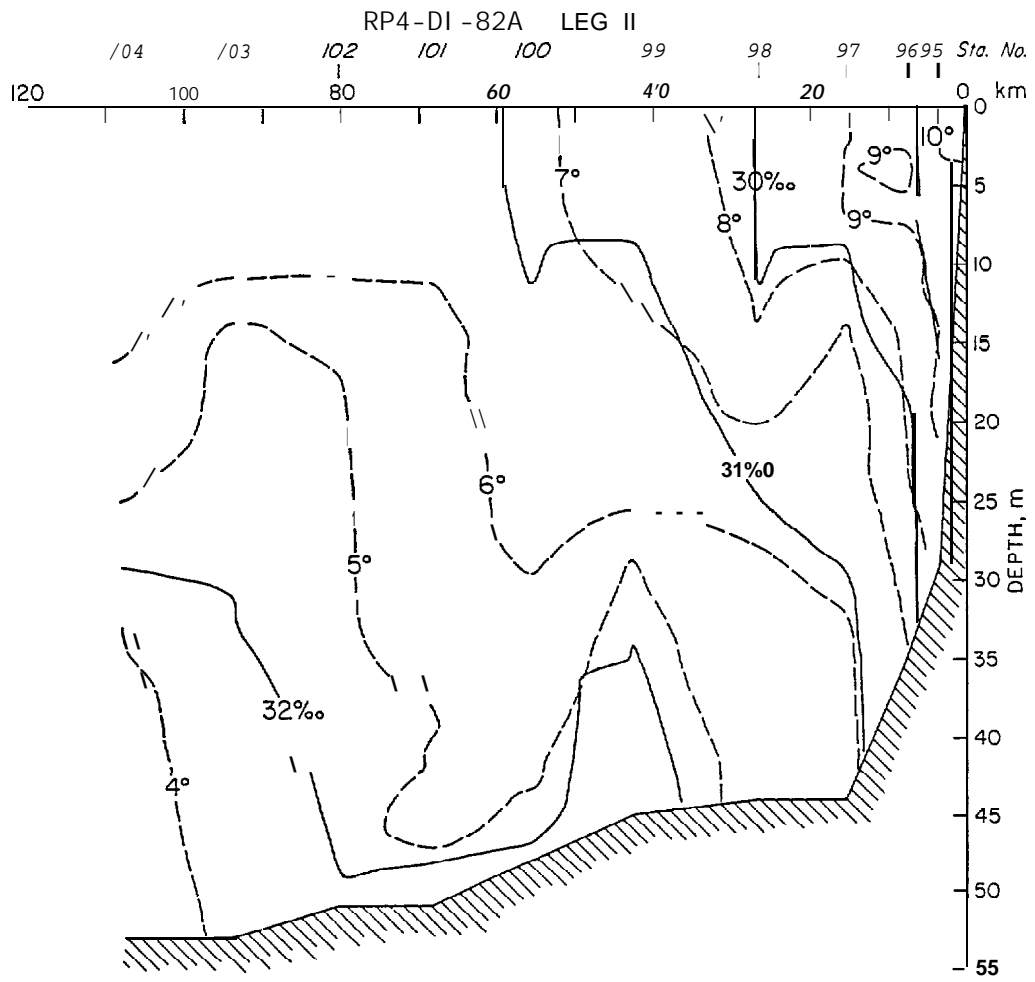


Figure 16. Cape Lisburne section

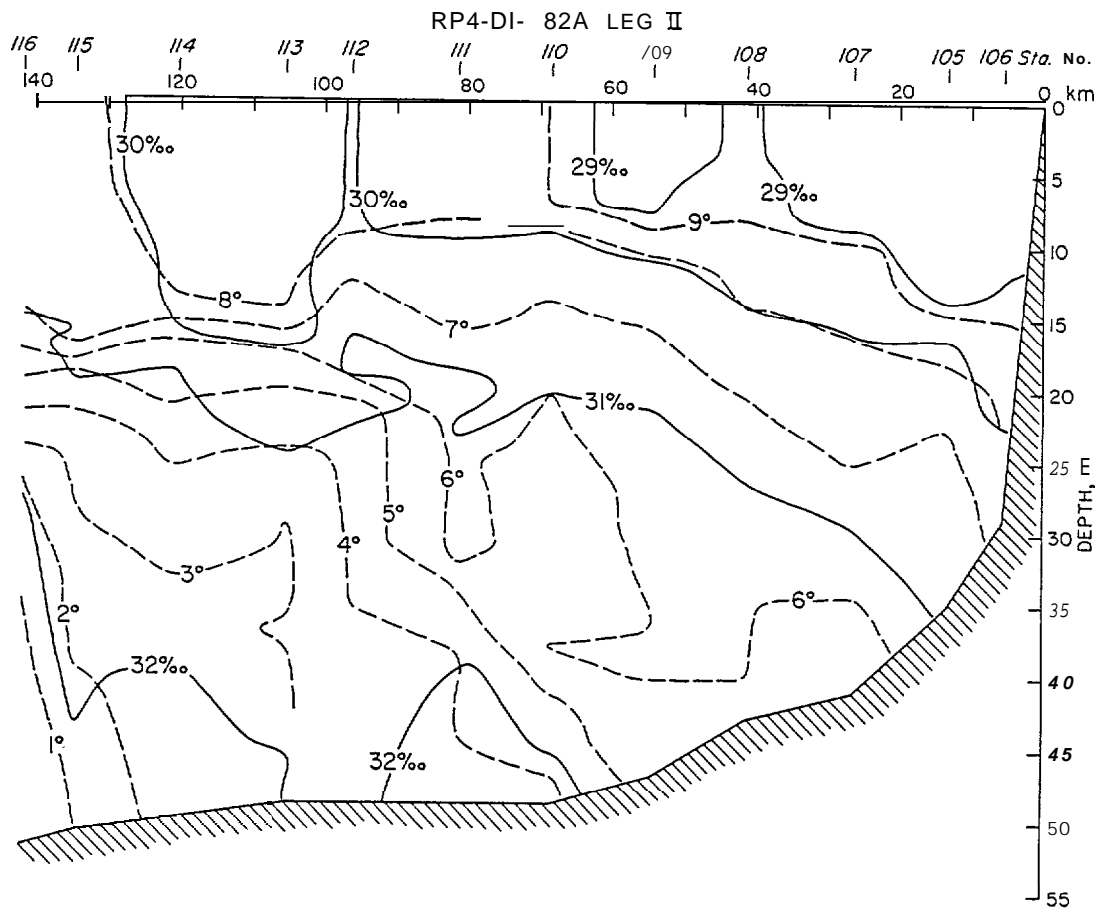


Figure 17. Cape Lisburne/northwest section

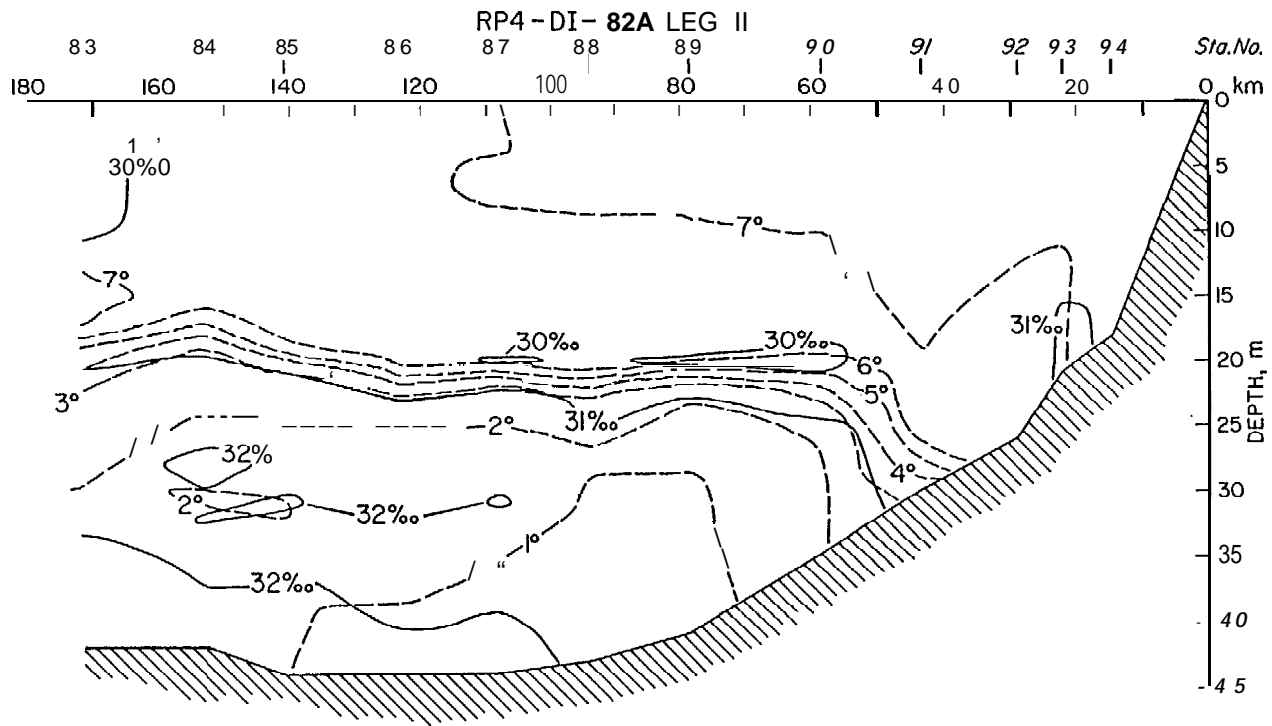


Figure 18. Pt. Lay section

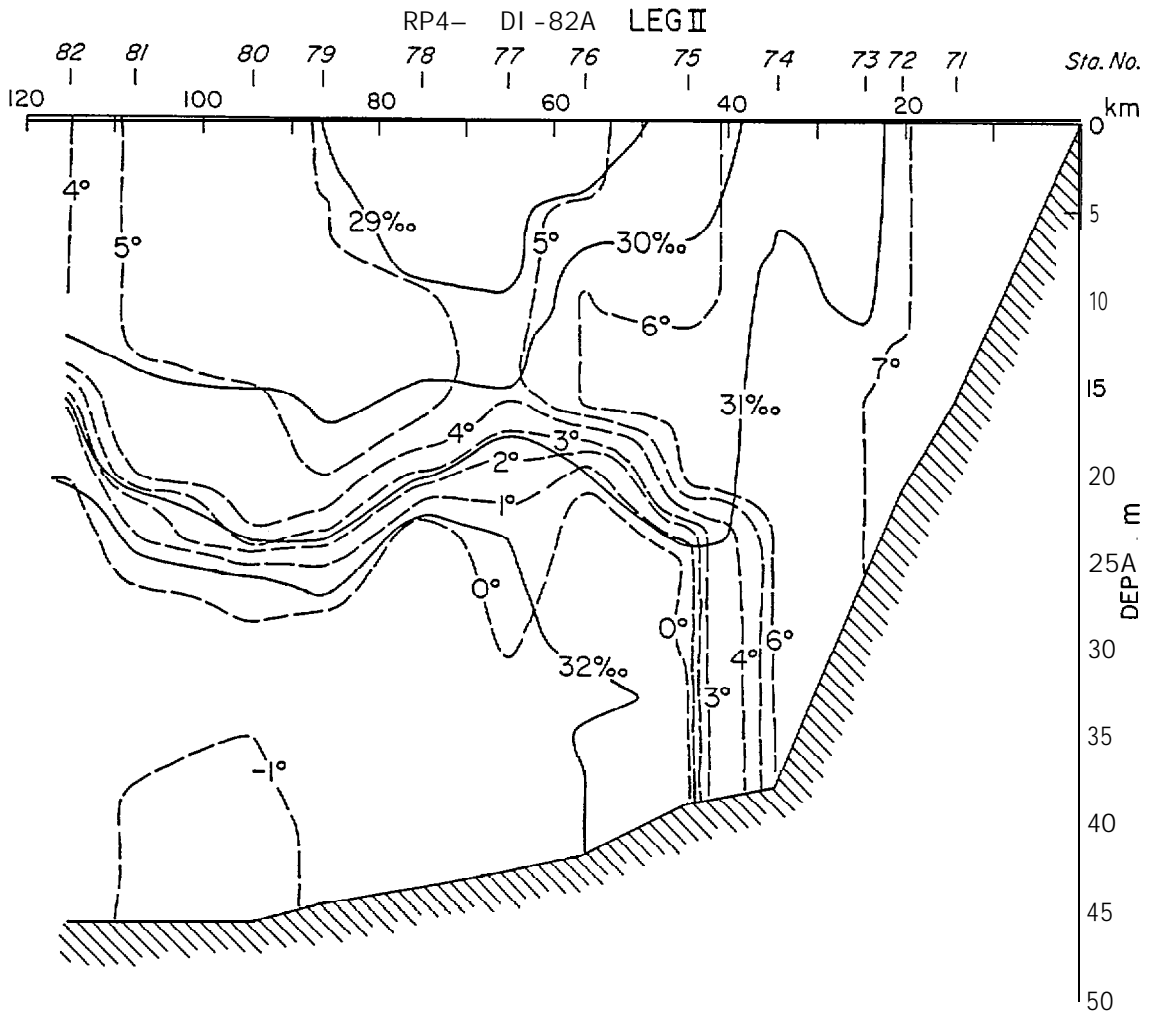


Figure 19. Icy Cape section

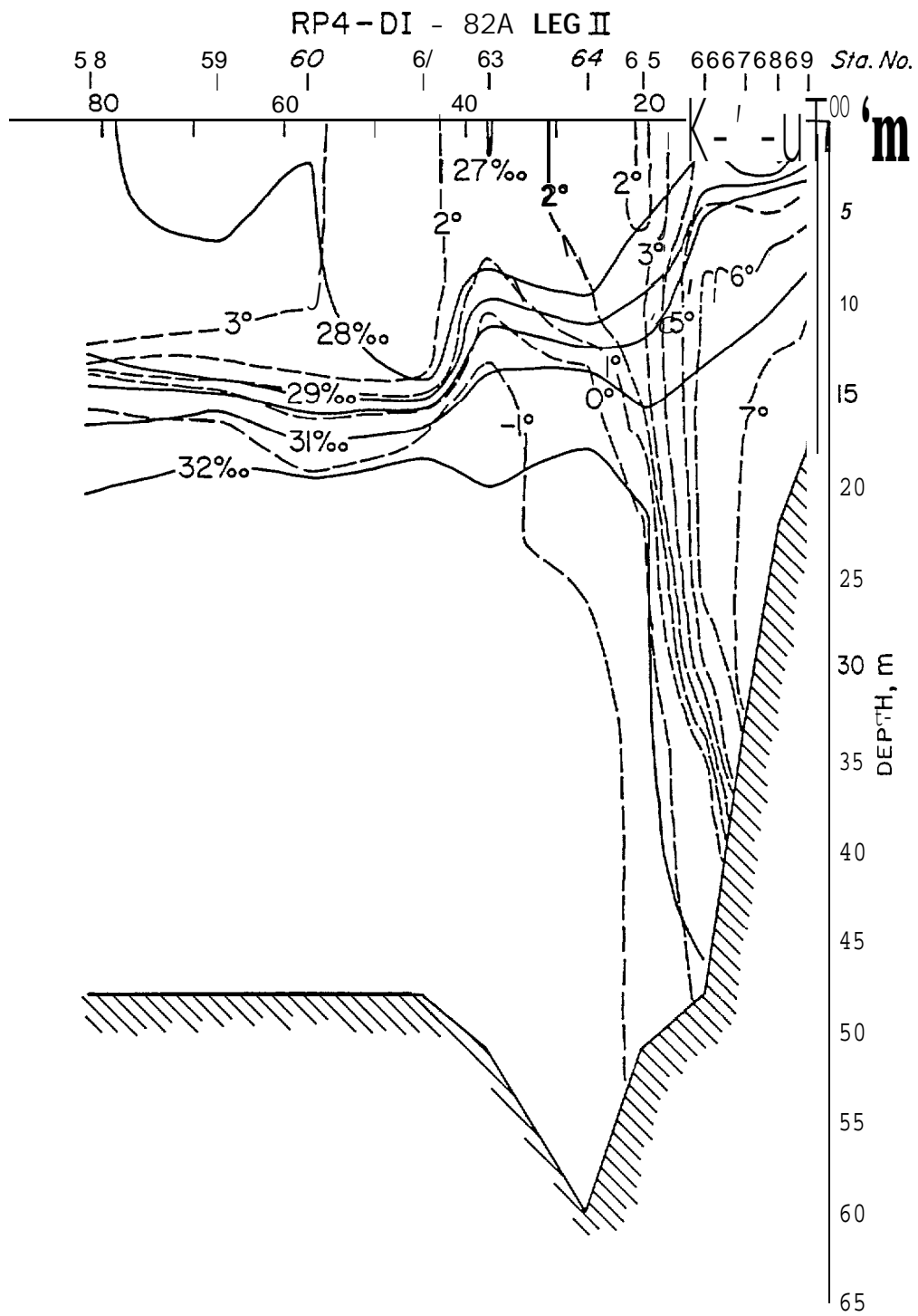


Figure 20. Wainwright section

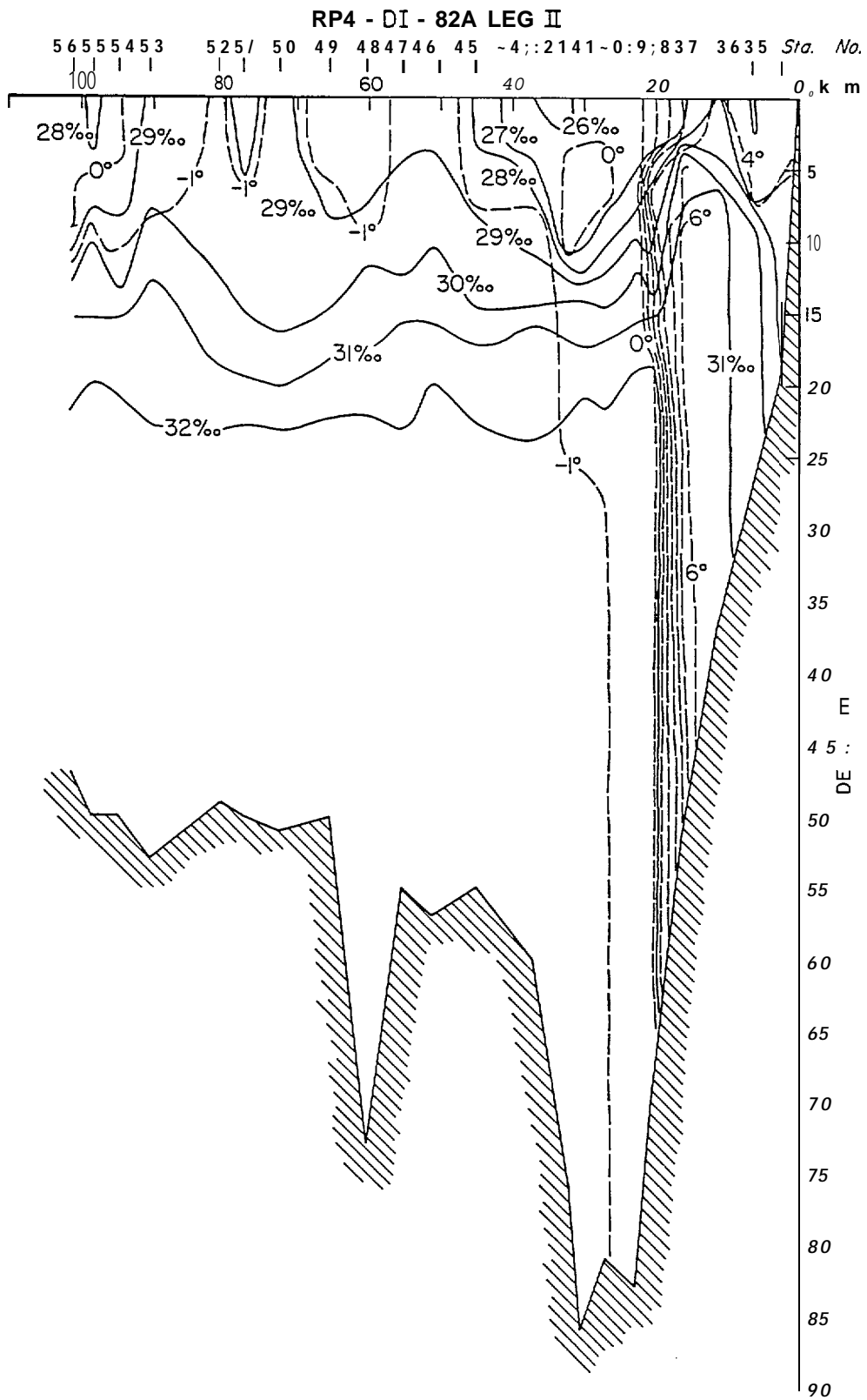


Figure 21. Pt. Franklin section

detailed discussion). However, recently it has also become clear that the flow is highly variable and can undergo **long** periods of reversal, with southward flow exceeding 50 cm sec<sup>-1</sup> having been observed west of Cape **Lisburne** (Coachman and Aagaard, 1981).

The second objective has been to determine the magnitude and extent of the density-driven flow associated with brine rejection from growing sea ice. Recent work by Aagaard, Coachman and **Carmack** (1981) has shown that the formation of dense water by this mechanism preferentially occurs along coasts with offshore winds, such as is frequently the case in the eastern **Chukchi** Sea during winter. Furthermore, it is likely that the principal density structure of the Arctic Ocean itself is to a large extent maintained by this process. The capability of the brine-induced density field to alter the local circulation has been shown for **the** northern Bering Sea by Schumacher, Aagaard, Pease and **Tripp** (1983).

### *The summer hydrography*

The locations of the summer CTD sections in 1981-82 are shown in Figs. 1-3 and the sections themselves in Figs. 4-21. Cruise **OC-81A**, Leg I, was conducted during 4-12 September 1981; **OC-81A**, Leg II, during 14-19 September 1981; and **DI-82A** during 16-27 August 1982.

A cursory examination of the sections shows enormous spatial and temporal variability. However, if we invoke the water mass classification of CAT, the hydrography becomes remarkably systematic. The two principal classifications of interest in these sections prove to be Alaskan coastal water (ACW) and resident **Chukchi** Sea water (RCW). The former is the low-salinity fraction of the inflow from the Bering Sea, supplemented by effluent from Kotzebue Sound. The ACW is relatively **warm** and has a broad

range of salinity, but **with** a rather sharply defined upper limit which can vary **interannually**, but **is** typically **32.1-32.5‰**. The RCW represents water remaining on the shelf from the **previous** winter **and/or** incursions from the upper Arctic Ocean. **This** water is quite cold and normally of salinity equal to or greater than ACW. None of these sections show any of the more saline Bering Sea water mass described by CAT, as they did not extend sufficiently far west. Many of the northern sections exhibit the cold low-salinity influence of ice melt. We now briefly examine these sections sequentially.

In early September 1981, the **Kivalina** and Cape **Lisburne** sections (Figs. 4-5) showed **only** ACW, with the warm low-salinity wedge near the coast probably containing a contribution from Kotzebue Sound. In interpreting the **Kivalina** section, note that the central part of the section, directed approximately along **isobaths**, is probably not normal to the **flow**. The **likely** flow pattern associated with this temperature and salinity distribution is probably northward in the vicinity of stations 2 and 3, i.e., on the west flank of the Cape Prince of Wales Shoal extension, southward on the east flank near stations 6 and 7, and then northward closer to the coast. That is, the section cuts across two large loops in the flow as the latter attempts to follow the isobaths.

In the Pt. Lay, Icy Cape, **Wainwright**, and Pt. **Franklin** sections (Figs. 6-9), no ACW is present. Instead there are only RCW, **mixtures** between it and ACW, and **ice-melt** and its mixtures. The absence of ACW can only mean that its flow along the coast has been interrupted over a substantial period of time, either by being diverted offshore (most probably in the Cape **Lisburne** divergence, cf. CAT) or by a **prolonged** general flow reversal in the eastern Chukchi. The steeply sloping **isopleths** near the coast over

upper Barrow Canyon (Figs. 8 and 9) must be a geostrophic adjustment of the RCW flowing rapidly northeastward along the coast, i.e., being flushed from the Chukchi, or conceivably being recirculated.

The northeasternmost section (Fig. 10) resembles the previous four, except that farthest offshore there is a clear subsurface core of ACW, centered near 20 m and overlaid by ice melt. This is almost surely a remnant of earlier flow of ACW along the coast, since no ACW is seen in the upstream four sections, even as far seaward as station 47.

The sections taken about a week later (Figs. 11-13) show substantially similar conditions, with only ACW in the Cape Lisburne section, whereas RCW, ice melt, and various mixtures occur in the downstream sections. While the water mass distribution thus remained the same over this time interval, the details of the temperature and salinity distributions were substantially different. In particular, the later sections were more saline and the two southernmost also colder. The differences are large, e.g., more than 2°C between the two occupations of the Cape Lisburne section. These differences illustrate the variability within each water mass. Note also that the repetition of the Wainwright section suggests the baroclinic coastal jet to have weakened (contrast Figs. 8 and 13).

The following year was substantially different in that ACW was observed in all the sections, rather than being restricted to the southern Chukchi. As during the previous year, the Kivalina and Cape Lisburne sections (Figs. 14-17) contained only ACW, but were overall somewhat warmer than during 1981. Note that the Kivalina section again suggests having transected a clockwise loop in the flow around the Cape Prince of Wales Shoal extension. The Pt. Lay section (Fig. 18) also contained only ACW, in marked contrast to the previous year (Figs. 6 and 12). Furthermore, the

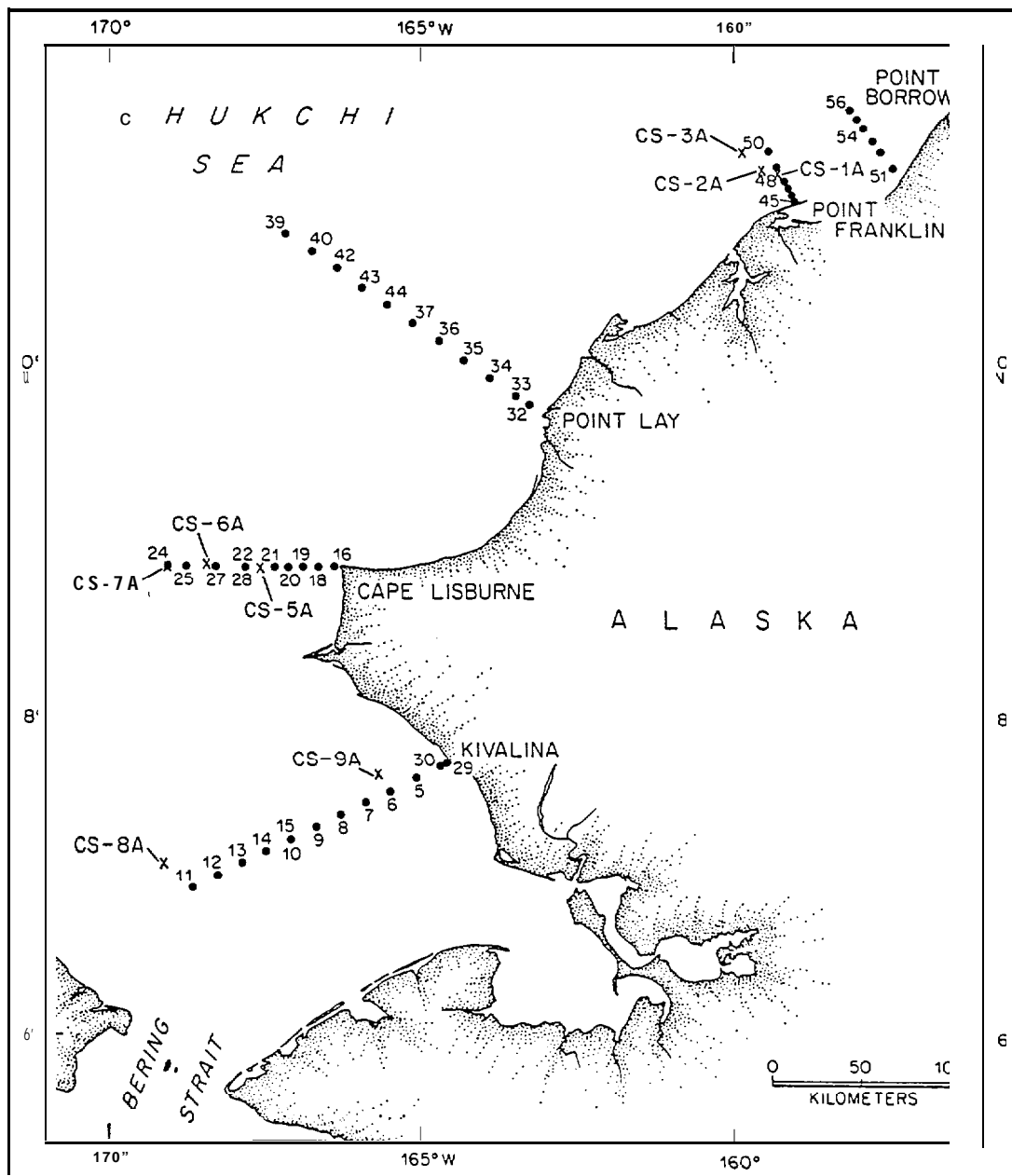


Figure 22. Station positions, 18 February - 14 March 1982, and 1981-82 mooring locations

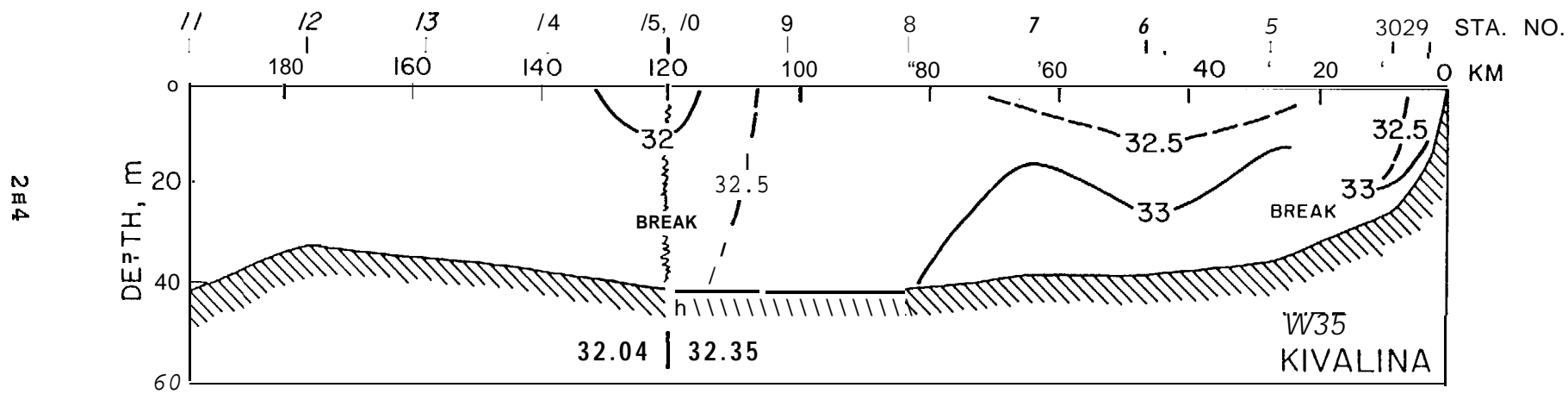


Figure 23. Kivalina section

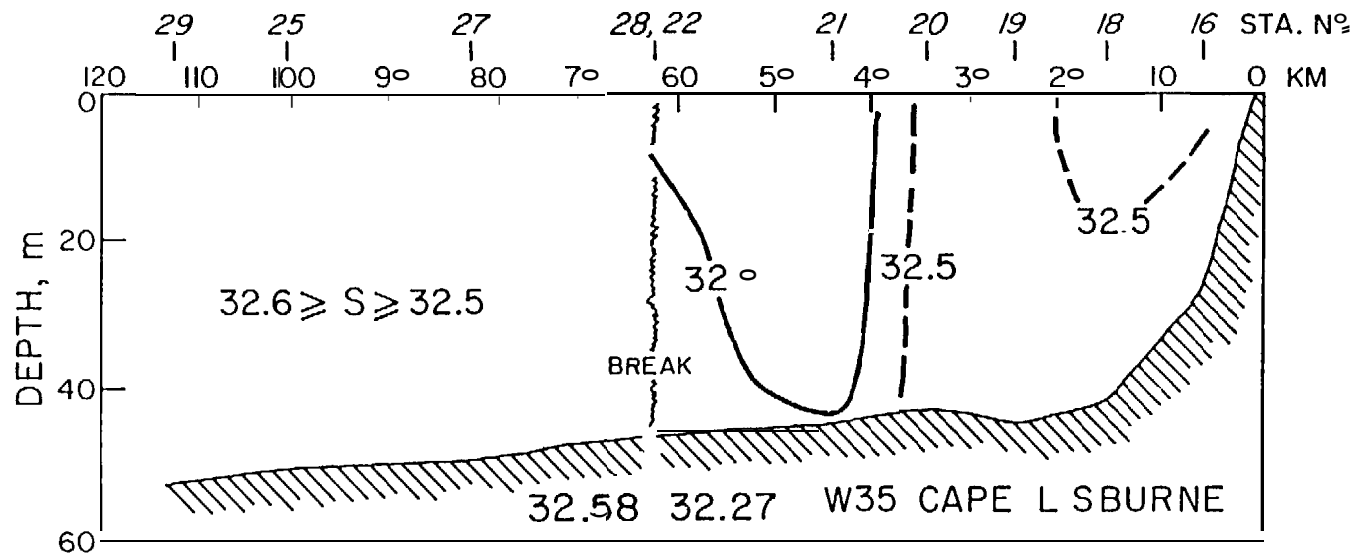


Figure 2c. Cape Lisburne section

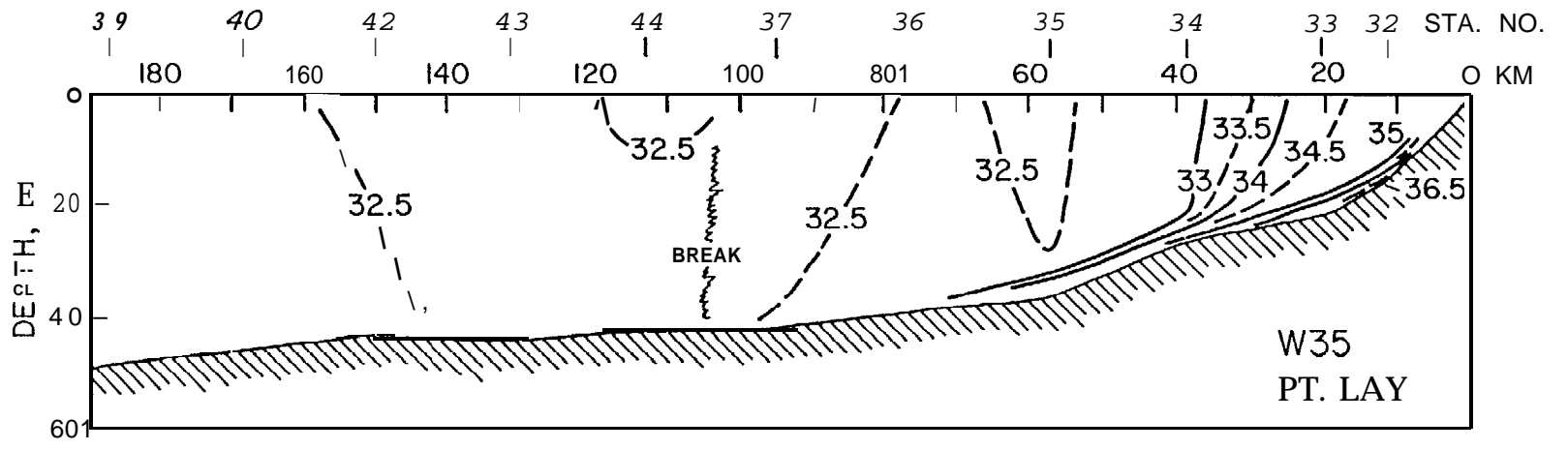


Figure 25. Pt. Lay section

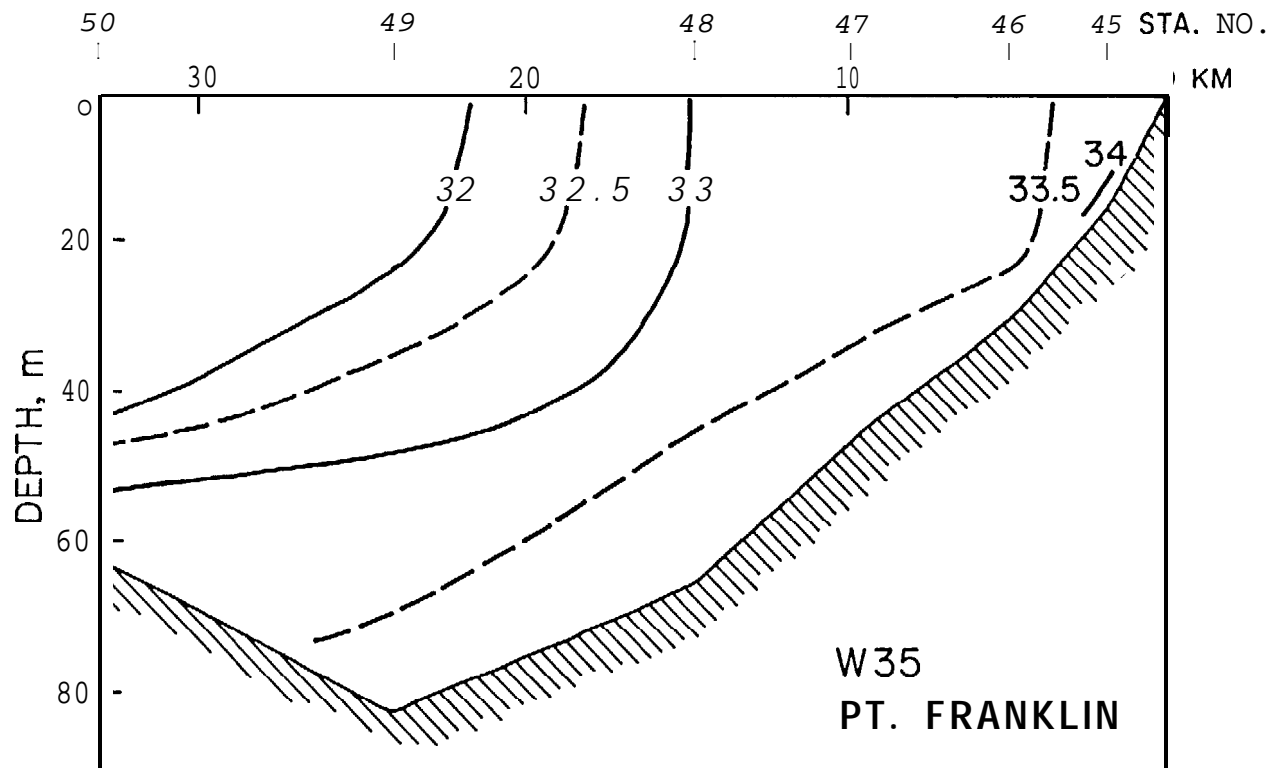


Figure 26. Pt. Franklin section

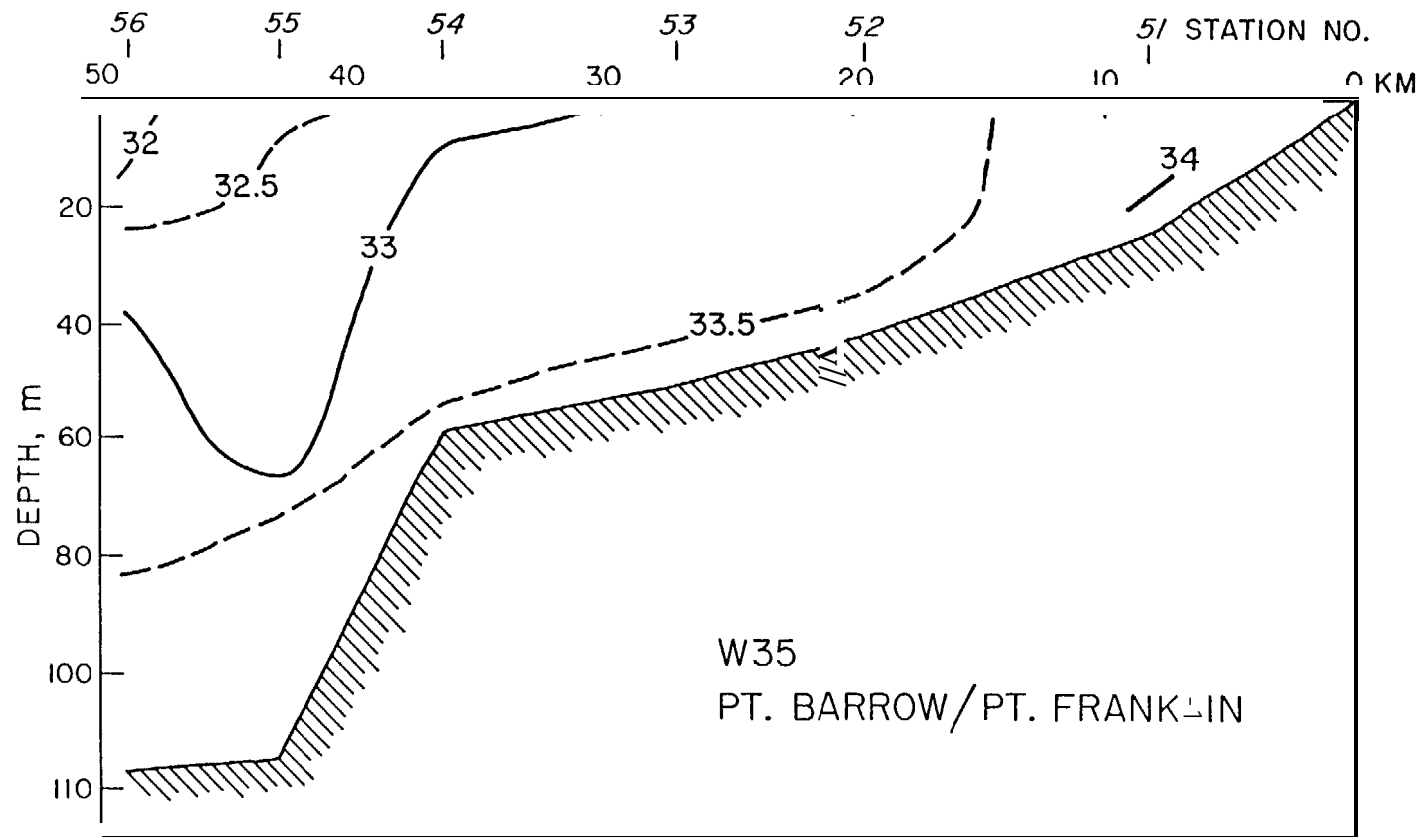


Figure 27. Pt. Barrow/Pt. Franklin section

isotherms near the coast in Fig. 18 are nearly horizontal, suggesting a relaxation of the coastal jet at the time of the section.

In the three northernmost sections, RCW is present, and in the Wainwright and Pt. Franklin sections (Figs. 20-21), also ice melt. The absence of ice melt in the Icy Cape section is a major change from conditions the previous year (contrast Figs. 7 and 19). Perhaps most remarkable in these sections are the nearly vertical isopleths near the coast, forming an exceptionally large horizontal gradient. In Fig. 21 the subsurface front spans 6°C in 5 km. The corresponding maximum geostrophic shear, centered between stations 38 and 39, is 68 cm sec<sup>-1</sup> between 15 and 50 db.

Overall, it is clear that during the 1982 observations, the Pacific influence in the Chukchi was far more extensive than it had been during the previous year's cruises. However, in both years the RCW, a residual shelf water from the previous winter, had been effectively flushed from the southeastern Chukchi at least as far as Cape Lisburne.

#### *The winter hydrography*

The Locations of the five winter CTD sections, taken during 18 February - 14 March 1982, are shown in Fig. 22, together with the sites of moored measurements to be discussed later. The CTD sections themselves are shown in Figs. 23-27. Only the salinity is given, since the temperature was uniformly within 0.01-0.02°C of the freezing point. The data were taken with a Neil Brown CTD system in which the sensor package had been modified for deployment through a hole augered in the ice.

The Kivalina section (Fig. 23) principally shows winter shelf water with properties essentially those of RCW, with salinity centered around

32.5 ‰. However, near the coast the salinity increases to more than 33‰, and the steeply sloping **isohalines** suggest a narrow coastal jet of dense water (as opposed to a buoyant coastal jet in summer). The **geostrophic** shear for 2/16 db between stations 29-30 is  $6.2 \text{ cm sec}^{-1}$ , or  $0.44 \text{ cm sec}^{-1} \text{ m}^{-1}$ . Whether this saline water primarily is formed locally or is advected from a formation site farther south, e.g., in northern Norton Sound, is not clear. However, the ice near the coast at the time of the section was so thin as to make helicopter landings nearly impossible. This suggests that rapid freezing was going on, and that the salinity was at least being augmented locally. In any case, the evidence for a **density-driven** coastal jet is **clear**.

The Cape **Lisburne** section (Fig. 24) contains only **RCW**. This in turn suggests the **saline jet** to be of an intermittent nature, and Schumacher, **Aagaard**, Pease and Tripp (1983) have in fact argued that the intermittence is determined by the forcing at synoptic meteorological time scales (a few days) .

The Pt. Lay section (Fig. 25) is truly remarkable in the magnitude of the salinity anomaly near the coast, about 4‰ above the ambient water. Water this saline has earlier been seen only in isolated shallow lagoons, and the observations show the efficacy of the salt-enhancement provided by the Ekman divergence along the coast. Note further that the dense water is seen to extend nearly 80 km seaward in a 5-10 m thick **layer** near the bottom. This probably represents offshore flow within a frictional **bottom** boundary layer in which the rotational constraint no longer is able to trap the flow near the coast. The **baroclinic** deformation radius is about 7 km, which should be the **scale** width of the jet outside the frictional domain. There is in fact some suggestion in Fig. 25 that the most densely packed

**isohalines** (inshore of station 32) might be contained within such a distance of the coast. The mean **geostrophic** shear inshore of station 34 is  $0.48 \text{ cm sec}^{-1} \text{ m}^{-1}$ , nearly the same as in the **Kivalina** section.

The two northernmost sections, across Barrow Canyon (Figs. 26-27), are quite similar. Both show moderately high salinity, with the densest water contained in a narrow band along the coast. Thus, while the sections clearly suggest brine enrichment effects, they do not represent extreme conditions (contrast Fig. 25). On the other hand, the deeper shear on the eastern side of the canyon is not much **lower** than in the **Kivalina** and Pt. Lay sections, *viz.*  $0.38 \text{ cm sec}^{-1} \text{ m}^{-1}$ .

#### *The current measurements*

We **turn** now to the direct measurement of currents. The mooring positions are shown in Fig. 22 and pertinent details of the 11 current meters are given in **Table 1**. (Mooring **CS-8A** provides only a pressure record, and is therefore ignored in this **analysis**.) Moorings **CS-1A - CS-3A** represent a cross-section of Barrow Canyon, with **CS-1A** located on the lower part of the coastal flank of the canyon, **CS-2A** near the canyon axis, and **CS-3A** on the offshore flank. The remaining moorings were all on relatively featureless portions of the shelf with depths between 42-52 m.

Table 2 summarizes the overall statistics of the current records. The variances in Table 2 are based on low-passed data (35 hr cutoff) and thus represent the variability at **subtidal** frequencies. Note **in Table 2** the extremely high proportion of the variance contained in the major axis component. This is particularly true for **CS-1A** and **-2A**, where essentially **all** the variance is along the major axis, corresponding to a **strictly** reciprocating current. Essentially, the flow at these sites is constrained

Table 1. Mooring Details

Mooring	Latitude	Longitude	Sounding	Instrument depth	First record	Last record
CS-1A	71°01.1'N	159°19.0'W	60.3 m	49.8 m	10 September 1981	21 August 1982
				54.3 m	10 September 1981	21 August 1982
CS-2A	71°03.3'N	159°34.9'W	82.5 m	70.0 m	10 September 1981	2 June 1982
				76.0 m	10 September 1981	7 July 1982
CS-3A	71°10.9'N	159°54.2'W	56.7 m	46.2 m	11 September 1981	14 September 1982
				50.7 m	11 September 1981	14 September 1982
CS-5A	68°51.7'N	167°38.1'W	47.5 m	41.5 m	7 September 1981	19 August 1982
CS-6A	68°51.6'N	168°20.3'W	51.2 m	40.7 m	7 September 1981	19 August 1982
				45.2 m	7 September 1981	19 August 1982
CS-7A	68°52.5'N	168°58.2'W	52.0 m	39.5 m	7 September 1981	18 August 1982
CS-9A	67°38.2'N	165°37.4'W	42.0 m	31.5 m	6 September 1981	17 August 1982

Table 2. Current Statistics

Mooring	Instrument depth	Mean velocity	Maximum hourly mean speed	Axis of maximum variance
CS-1A	49.8 m	21.9 cm sec <sup>-1</sup> , 058°T	99.7 cm see-1	050°T, containing 96% of variance
	54.3 m	19.2, 054"	92.4	048°, 98%
CS-2A	70.0 m	15.8, 074°	109.3	059°, 99%
	76.0 m	16.5, 067°	103.1	055°, 98%
CS-3A	46.2 m	7.8, 137°	88.3	078°, 88%
	50.7 m	6.9, 134°	94.2	075°, 88%
CS-5A	41.5 m	5.0, 356°	57.0	359°, 83%
CS-6A	40.7 m	6.6, 348°	61.9	359°, 83%
	45.2 m	5.8, 338°	56.5	348°, 84%
CS-7A	39.5 m	6.5, 336°	48.4	356°, 75%
CS-9A	31.5 m	5.9, 345°	74.5	318°, 85%

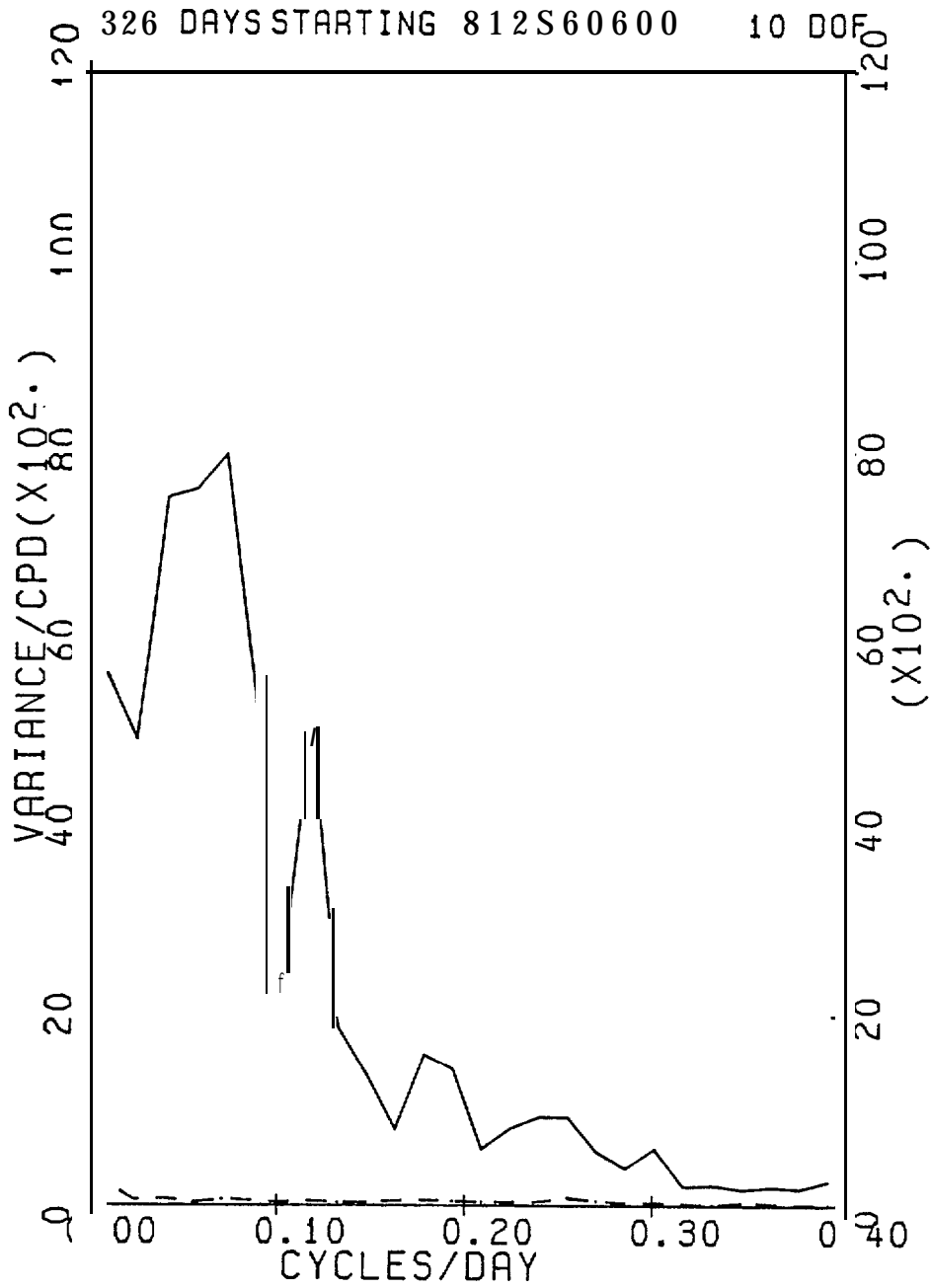


Figure 28. Power spectrum, current record CS-1A lower. Principal axis 048°T. In these spectra the principal axis component is shown by the solid line, and the minor axis component by the dashed line. Variance units are  $\text{cm}^2/\text{sec}^2$ . There are 10 degrees of freedom.

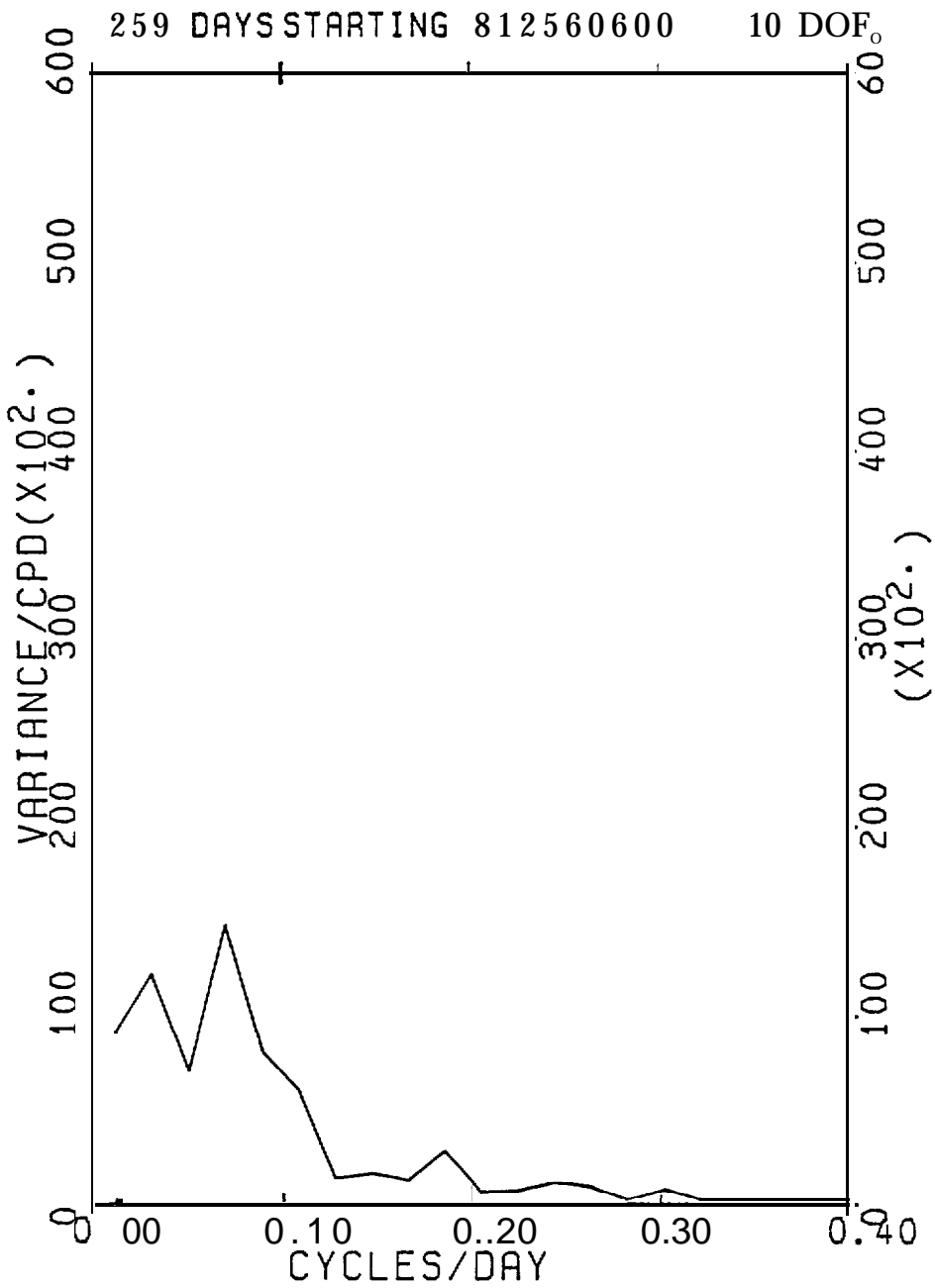


Figure 29. Power spectrum, current record CS-2A upper. Principal axis 059°T.

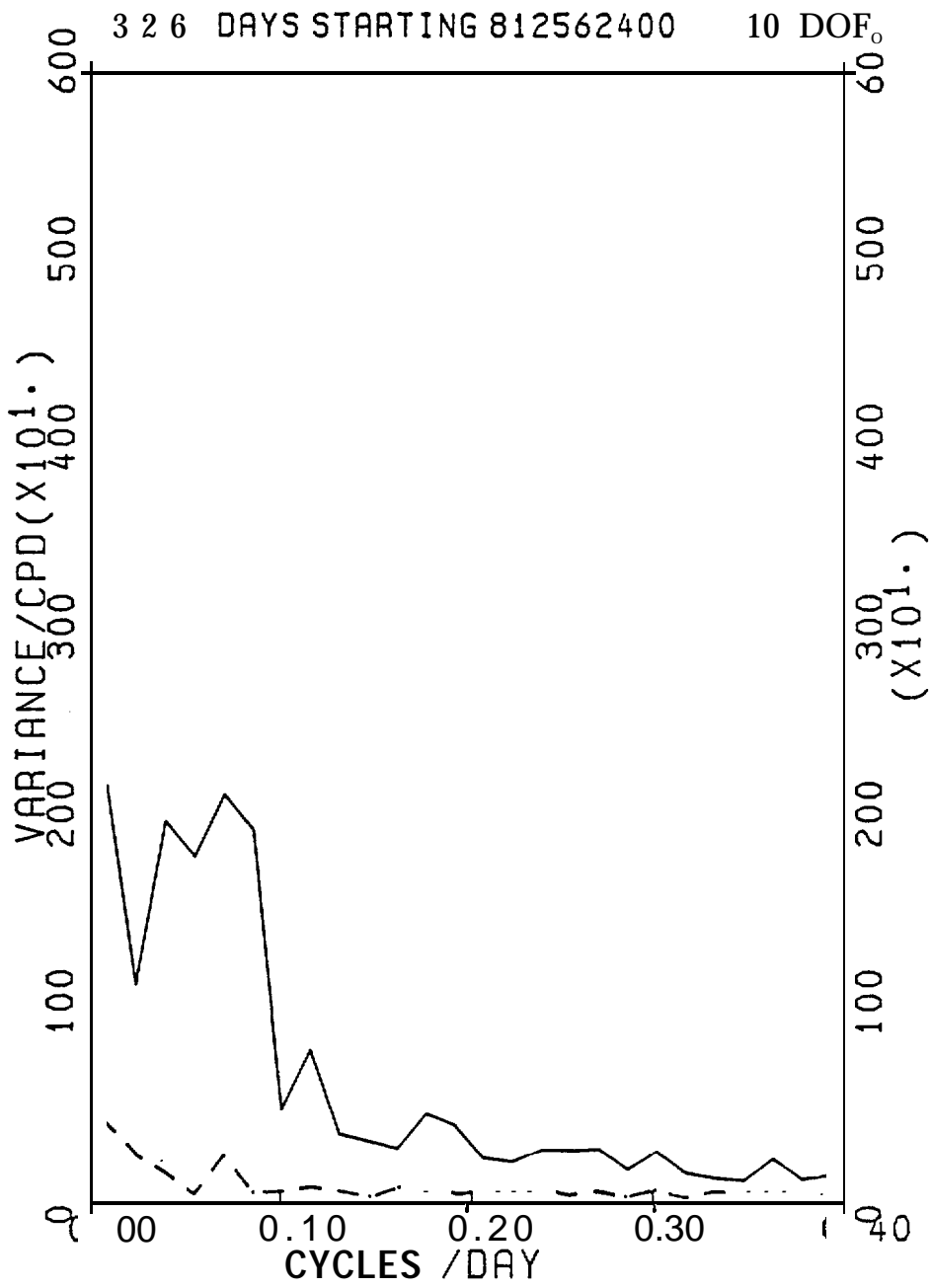


Figure 30. Power spectrum, current record CS-3A upper. Principal axis 078°T.

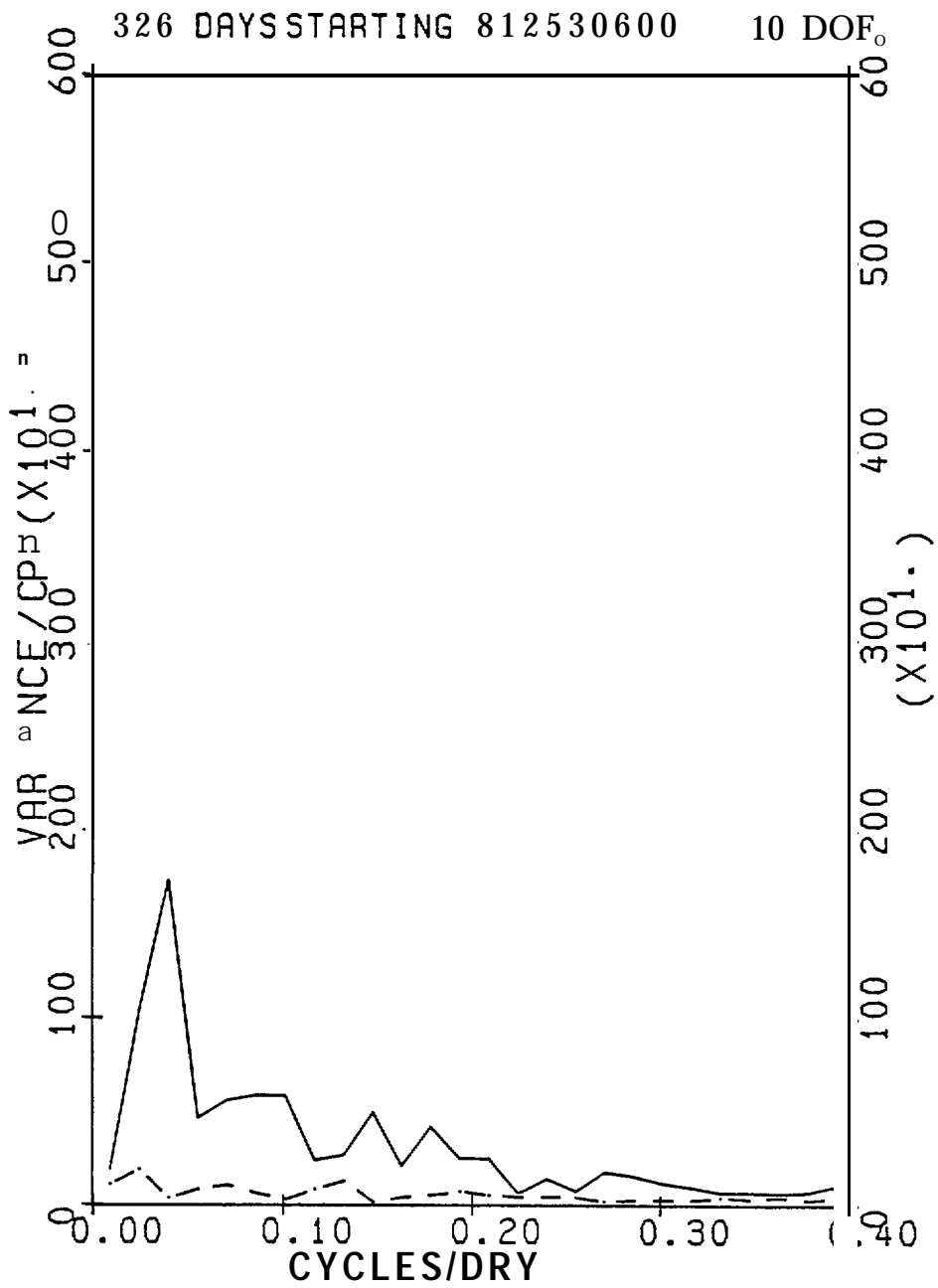


Figure 31. Power spectrum, current record CS-5A. Principal axis 359°T.

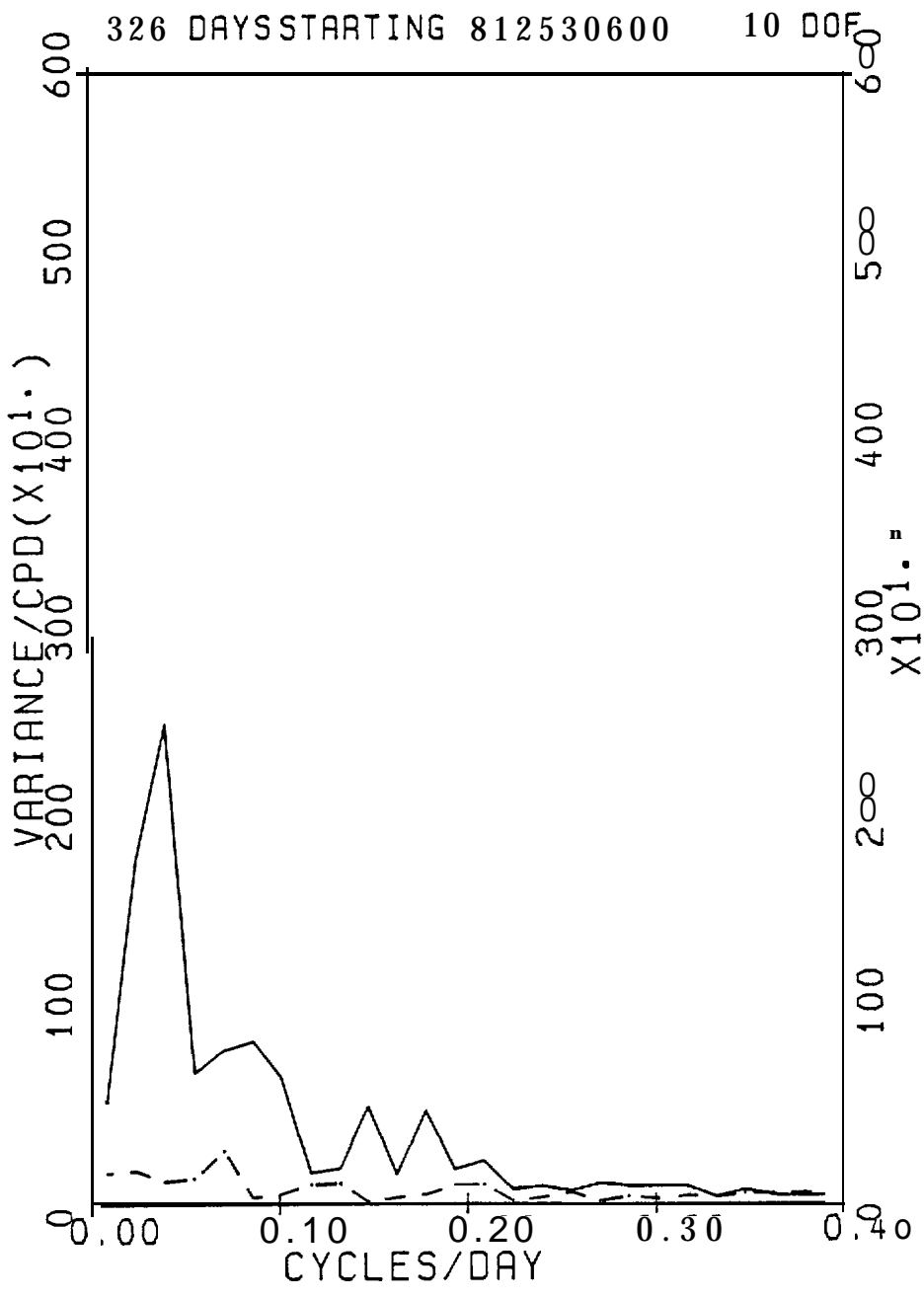


Figure 32. Power spectrum, current record CS-6A upper. Principal axis 359°T.

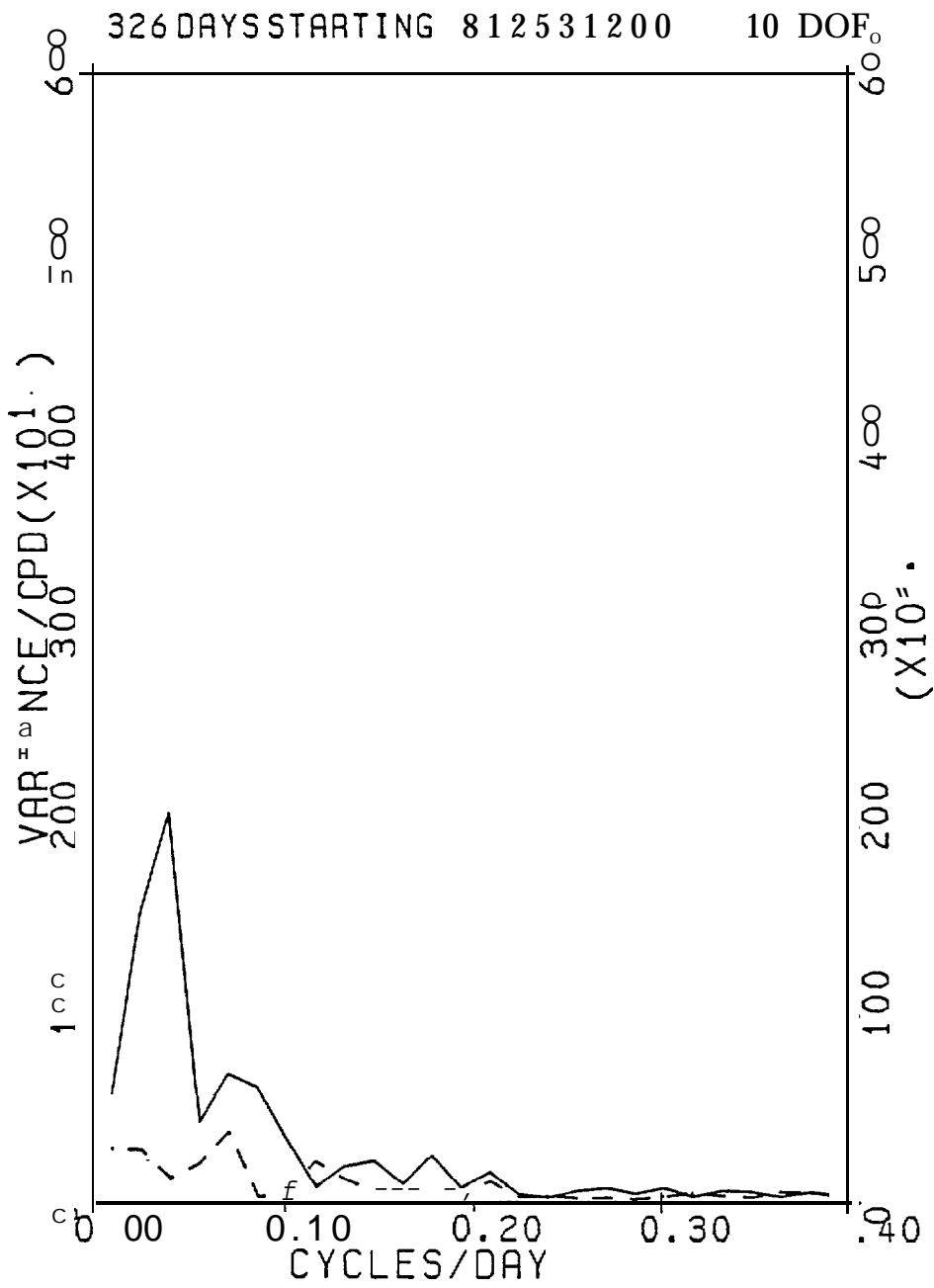


Figure 33. Power spectrum, current record CS-7A. Principal axis 356°T.

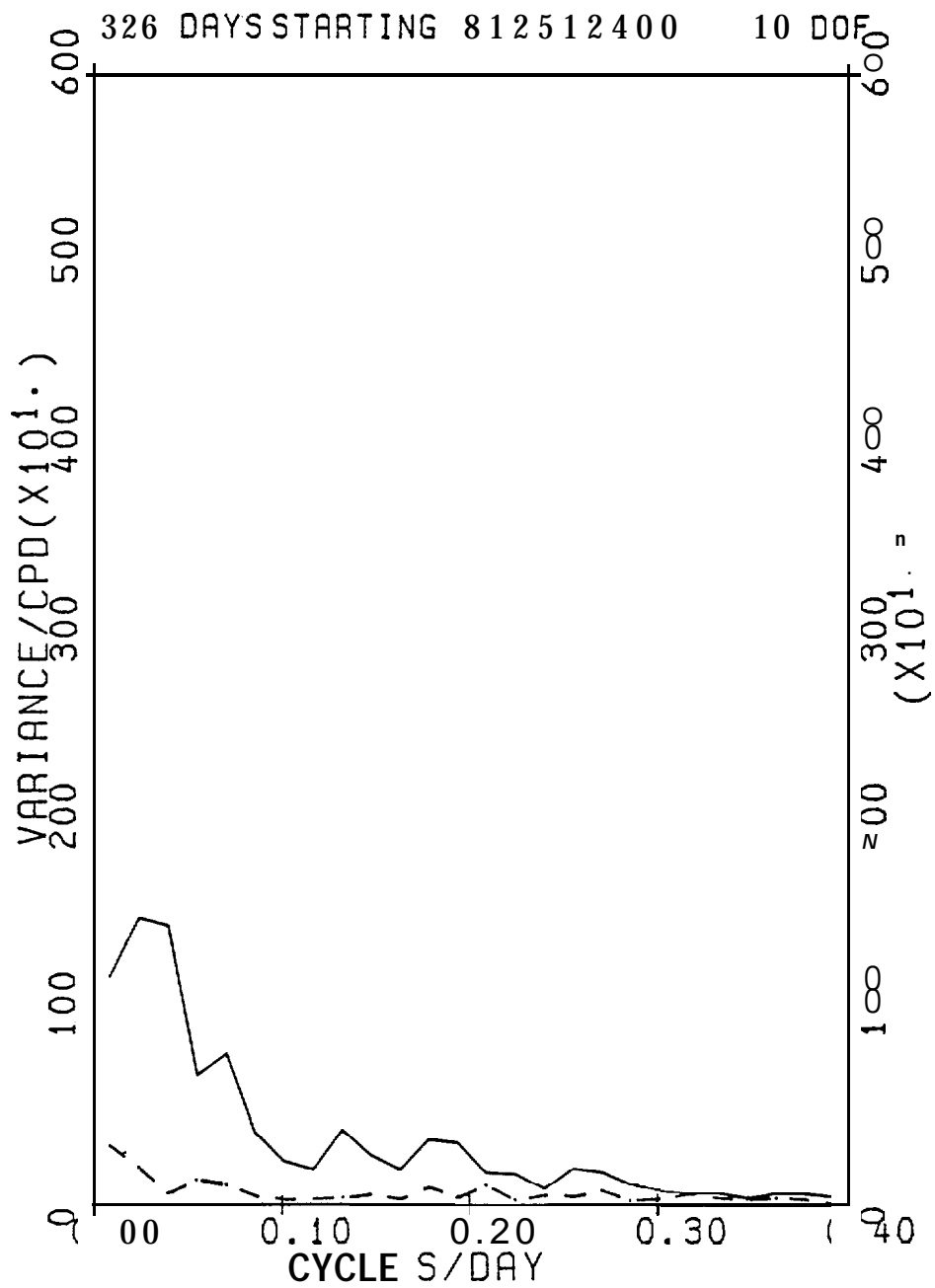


Figure 34. power spectrum, current record CS-9A. Principal axis 318°T.

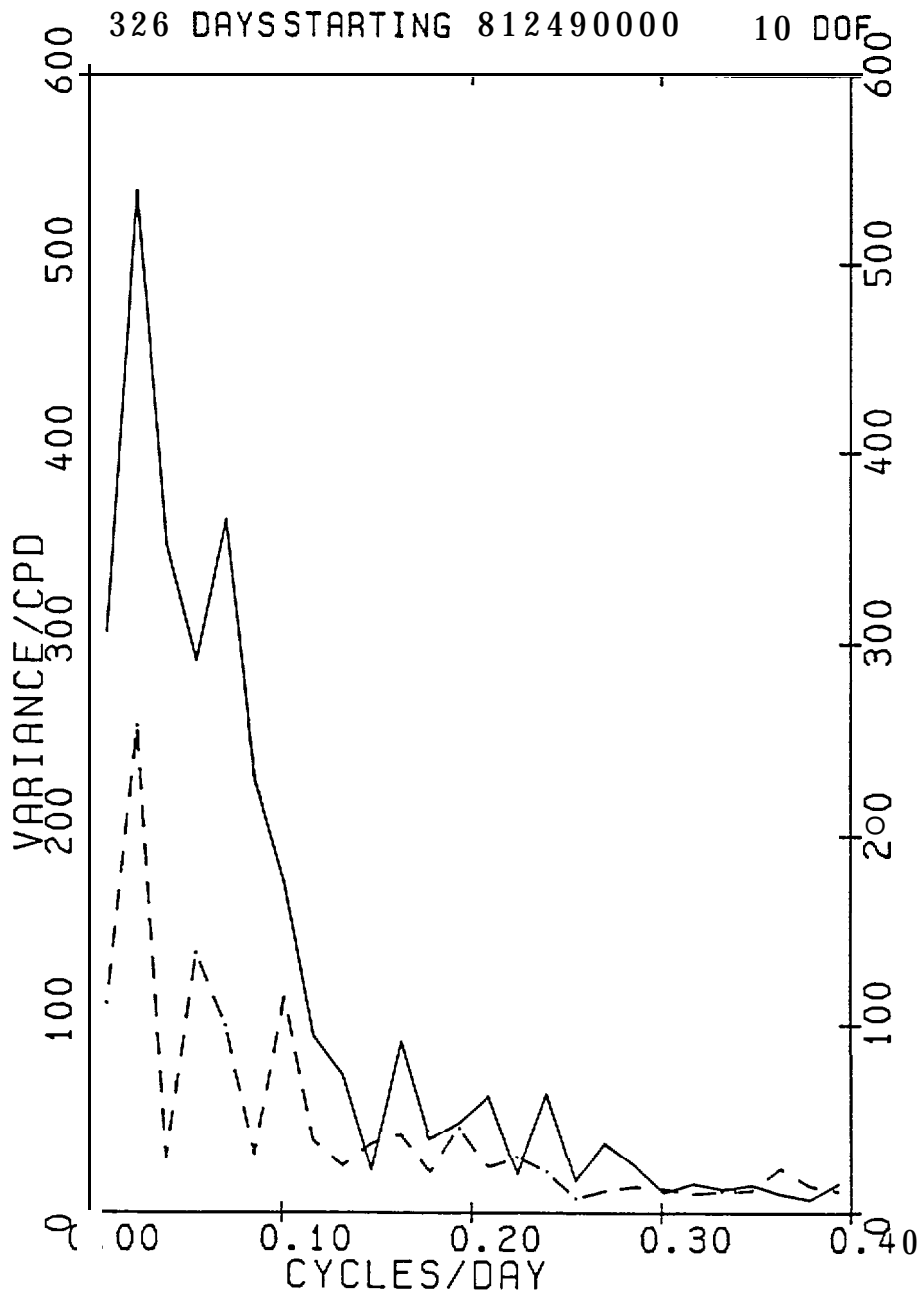


Figure 35. Power spectrum, geostrophic wind at 68°N, 166°W. Principal axis 016°T. Variance units are  $m^2 \text{ sec}^{-2}$ .

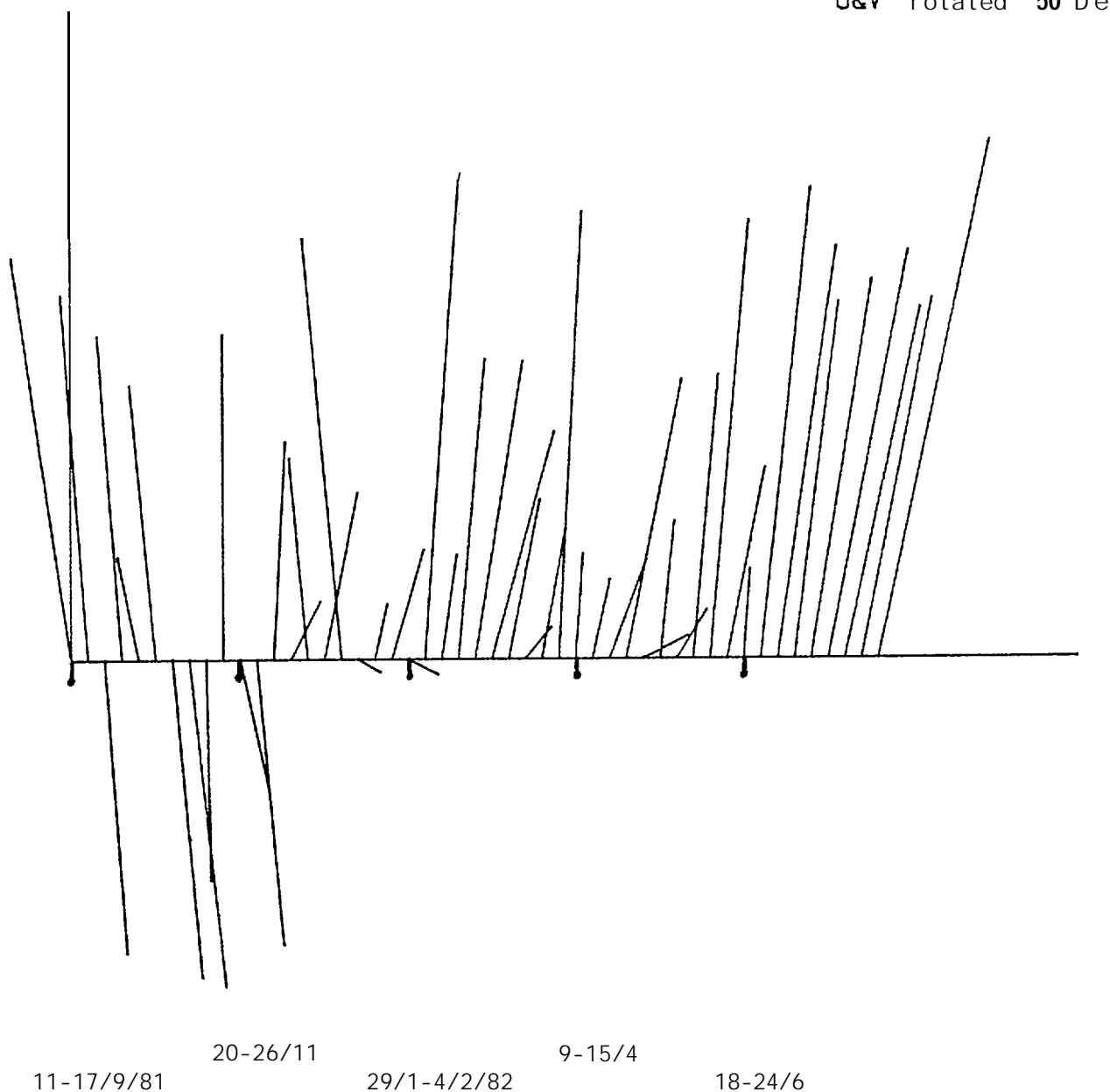


Figure 36. Weekly mean velocity, current record CS-1A upper. Principal axis (up) 050°T.

CS-1A 54. 3M 7-DAY MEAN

20 cm/sec/in  
U&V rotated 48 Deg

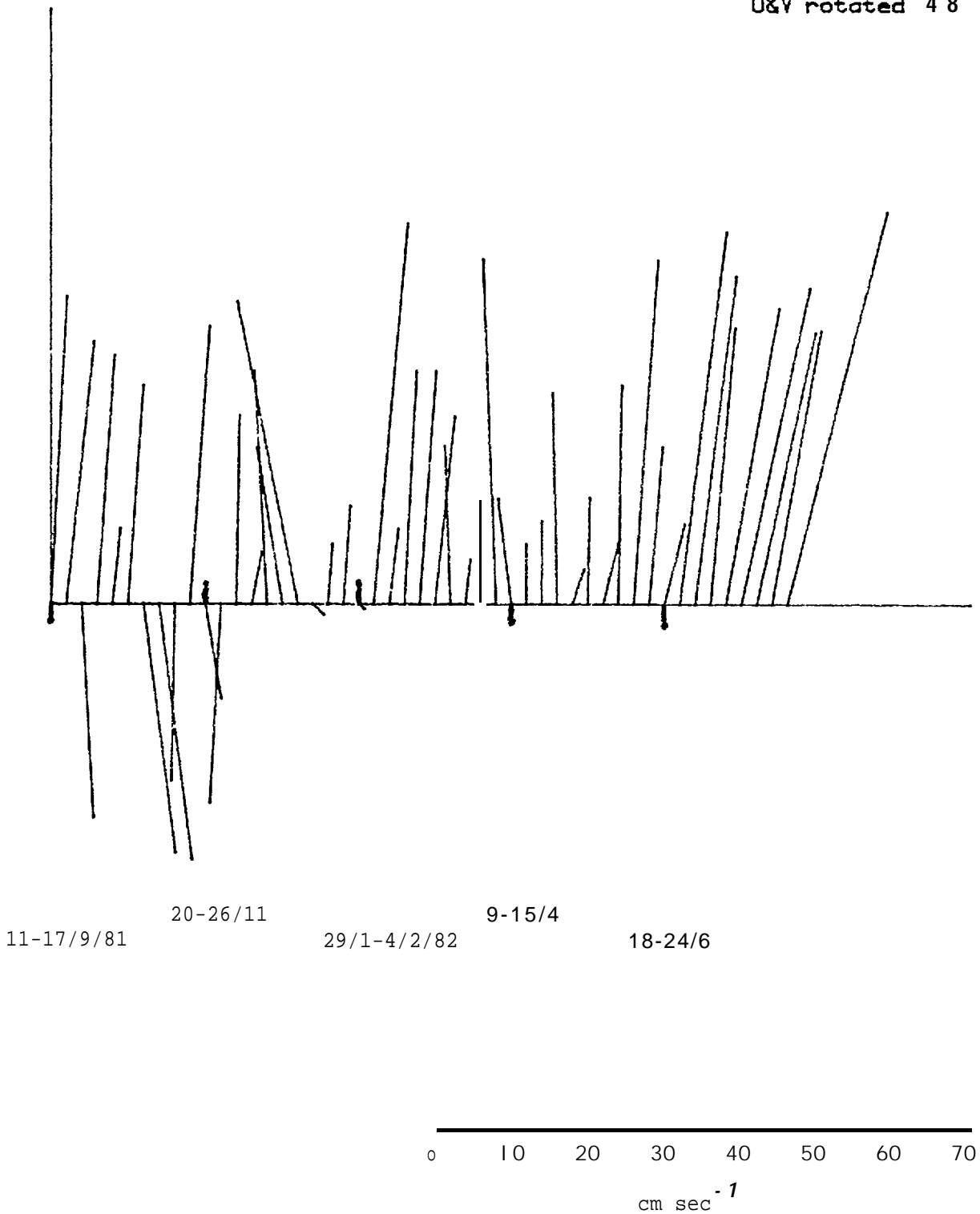


Figure 37. Weekly mean velocity, current record CS-1A lower. Principal axis 048°T.

CS-2A 70.0 7-DAY MEAN

20 cm/sec/in  
U&V rotated 59 Deg

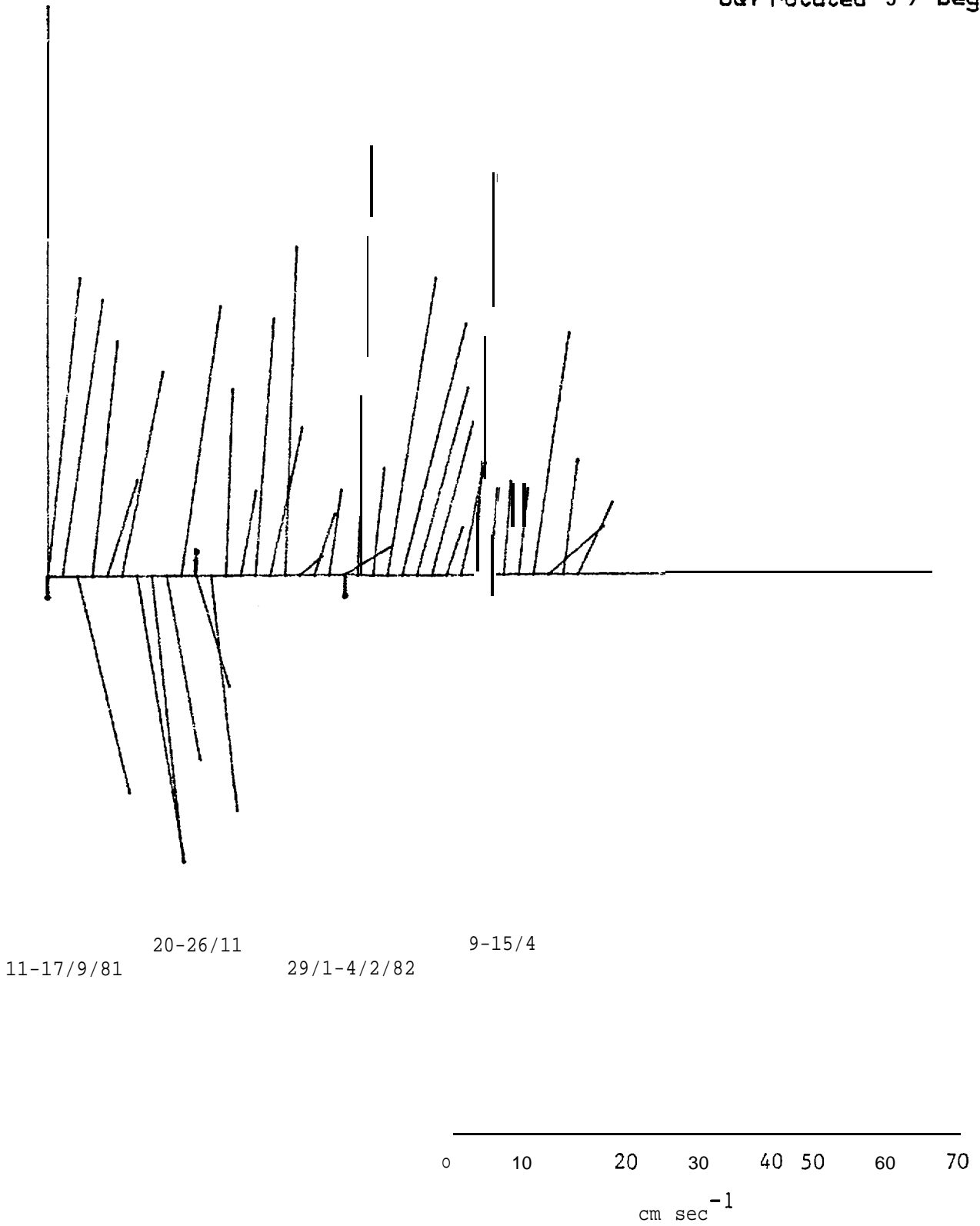


Figure 38. Weekly mean velocity, current record CS-2A upper. Principal axis 059°T.

CS-2A 76. ØM 7-DA% MEAN

20 cm/sec/in  
U&V rotated 55 Deg

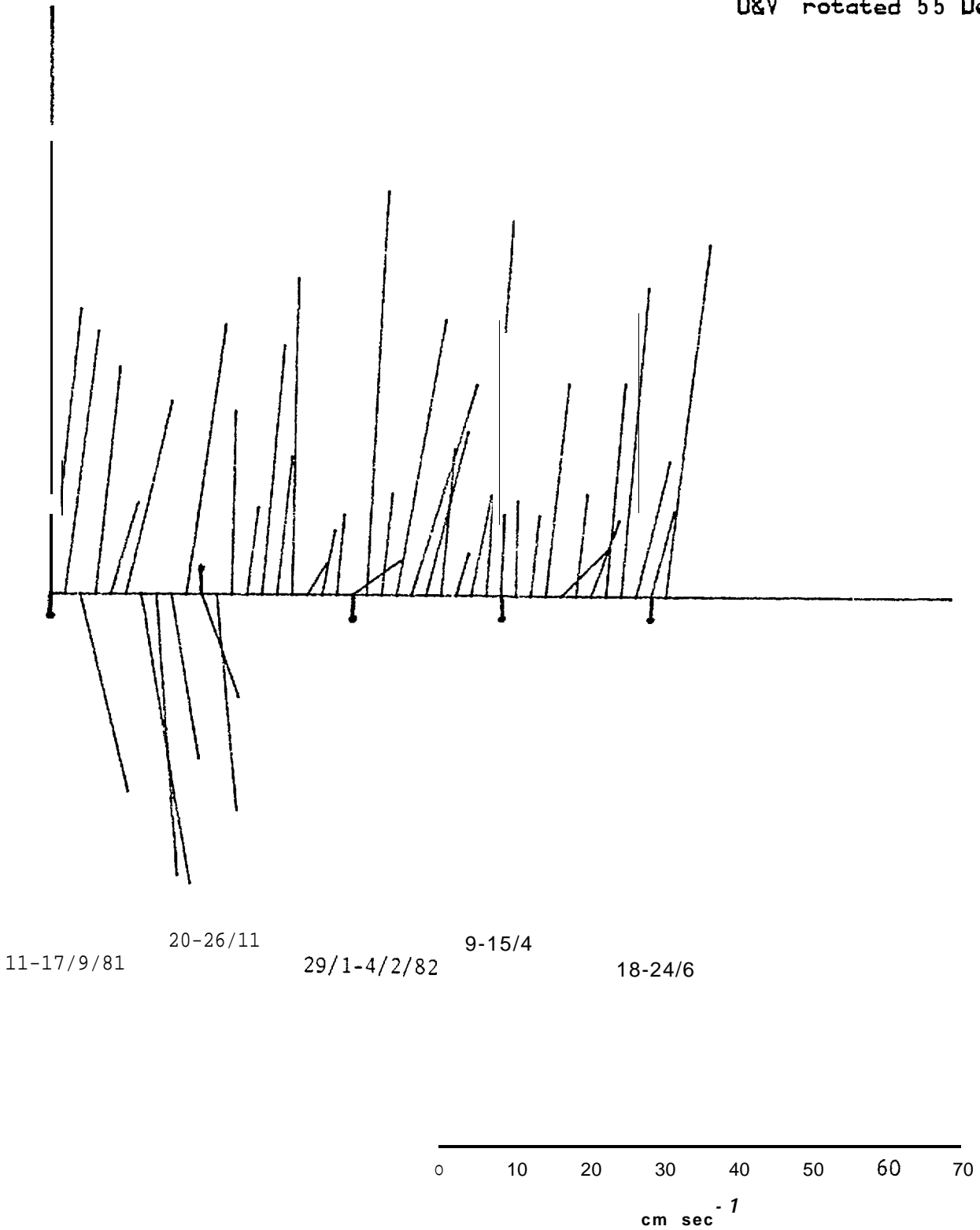


Figure 39. Weekly mean velocity, current record CS-2A lower. Principal axis 055°T.

CS-3A 46. 2M 7-DAY MEAN

20 cm/sec/in  
U&V rotated 78 Deg

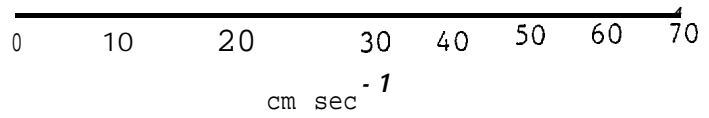
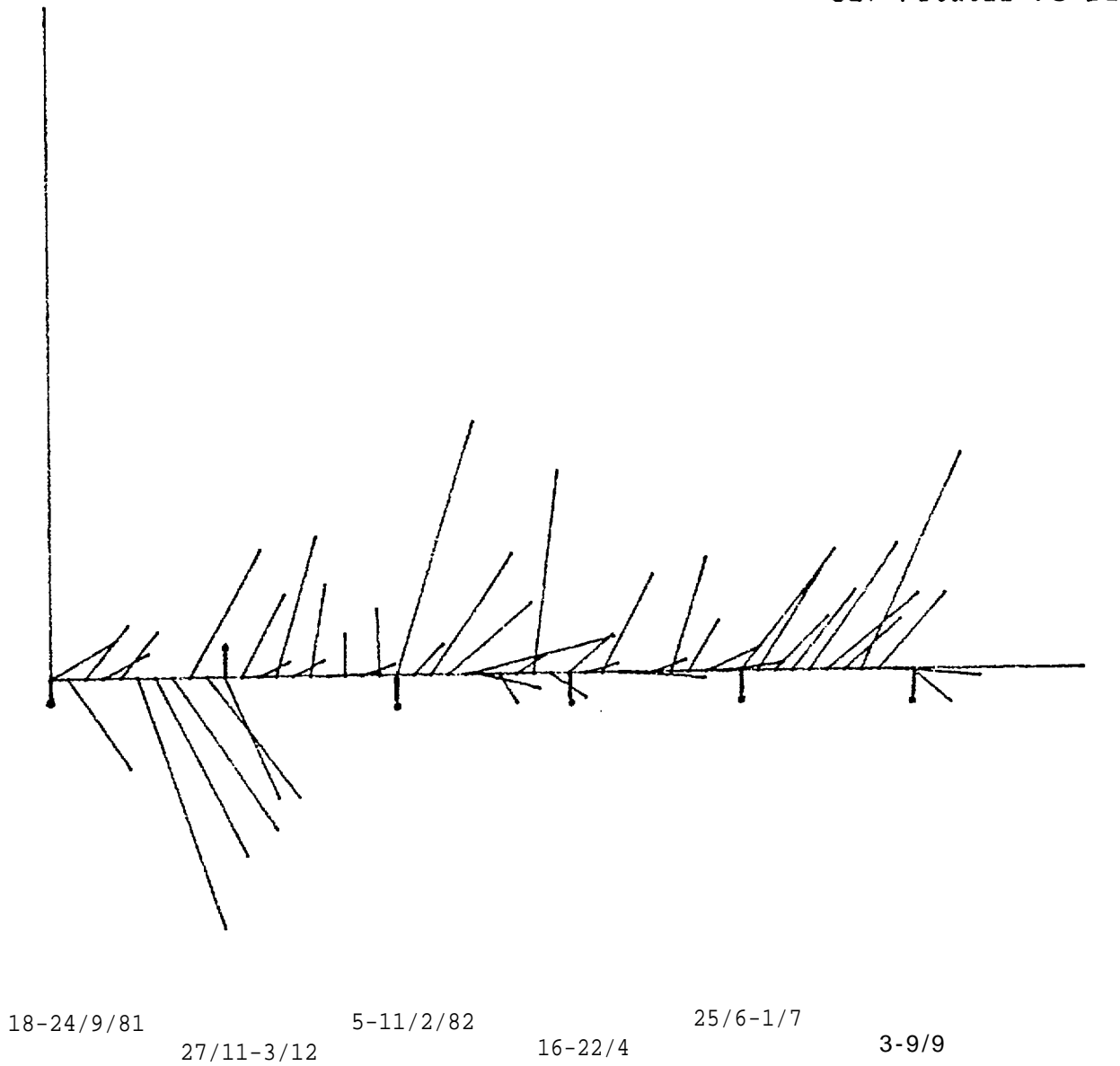


Figure 40. Weekly mean velocity, current record CS-3A upper. Principal axis 078°T.

CS-3A 50. 7M 7-DAY MEAN

20 cm/sec/in  
U&V rotated 75 Deg

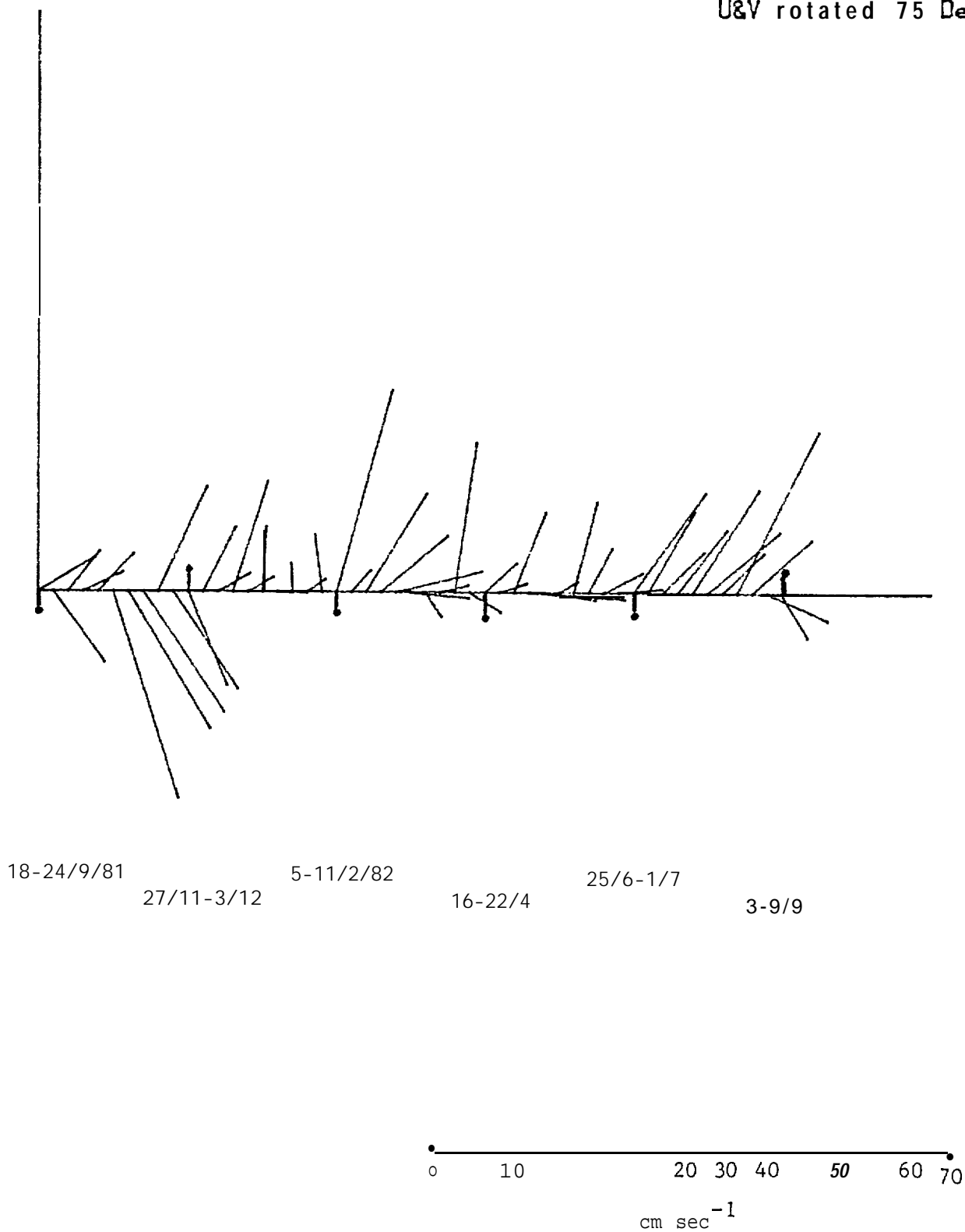


Figure 41. Weekly mean velocity, current record CS-3A lower. Principal axis 075°T.

CS-5A 41. 5M 7-DAY MEAN

20 cm/sec/in  
U&V rotated 359 Deg

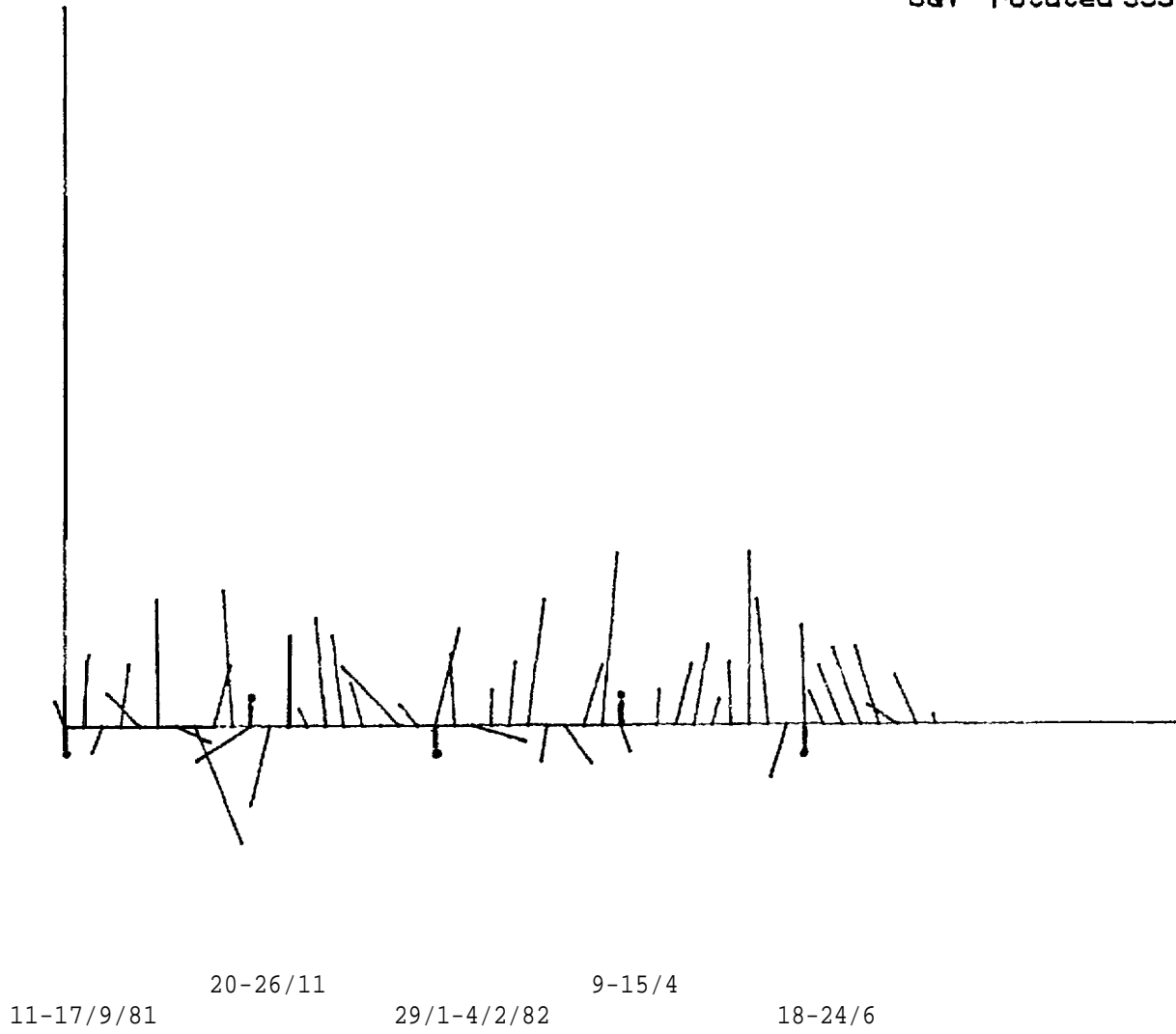


Figure 42. Weekly mean velocity, current record CS-5A. Principal axis 359°T.

CS-6A 40.7M 7-DAY MEAN

20 cm/sec/in  
U&V rotated 359 Deg

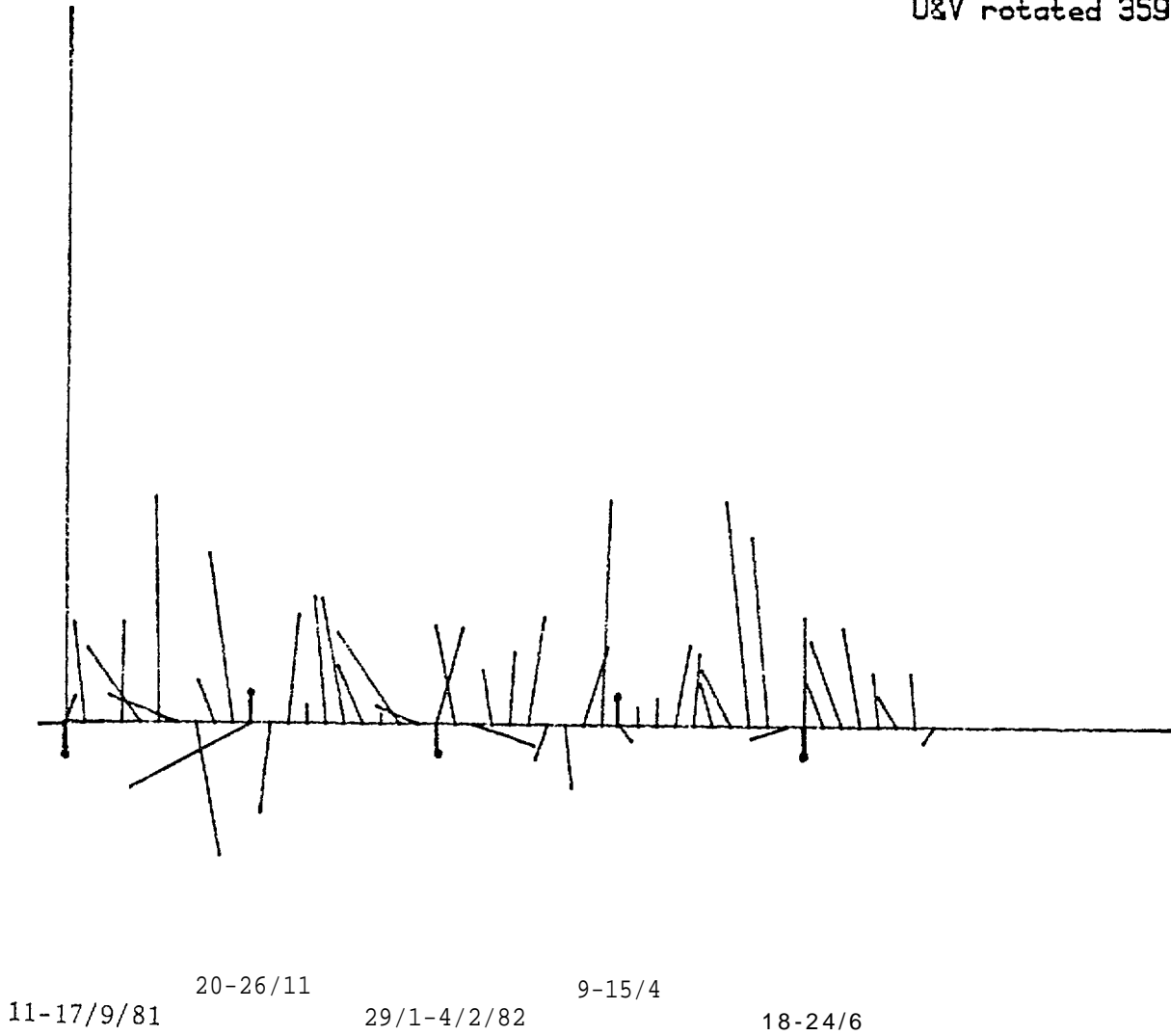


Figure 43. Weekly mean velocity current record CS-6A upper. Principal axis 359°T.

CS-6A 45.2M 7-DA% MEAN

20 cm/sec/in  
U&V rotated 348 Deg

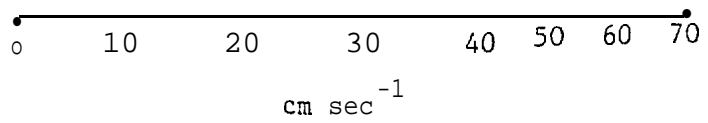
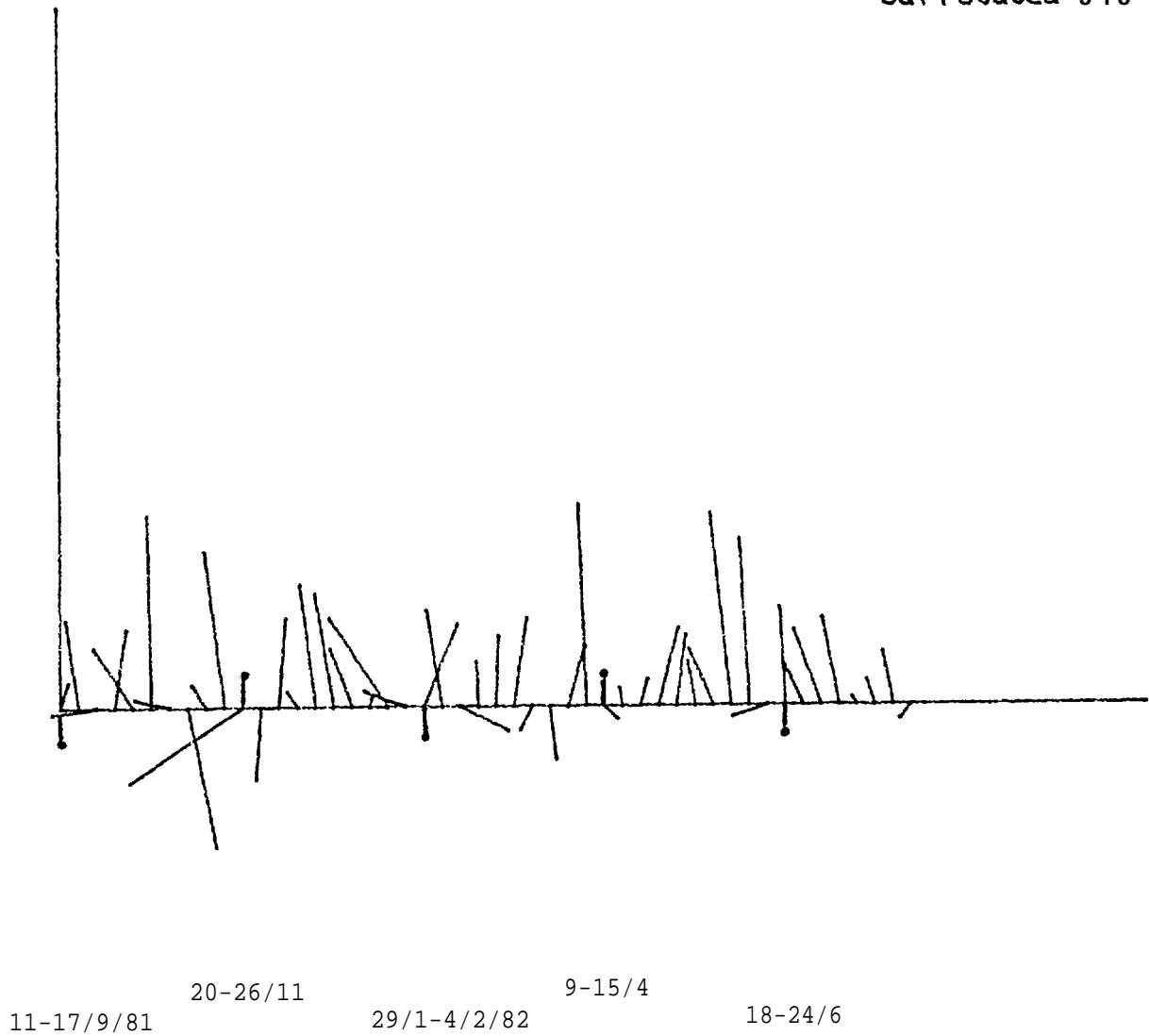


Figure 44. Weekly mean velocity, current record CS-6A lower. Principal axis 3480T.

CS-7A 39.5M 7-DAY MEAN

20 cm/sec/in  
U&V rotated 356 Deg

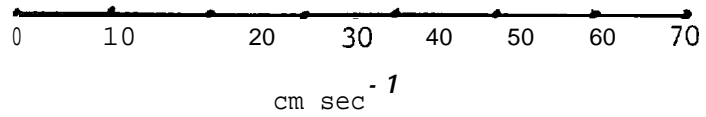
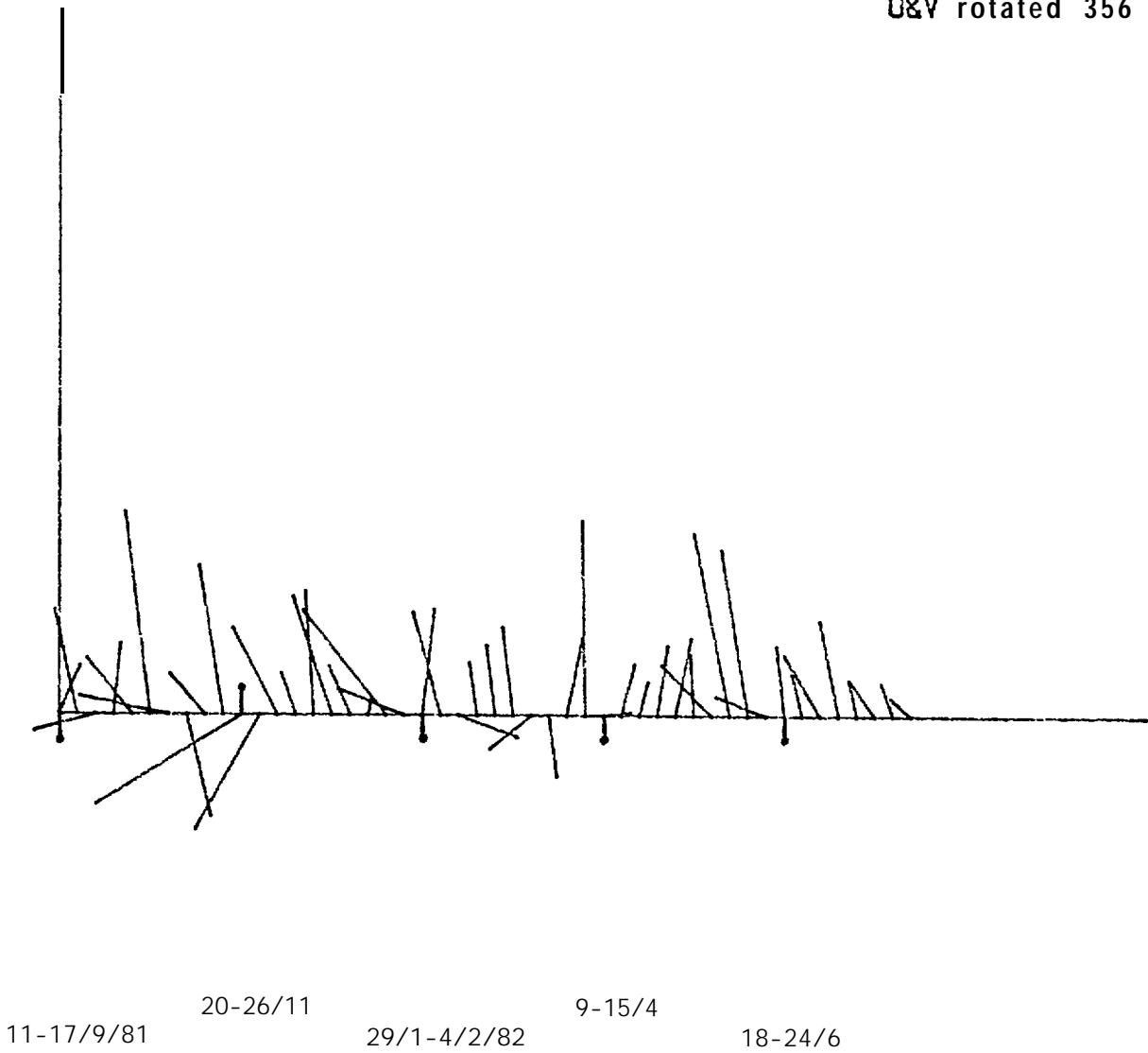


Figure 45. Weekly mean velocity, current record CS-7A. Principal axis 356°T.

CS-9A 31.5M 7-DAY MEAN

20 cm/sec/in  
U&V rotated 318 Deg

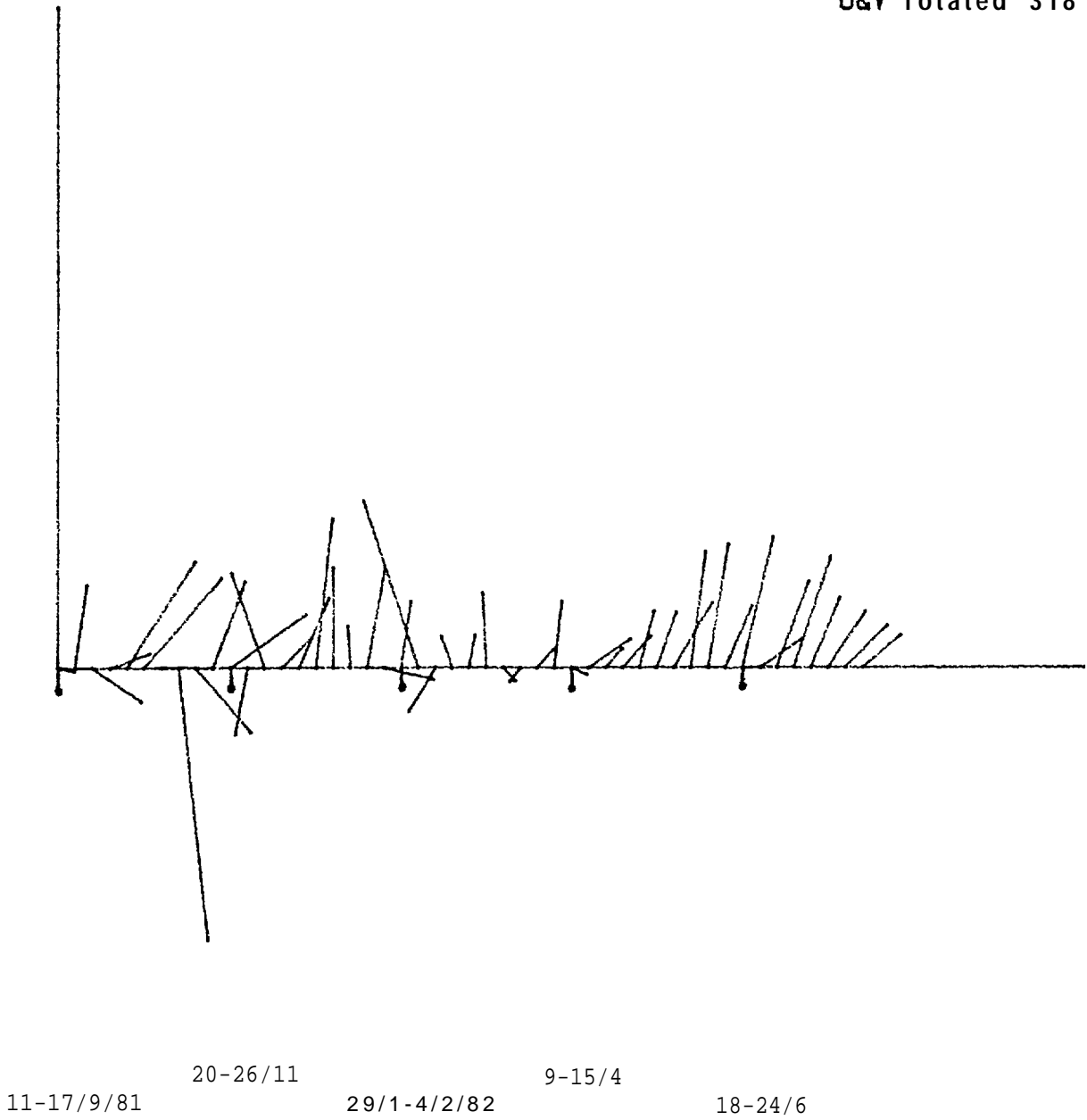


Figure 46. Weekly mean velocity, current record CS-9A. Principal axis 318°T.

to move **along** the relatively steep sides of Barrow Canyon. Farther offshore the current takes on a **more** two-dimensional character, with variability being more **nearly** rotating. Thus at **CS-7A**, which is farthest from the constraining influence of the coast **and/or** steep topography, one-fourth of the variance is offshore.

Statistical properties of a current record from each mooring, in the form of the component power spectra, are shown in Figures 28-34. (Note that the vertical scale in Fig. 28 is expanded.) The orientation of the axes is given in each case (compare Table 2). The dominance of the variance in the principal axis component is again **clear**. Most of the energy lies at time scales of five days or more. Figure 35 shows the generally similar power spectra for the geostrophic wind calculated at **68°N, 116°W**, a point about halfway along the coast from **Kivalina** to **Cape Lisburne**. Note that the principal axis is directed approximately **north-south**.

Figures 36-46 show the weekly mean flow recorded by the various instruments. All the plots have been rotated into the appropriate **principal** coordinate system, with the vertical figure axis representing the major current component. For example, in Fig. 36 the **vertical** axis is aligned along **050°T** (cf. Table 2). On a **weekly** basis, the flow was quite comparable at **CS-1A** and **-2A**, but significantly slower over the seaward side of the canyon at **-3A**. The temporal variability is large, with successive weekly means in some instances varying by a factor of ten or more. Particularly noticeable are the large flow reversals during the first three months of the record, extending over at **least six** weeks. These occurred at all three sites, but **CS-3A** recorded subsequent weaker ones as well, sprinkled throughout the deployment period (note the shift in time origin for the **-3A** records).

At CS-5A, -6A, and -7A the flow was rather similar, although slightly slower at -5A than at the other two sites. However, these speeds were **all** much **lower** than at CS-1A and -2A, and also **somewhat** lower than at -3A. The flow reversals at the three Cape Lisburne moorings are on the whole quite similar, and at the beginning they also mostly coincide with those at the northern moorings, though weaker. There is a partial coincidence of the later, smaller reversals with those at CS-3A. At CS-9A the flow is comparable to that at -5A, and the majority of the reversals agree in their timing.

These impressions of a rather coherent velocity field are quantified in Table 3, which correlation matrix is based on the low-passed velocity data and thus includes all sub-tidal time scales. First, with respect to vertical coherence, note that only at CS-1A is the vertical correlation noticeably reduced from unity, corresponding to a shear flow with slight vertical differences in time behavior. Reference to Fig. 21 shows that this is precisely the location of the very strong front discussed earlier, with extremely large **baroclinic** shear.

The records from moorings CS-1A and -2A are seen to be very highly correlated with each other (0.92-0.98), but somewhat less so with -3A (0.73-0.81). There is then a big drop in correlation to the Cape Lisburne moorings (0.40-0.54) and a further drop to CS-9A (0.30-0.38). The Cape Lisburne moorings themselves are highly correlated (0.83-0.94) and are also fairly **well** correlated with CS-9A (0.62-0.70). These statistics thus support the conclusions drawn from the **weekly** mean flow depictions (Figs. 36-46).

Table 2 also shows the correlations between the current records and the **geostrophic** wind calculated at  $68^{\circ}\text{N}, 166^{\circ}\text{W}$ . The correlations are

Table 3. Correlation of Major Axis Current Components, Zero Lag\*

	CS-1A lower	CS-2A upper	CS-2A lower	CS-3A upper	CS-3A lower	CS-5A	CS-6A upper	CS-6A lower	CS-7A	CS-9A
CS-1A upper	0.92	0.92	<i>0.92</i>	<b>0.74</b>	<b>0.73</b>	0.42	0.49	0.51	0.51	<i>0.36</i>
CS-1A lower		0.98	<i>0.98</i>	<b>0.77</b>	<b>0.75</b>	0.46	0.51	0.54	0.53	0.36
CS-2A upper			1.00	<b>0.81</b>	<b>0.80</b>	<i>0.46</i>	0.51	0.54	0.54	0.37
CS-2A lower				<b>0.81</b>	<b>0.80</b>	0.47	0.52	0.54	0.54	0.38
CS-3A upper					<b>0.98</b>	0.42	0.44	0.45	0.46	0.32
CS-3A lower						0.40	0.42	0.44	0.45	0.30
CS-5A							0.92	0.92	0.83	0.62
CS-6A upper								0.99	0.94	0.69
CS-6A lower									0.94	0.70
CS-7A										0.70
geostrophic wind 68° N, 166°W	0.62	<i>0.65</i>		<i>0.69</i>		<i>0.63</i>	<i>0.67</i>		0.68	<i>0.48</i>

\*Except for the wind-current correlation, which is for the wind leading by 18 hours. Principal axis for the geostrophic wind is 016°T.

remarkably high, particularly when we consider that we're using a **geostrophic** wind representation at a single point along a changing coastline. In this connection, note also that the largest improvement in correlation obtained by lagging the current 18 hours (a little **more** than 0.1) came at the northernmost moorings. In other words, the phase difference suggested by the slightly lagged **maximum** correlations may not so **much** represent the wind locally leading the current by **18** hours, as it does the calculated wind not representing the instantaneous wind along the entire coast. The principal point, however, is that even a crude representation of the longshore wind component is **highly** correlated with the current (in the mean, the correlation coefficient is about 0.66 if **CS-9A** is ignored). Nearly one-half the **total** current variance can thus be predicted by this scheme, suggesting both that wind-driven coastal dynamics is the key physical mechanism operating and that the coastal flow is in fact highly predictable. The reason for the significantly lower correlation at **CS-9A** **is** not clear, but Table 2 shows that it occurs both with the wind and with the other current records. The cause may lie in the proximity to Bering **Strait or in more local dynamical control.**

The coherence of the current field and of the current and the wind are shown for two of the moorings in spectral representation in Figs. 47-50. The fairly high coherence between **CS-6A** upper and **CS-9A** (Fig. 47) is generally **distributed** over the low-frequency bands and the coherent signals are essentially in phase (Fig. 48). In the comparison between the **geostrophic** wind and the **CS-6A** upper record, the coherent signals are also scattered across the low-frequency bands (Fig. 49), and there is some suggestion of the wind leading the current slightly (Fig. 50), as was discussed in connection with **Table 3.**

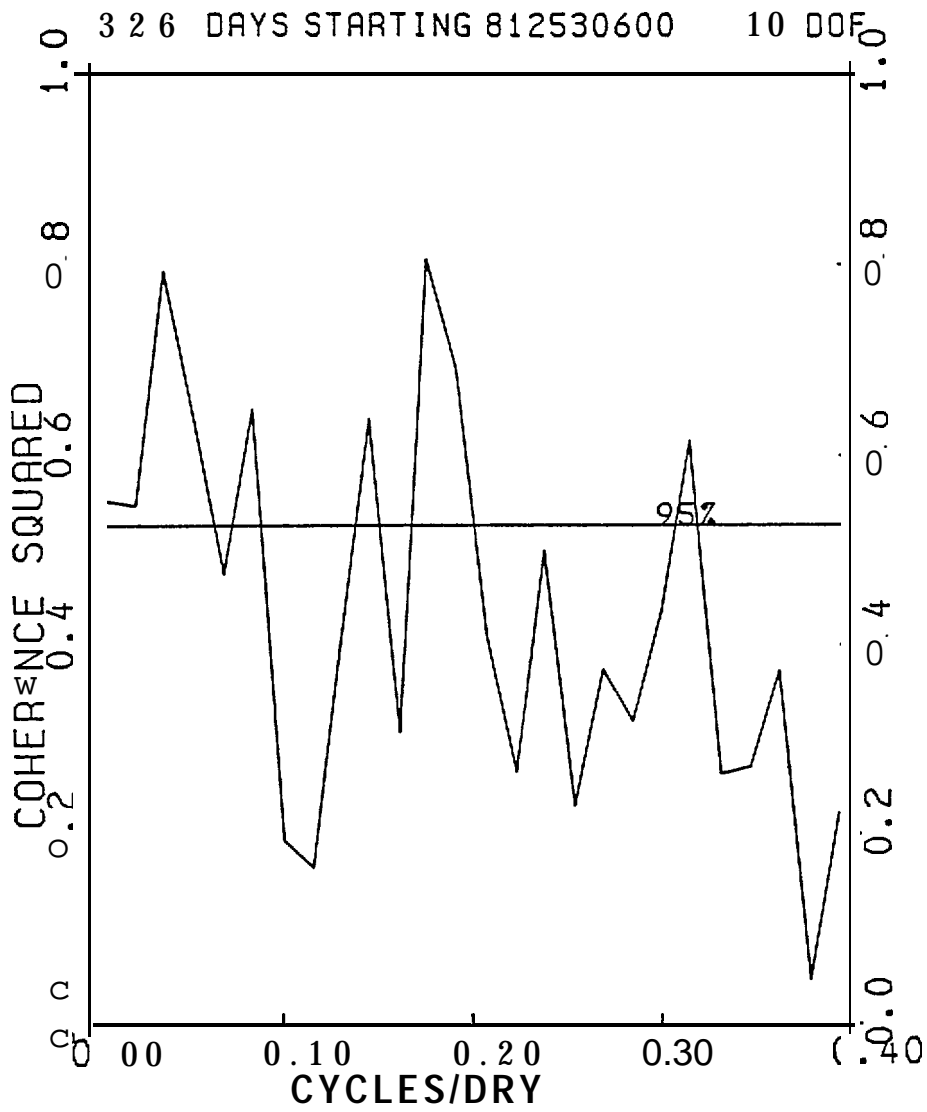


Figure 47. Coherence spectrum, current records CS-6A upper and CS-9A, principal axis components.

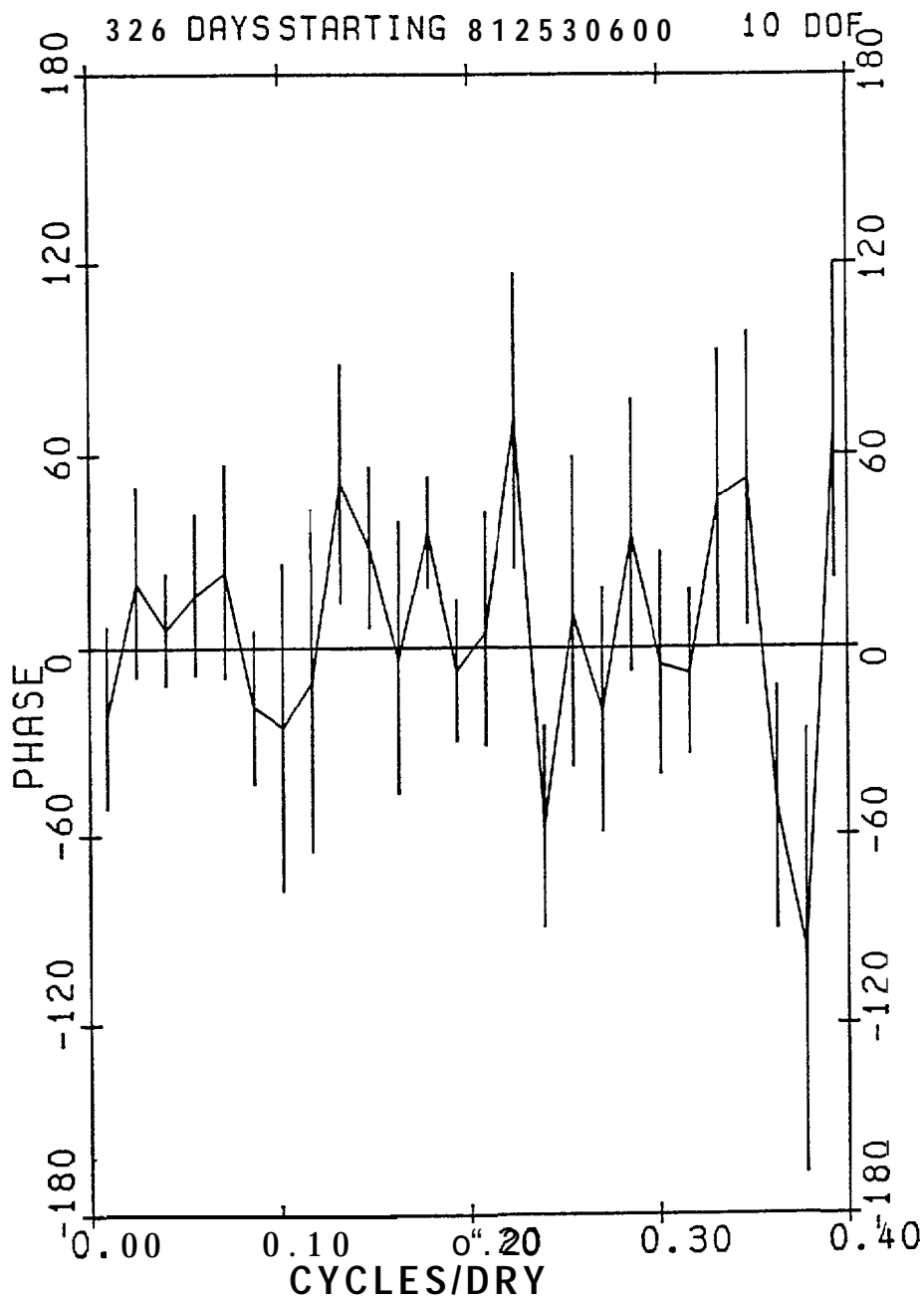


Figure 48. Phase spectrum, current records CS-6A upper and CS-9A, principal axis components. Vertical bars represent 95% confidence limits.

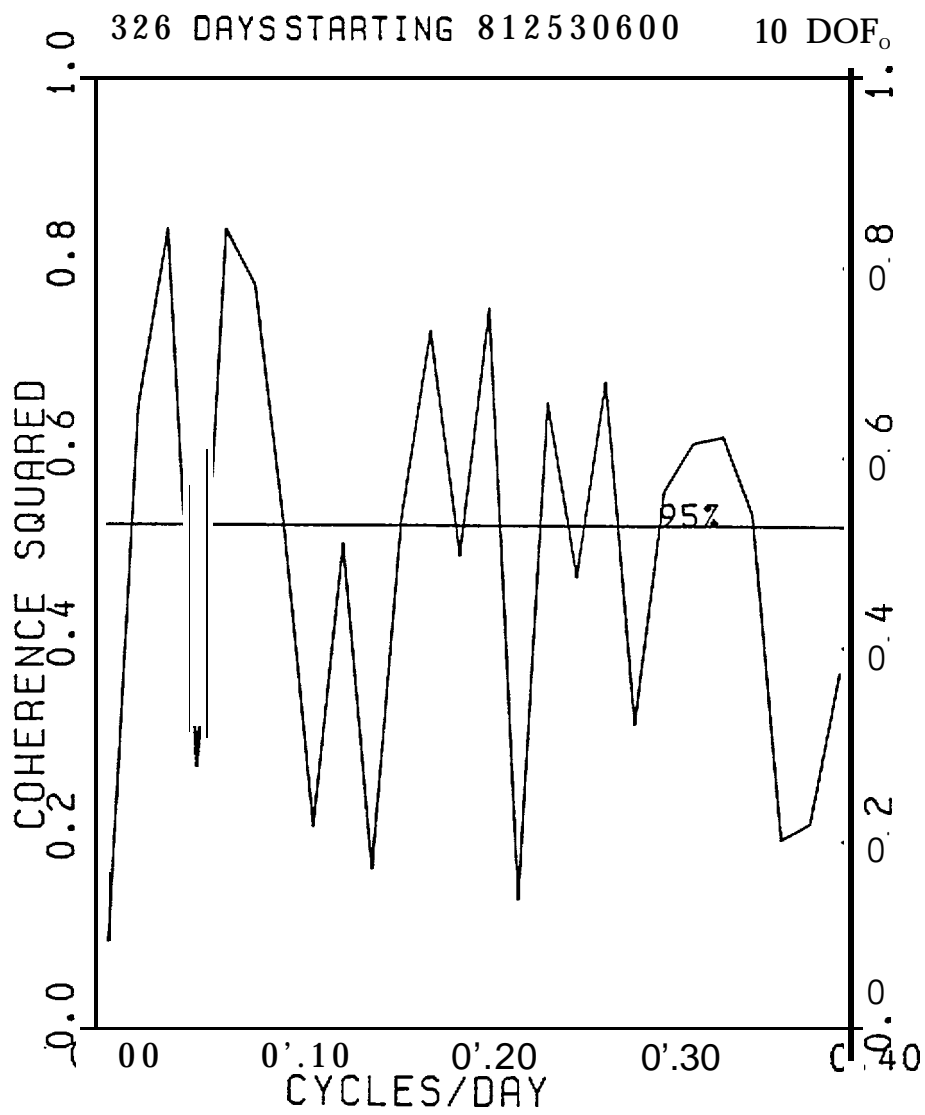


Figure 49. Coherence spectrum, geostrophic wind at 68°N,1660W and current record CS-6A upper, principal axis components.

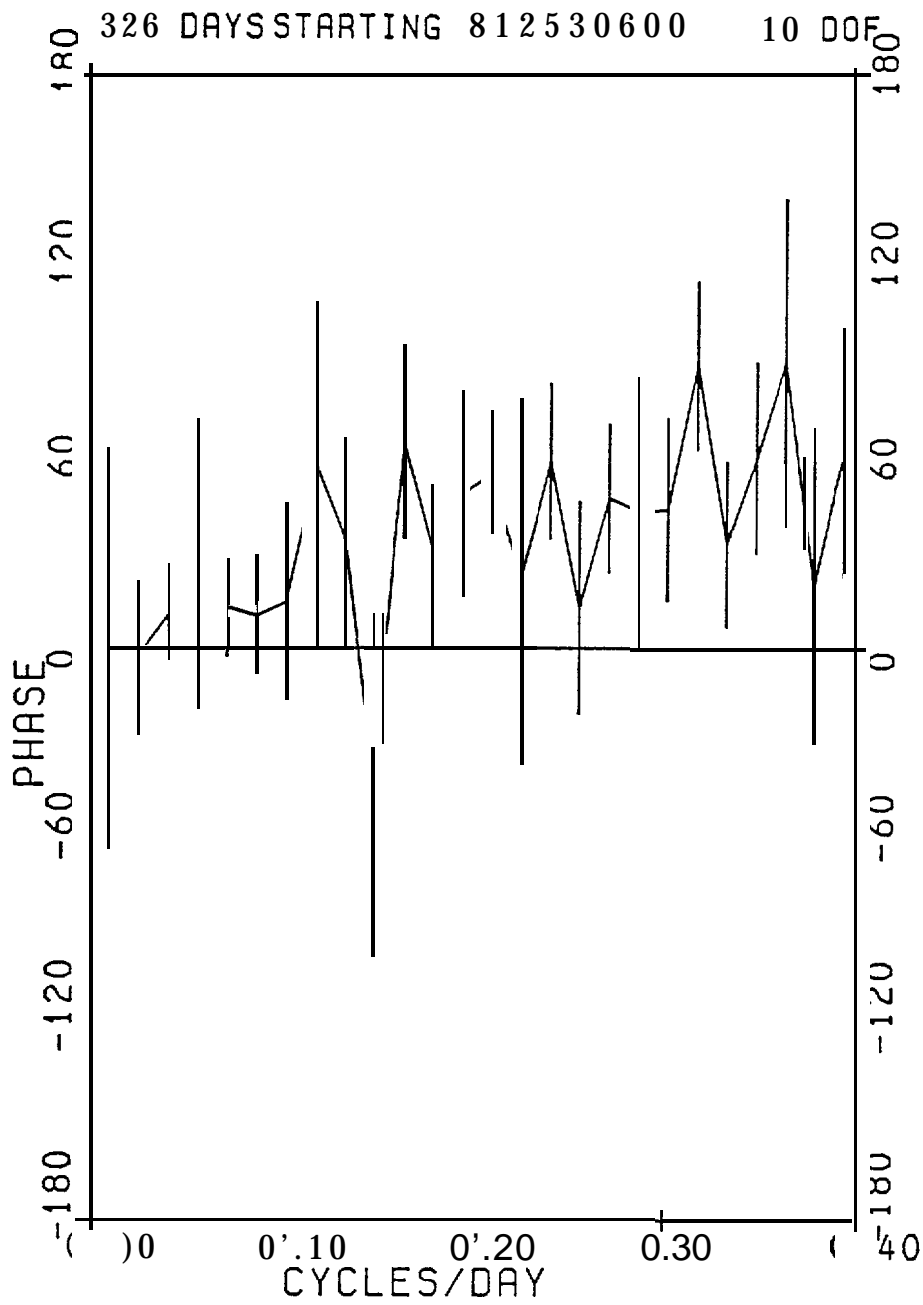


Figure 50. Phase spectrum, geostrophic wind at 68°N,1660W and current record CS-6A upper, principal axis components,

The large **flow** reversals in the early part of the record, reaching over  $40 \text{ cm sec}^{-1}$  on a daily mean basis, are of particular interest, and Figs. 51-57 have therefore been prepared, spanning these events with daily mean currents at one instrument from each mooring. On this time scale the CS-1A and -2A records are nearly identical. At -3A the southerly flow events are comparable to those at the other two moorings in the section, but the northerly events are much weaker. The Cape Lisburne records resemble each other closely both in phase and amplitude but are **significantly** different from the ones at the northern moorings and also from -9A. Overall, the impression during this period is of a decrease in **flow** reversals at the more southerly moorings (with the least at -9A), but no clear phase difference. On the other hand, as we saw from the weekly means, later in the year there were reversals at the four southerly moorings (Figs. 41-45), but not in the central and eastern part of the Barrow Canyon section (Figs. 35-38).

### *Serial observations of the dense jet*

The lower instrument at mooring CS-2A carried both conductivity and temperature sensors, from which we have calculated the **salinity** time series. Figure 58 shows the daily mean characteristics of the water flowing past the mooring during a seven-week period in February-March 1982. At the beginning of the period, the salinity increased about  $2.50\%$ , and then went through several salinity oscillations before reaching a daily mean of  $35.7\%$  in late February. It then declined to a plateau which was still  $1.5\text{-}2.0\%$  above ambient values. The temperature series is a mirror image of the salinity, faithfully following the freezing point.

CS-1A 49.8M DAILY MEAN

20 cm/sec/in  
U&V rotated 50 Deg

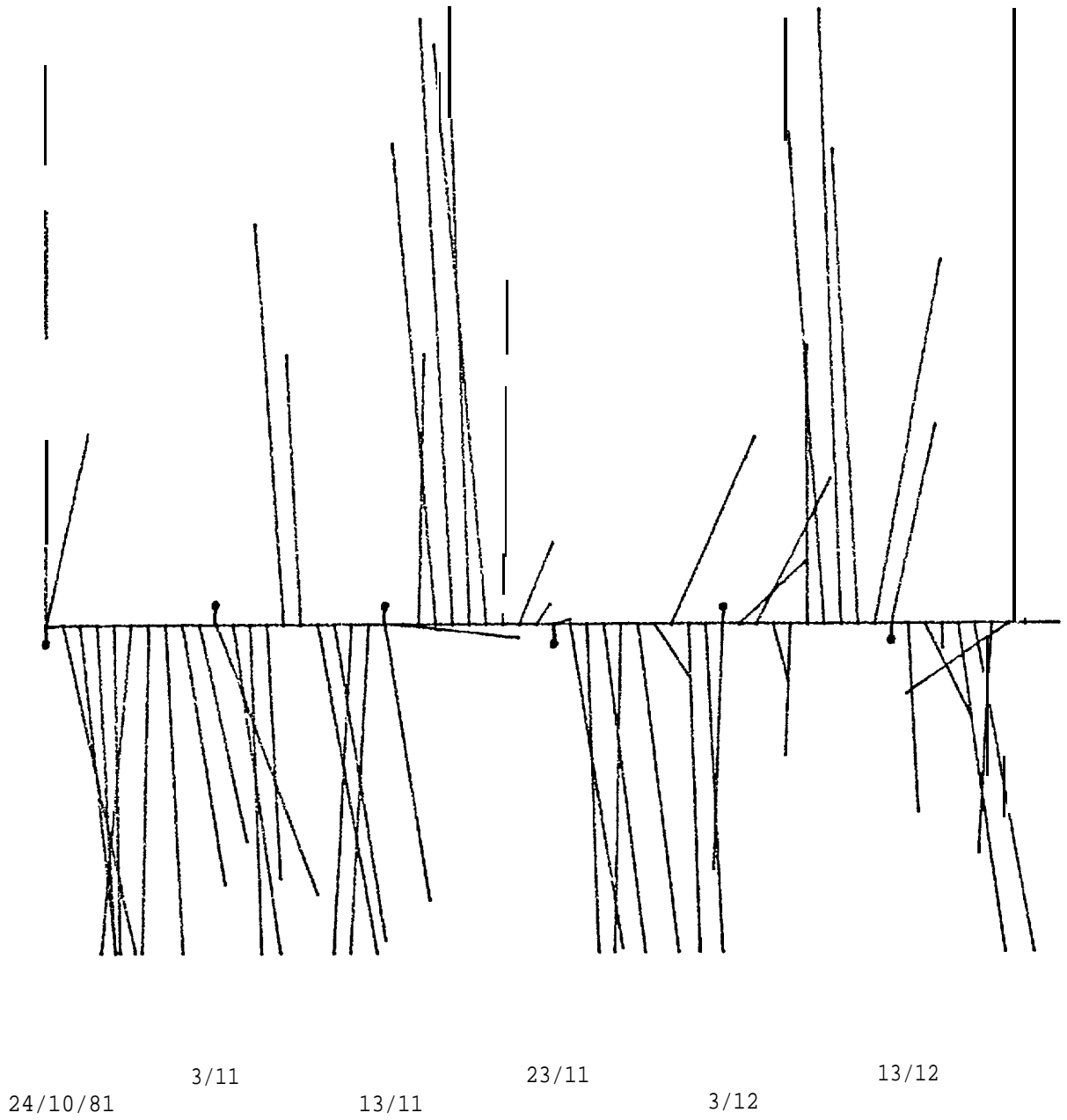


Figure 51. Daily mean velocity, current record CS-1A upper, 24 October - 21 December 1981.

CS-2A 76. ØM DAILY MEAN

2Ø cm/sec/in  
U&V rotated 55 Deg

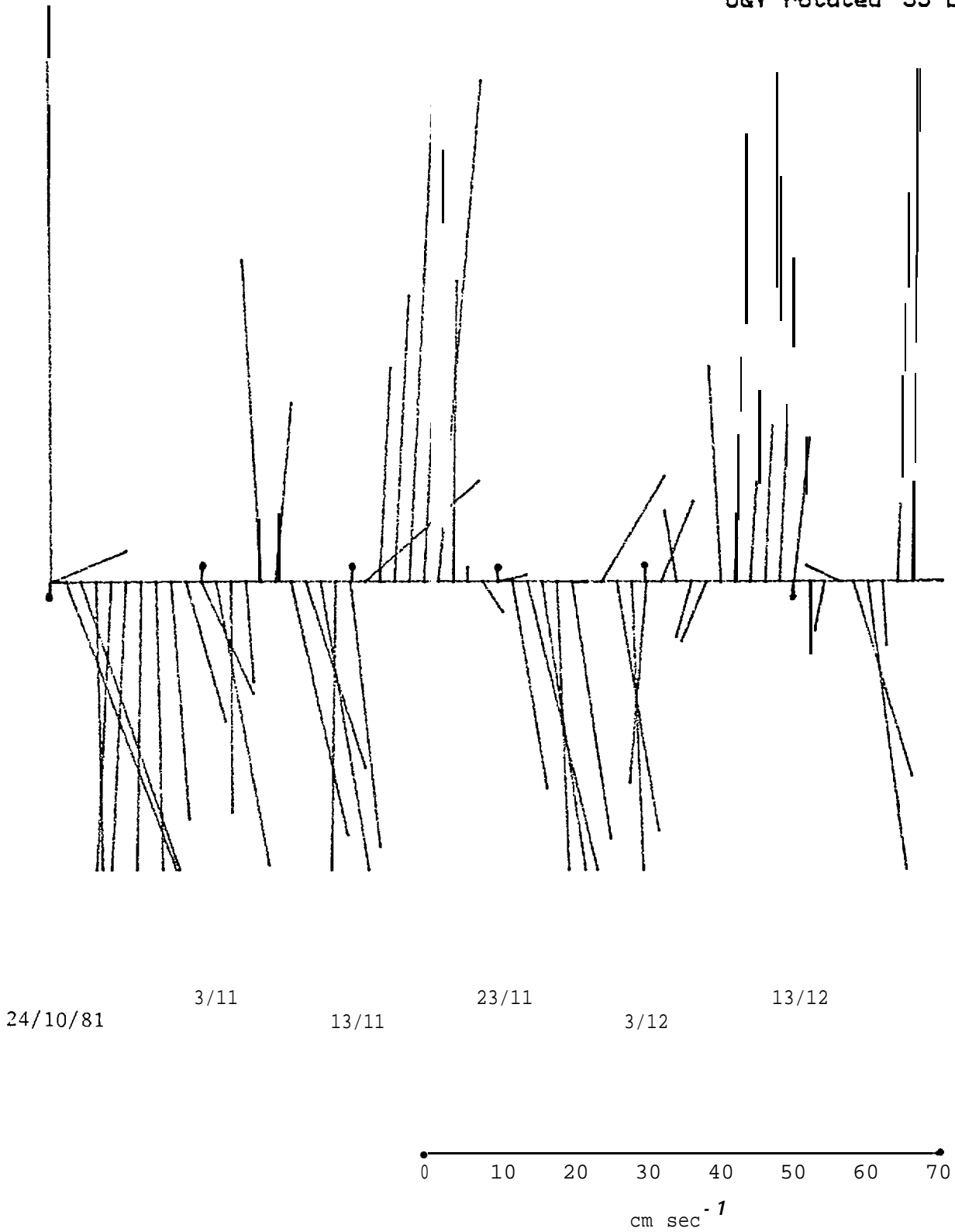


Figure 52. Daily mean velocity, current record cS-2A lower, 24 October - 21 December 1981.

CS-3A 50.7M DAILY MEAN

20 cm/sec/in  
U&V rotated 75 Deg

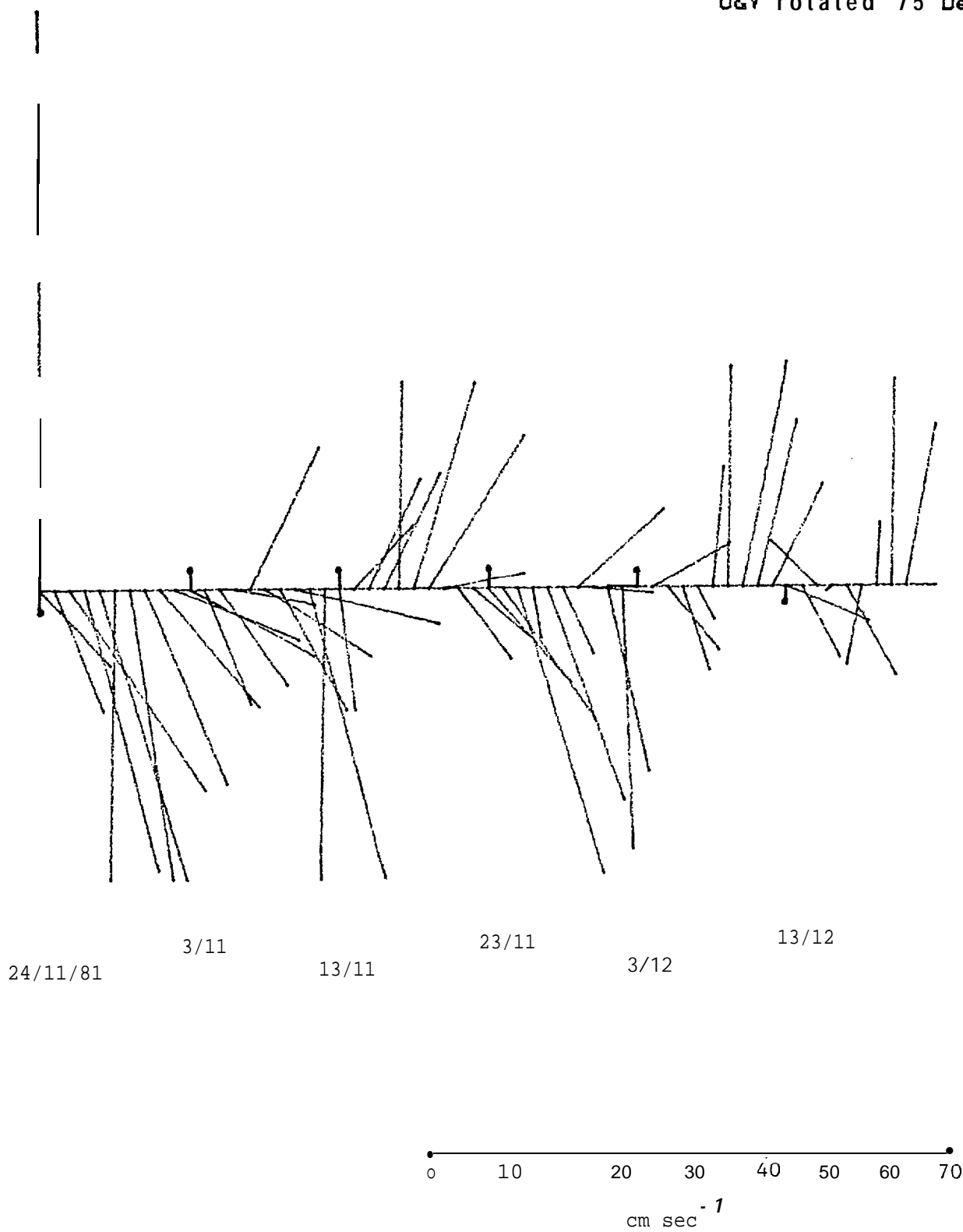


Figure 53. Daily mean velocity, current record CS-3A lower, 24 October - 21 December 1981.

CS-5A 41.5M DAILY MEAN

20 cm/sec/in  
U&V rotated 359 Deg

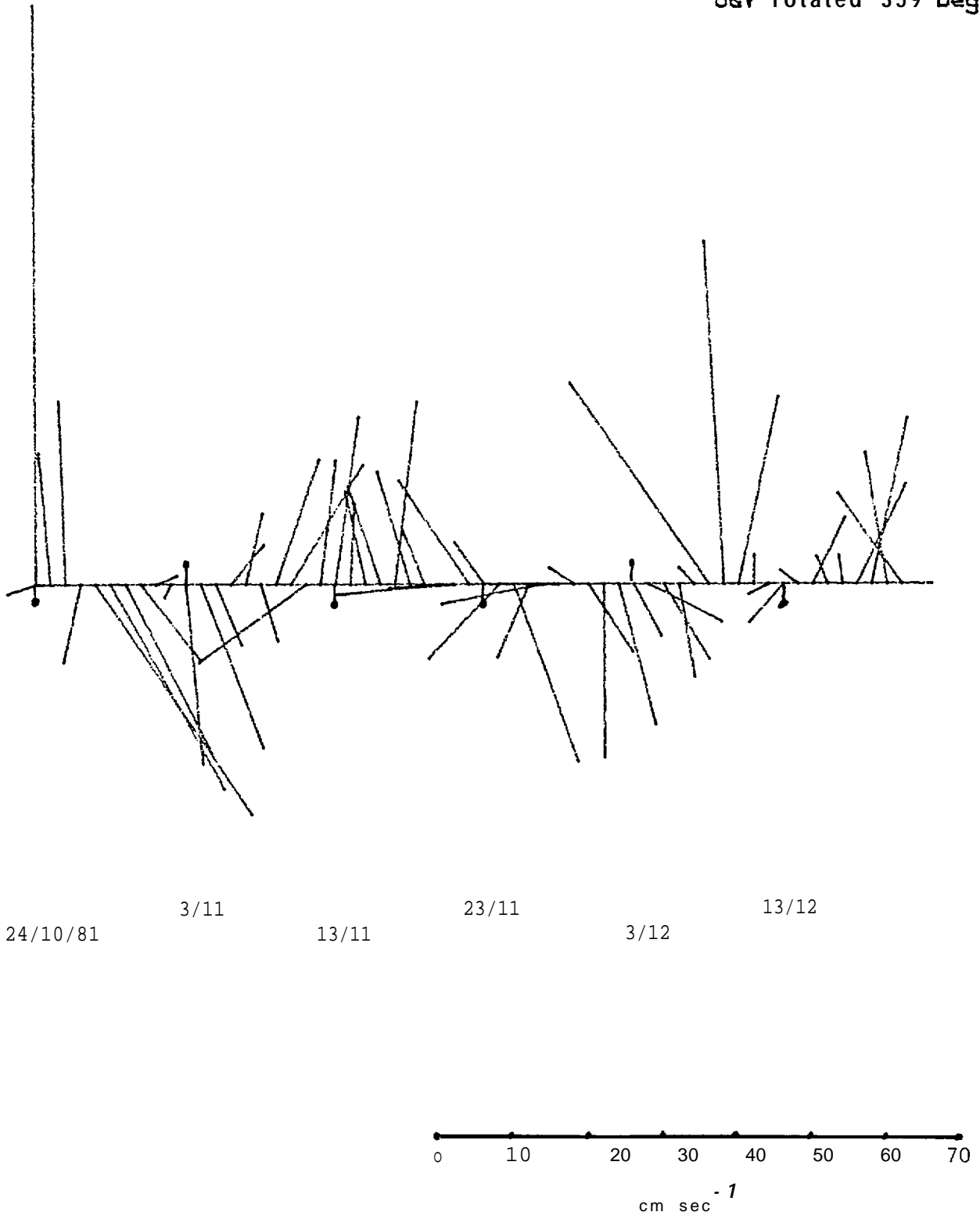


Figure 54. Daily mean velocity, current record CS-5A, 24 October - 21 December 1981.

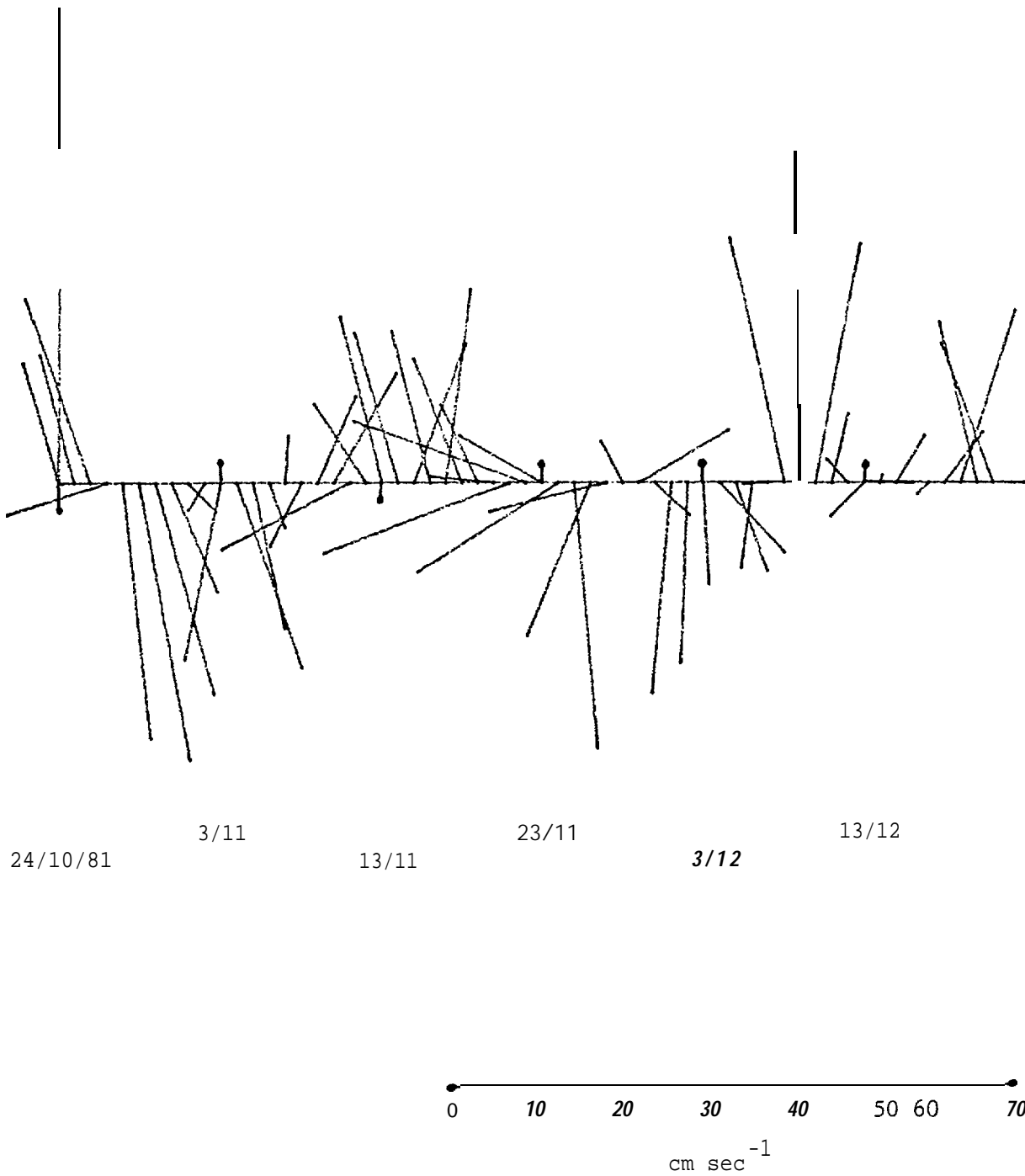


Figure 55. Daily mean velocity, current record CS-6A lower, 24 October - 21 December 1981.

CS-7A 39. 5MDAILY MEAN

20 cm/sec/in  
U&V rotated 356 Deg

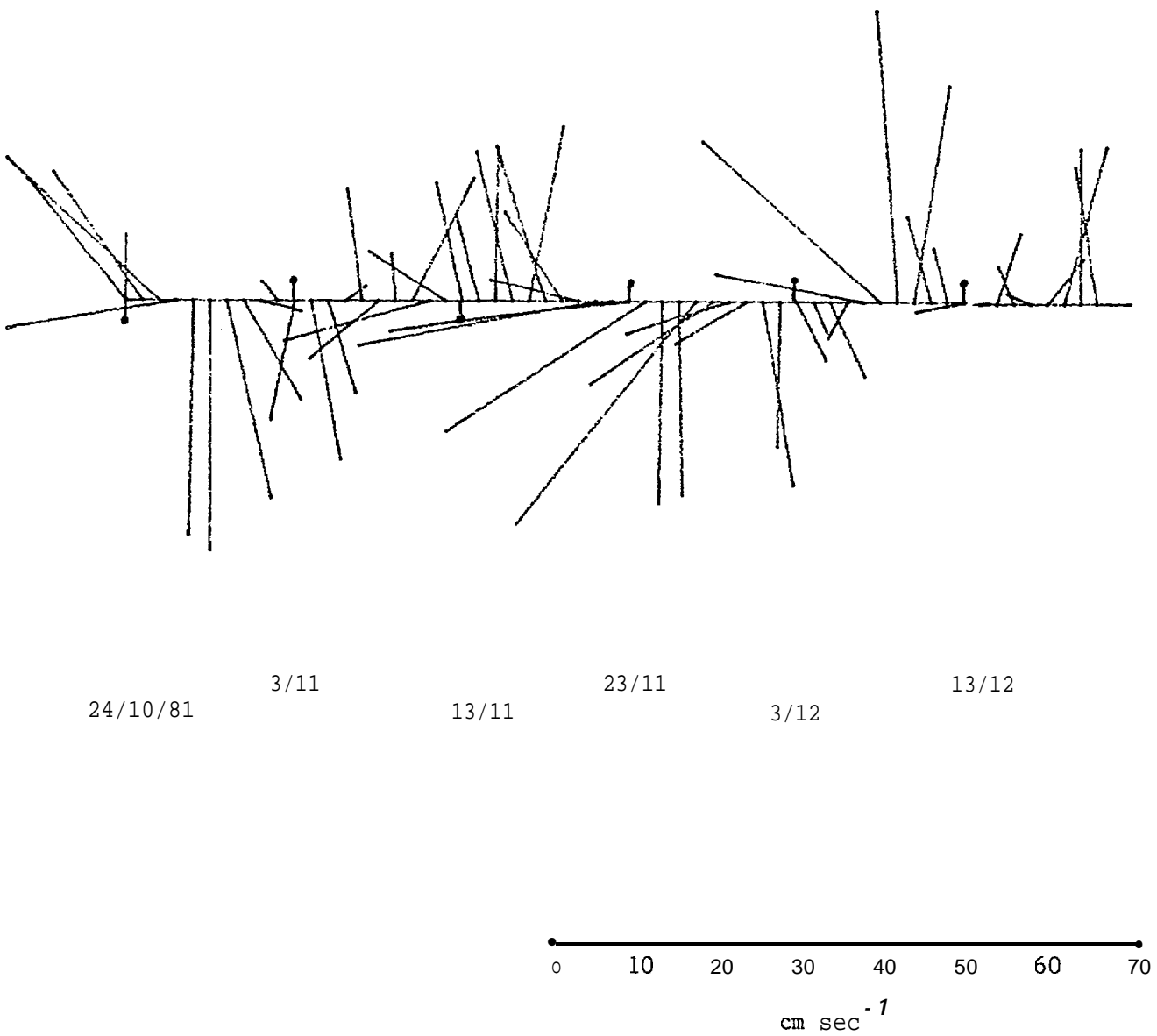


Figure 56. Daily mean velocity, current record CS-7A, 24 October - 21 December 1981.

CS-9A 31.5M DAILY MEAN

20 cm/sec/in  
U&V rotated 318Deg

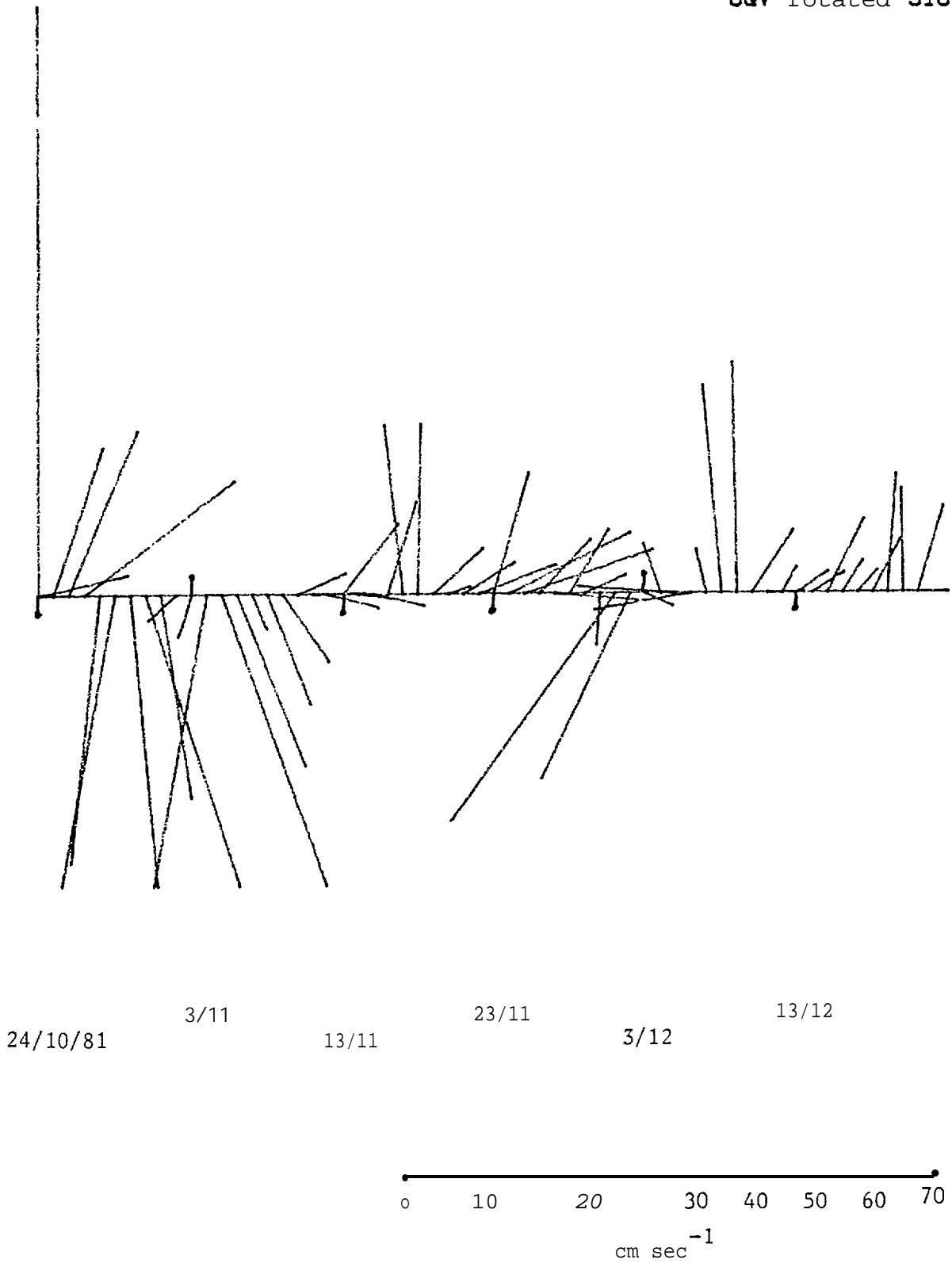


Figure 57. Daily mean velocity, current record CS-9A, 24 October - 21 December 1981.

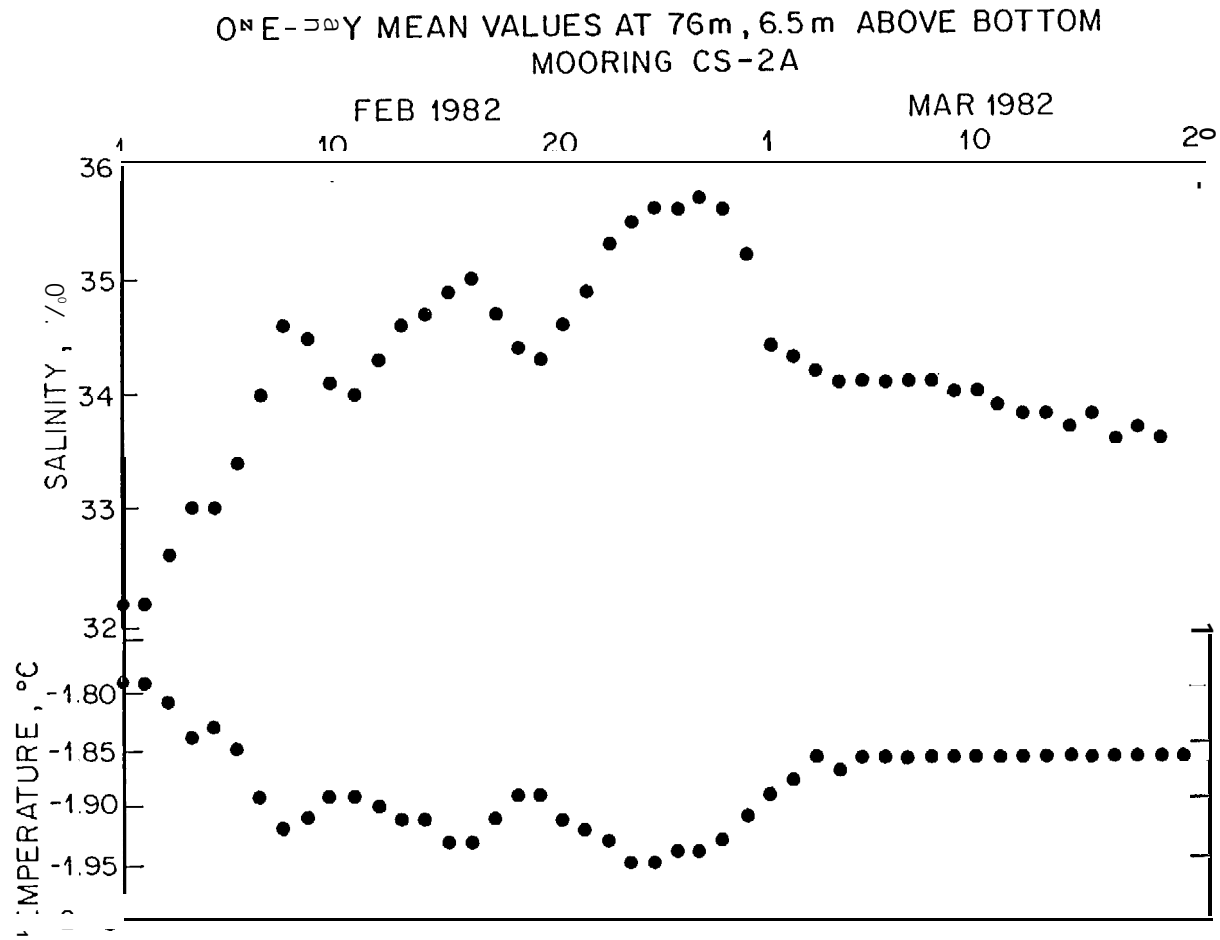


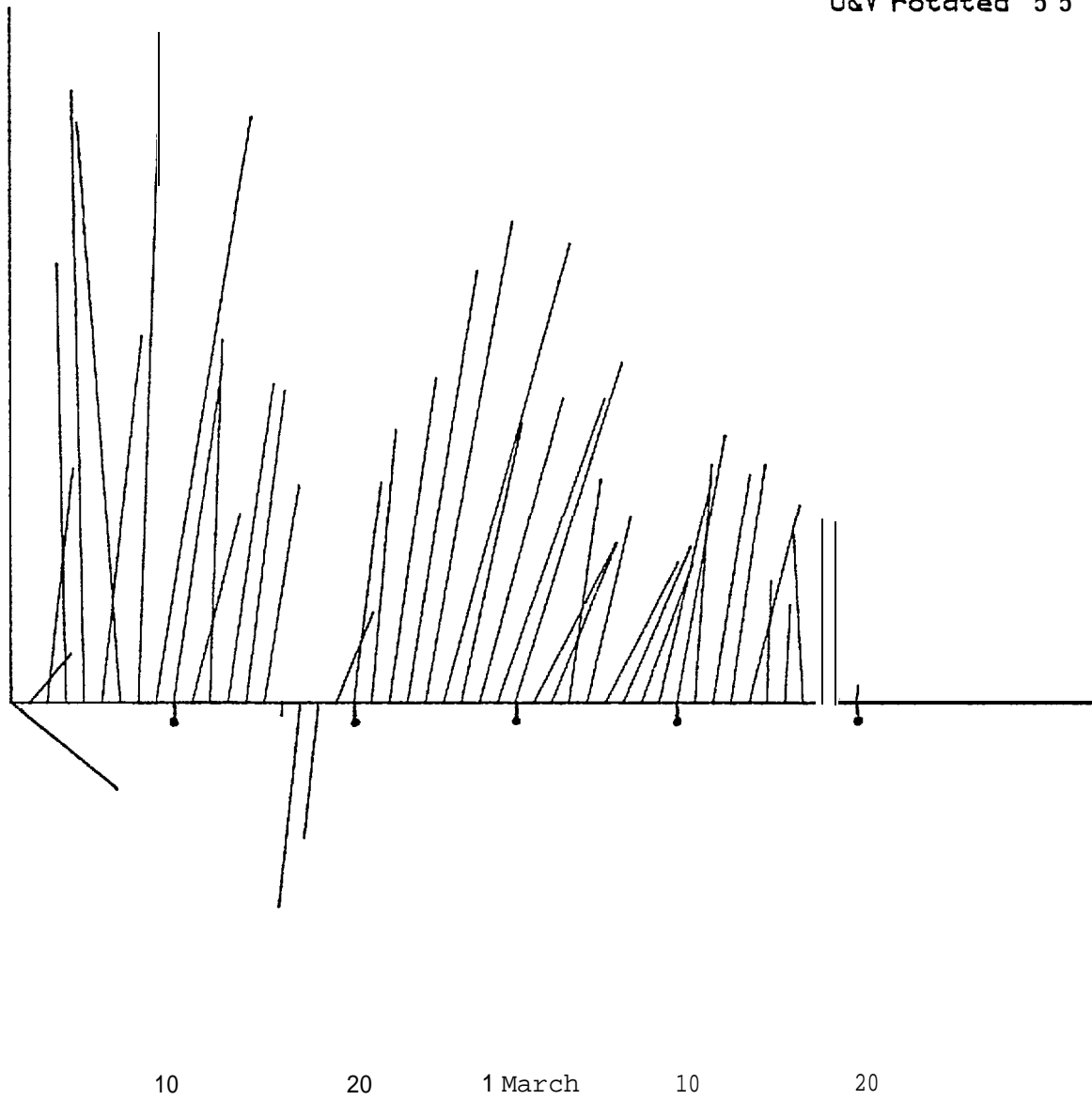
Figure 58. Daily mean salinity and temperature, current record CS-2A lower, 1 February - 20 March 1982.

The daily mean velocity over the same period is shown in Fig. 59. **While** there are obvious ties between the salinity and velocity signals (e.g., the salinity decline from 16-19 February corresponds to a velocity reversal, so that the decline actually represents **less** saline water which had earlier passed the instrument now being advected back past the instrument again), there are **no** correlations to suggest that the velocity variations themselves are forced by a variable pressure field associated with the **hypersaline** water (compare Figs. 58 and 59). Furthermore, the calculated **baroclinic** shears are typically in the range  $5-10 \text{ cm sec}^{-1}$ , whereas the measured speeds **along** the coast **are** considerably higher, suggesting other forcing. Finally, the actual shears observed within the saline layer, as determined from the current records, were almost always negative (speed decreasing toward the bottom), even during the times when the density observations indicated a positive **baroclinic** shear. Friction **is** therefore a major **dynamical** consideration within the dense layer. This was **also** the indication **of** the great seaward extent of the dense bottom Layer (Fig. 25). We may conclude that to first order at Least, the observed **velocity** variations are due to causes other than perturbations in the density field, e.g., to wind forcing. Conceptually, then, the wind plays an important role both in the formation of the dense water, and in its variable **flow** along the coast.

Finally, if we consider only the week in late February when the **daily** mean salinity at mooring CS-2A exceeded  $35\text{‰}$ , the corresponding flow was about  $40 \text{ cm sec}^{-1}$ , implying a longshore extent of **the** very dense water of about 250 km. This would correspond to a point upstream about halfway between Pt. Lay and Cape **Lisburne**, which is **at least** consistent with the

CS-2A 76.0M DAILY MEAN

20 cm/sec/in  
U&V rotated 55 Deg



0 10 20 30 40 50 60 70  
cm sec<sup>-1</sup>

Figure 59. Daily mean velocity, current record CS-2A lower, 1 February - 20 March 1982.

observations portrayed in Figs. 24-26. Enormous stretches of the coastline **are** thus seen to be involved in the saline events.

### *Conclusions*

The objectives of this study have been to 1) determine the characteristics of the **longshore** flow, and 2) ascertain whether brine rejection drives a significant winter circulation. These phenomena are of particular interest with respect to their possible role **in** pollutant transport and dispersal.

We have found that the **flow** is primarily **alongshore** (at some sites entirely so) and generally northward. Currents of 100 cm sec<sup>-1</sup> are not unusual. The flow is highly variable, including directional reversals which can persist for several weeks. There also appear to be large interannual differences, so that in **some** summers the unmixed Bering Sea inflow is missing from the northeastern **Chukchi**. A large portion of the flow variability is wind-driven, with little if any phase lag. This variability is therefore predictable.

**In** general, however, there is also a **baroclinic** circulation throughout the year. In summer this principally takes the form of a **longshore** buoyant jet, whose velocity signature can exceed 65 cm sec<sup>-1</sup>. Strong shears can exist over 40 km out from the coast, i.e., well beyond the **baroclinic** deformation radius. In **winter**, a jet of dense water is formed on an intermittent basis **by** brine rejection. Salinities have been measured in this water which exceed any ever observed in the Arctic outside coastal lagoons, and the dense water has been seen to spread offshore some 80 km within a frictional **bottom** boundary layer.

## References

- Aagaard, K., L.K. Coachman and E. Carmack. 1981. On the halocline of the Arctic Ocean. Deep-Sea Res. 28A: 529-545.
- Coachman, L.K. and K. Aagaard. 1981. Reevaluation of water transports in the vicinity of Bering Strait. Pp. 95-110 in The Eastern Bering Sea Shelf: Oceanography and Resources, vol. 1, D.W. Hood and J.A. Calder (eds.). Dept. of Commerce/Natl. Oceanic and Atmos. Admin., Washington, D.C.
- Coachman, L.K., K. Aagaard and R.B. Tripp. 1976. Bering Strait: The Regional Physical Oceanography. University of Washington Press, Seattle, 172 pp.
- Kowalik, Z. 1981. A study of the  $M_2$  tide in the ice-covered Arctic Ocean. Modeling, Identification and Control 2: 201-223.
- Matthews, J.B. 1970. Tides at Pt. Barrow. Northern Engineer 2: 12-13.
- Schumacher, J.D., K. Aagaard, C.H. Pease and R.B. Tripp. 1983. Effects of a shelf polynia on flow and water properties in the northern Bering sea. J. Geophys. Res. 88: 2723-2732.